Biomimetic Whiskers for Active and Passive Sensing

Sejoon Ahn

The Graduate School
School of Electrical and Electronic Engineering
Yonsei University

Biomimetic Whiskers for Active and Passive Sensing

A Masters Thesis
Submitted to the Department of
Electrical and Electronic Engineering
and the Graduate School of Yonsei University
in partial fulfillment of the
requirements for the degree of
Master of Engineering

Sejoon Ahn

July 2013

This certifies that the master's thesis of Sejoon Ahn is approved.

Thesis Supervisor: DaeEun Kim

Euntai Kim

Hyun Myung

The Graduate School
School of Electrical and Electronic Engineering
Yonsei University
June 2013

Abstract

Many types of animals such as rats and pinnipeds use their whiskers as their primary sensor in order to perceive their environment.

Rats use their whiskers to sense their environment by actively moving them back and forth continuously. Rats are able to discriminate different textures or extract features of a nearby object (such as size, shape and distance).

Pinnipeds, such as the harbor seal and the California sea lion, are known to have highly sensitive whisker sensors which can detect hydrodynamic trails generated by preys such as from swimming fish. They can sense the trails even after the prey (fish) has gone a long distance. Hydrodynamic stimuli can be sensed with high accuracy by pinnipeds.

Inspired by the ability of rats, engineers have derived mathematical models for whiskers' 'contact distance estimation' and also made artificial whiskers. Many methods for contact distance estimation (the distance between the base of the whisker to the object - whisker contact point) have been proposed based on numerical or analytical models of the whiskers. These methods could be classified by 'the shape of whiskers(cylinder or tapered)', 'sensors used at the base' and 'sensing strategy, (active or passive)'.

In this dissertation, we first analyze the linear cylinder whisker model proposed by Kim and Möller. Under an active sensing situation, this model only measures the protraction angle and a single deflection angle a little away from the base. With the two angle information, the model can estimate the contact distance without knowing the whisker's property or the moment at base. We analyze this linear model in the perspective of robustness to noise. Also, how accurately this model estimates the contact distance in large deflection is analyzed by comparing linear simulation results with numerical nonlinear results. Extending this model, we propose a linear tapered whisker model. It is shown that the contact distance can be estimated using only two angles (protraction angle and a deflection angle on the whisker) as well. The same analysis has been done on the tapered model. Results show that tapered whiskers are more robust to noise than linear cylindrical whiskers. Also, it is shown that knowing two deflections, the contact distance could be estimated.

Also, a simple but effective microphone based sensor has been designed and manufactured inspired from the pinniped whisker systems. This chapter was concentrated on the passive sensing.

Five different microphone sensors were made which had either a short (approx. 7cm) whisker shaft or a long (approx. 10cm) whisker shaft. Two of the sensors had a short whisker shaft and the other three had a long whisker shaft. Five of these sensors have been conducted under several experiments. First, all of them were tested with an impulse-like response to check if any defects were present, and if the length and natural frequency relationship was well shown from the results. For the fifth sensor, the impulse-like response within water was conducted.

Also a successful modeling of the whisker sensor has been done, which mimics the main key features shown in the experimental impulse-like response. For passive experiments, a whisker sensor was sensing hydrodynamic stimuli while varying the source's location. The results showed that passive sensing may be not enough for sensing hydrodynamic trails.

As an extension, the hydrodynamic trail which was generated by the motor was sensed by the whisker sensors either passively or actively. It was shown in the results that the relatively slow movements of the whisker sensor (moving towards the motor) can make the trail be sensed with higher sensitivity. However for the case where the whisker was moving too fast, the movement induced VIV effect becomes dominant (data not shown). Keeping in mind that the relative velocity of the predator and the prey cannot be extremely high, the slowly moving whisker (approx. $20cm/s$) may be a strategy pinnipeds might use.

Also, the VIV (vortex induced vibration) effect was measured from the results. Because the whisker shafts were all approximately similar to a circular cylinder, unlike the harbor seal's bumpy whisker, it did not suppress any VIV. The evident relation between the VIV and the moving velocity, the relationship between the length and VIV frequency has been shown from the results. Such differences of whisker length could be a cue for the use of various whiskers with different length.

Through the relationships between 'whisker length', 'whisker moving speed', and 'the corresponding VIV frequencies', it was shown that the longer the whisker, the lower the frequency it will have compared to shorter whiskers (with same speed) but will increase its frequency faster as speed increases. Also, the longer the whisker, the VIV frequency will appear more clearly, which resulted in a smaller 'dispersion value' than the others. Another experiment was to measure the VIV frequency when external stimuli or fluid flow exists. Though the experiment used stimuli generated by a propeller which is far from linear, it could be concluded that if there is external linear flow, the flow velocity could be estimated using the characteristics of a whisker sensor.

Acknowledgements

This thesis could not have been written if it were not for the support of many people. I first thank my supervisor, Prof DaeEun Kim, and Prof Euntai Kim and Prof Hyun Myung, the professors who volunteered to be a part of my Thesis Committee. They all guided me with great enthusiasm and support which expanded my view. My thesis could be completed because of their enormous help.

I express my overflowing gratitude for the support of the members of Biological Cybernetics Lab. I'd like to give special thanks to Jaehong Lee and Eunseok Jung. Without their hardware design and circuit design, most of my work could not have been done. I'd also like to thank Changmin Lee, Hyungu Yim, Seungmin Baek, Joongbo Shin, Wonki Lee for their friendship, support and interactions.

Finally, I'd like to thank my mom and dad, brother and sister for supporting me throughout all my studies. Last but not least, I thank God, my Creator, Savior and Heavenly Father, who made everything possible.

Declaration

I declare that this thesis was composed by myself, that the work contained herein is my own except where explicitly stated otherwise in the text, and that this work has not been submitted for any other degree or professional qualification except as specified.

(*Sejoon Ahn*)

Table of Contents

List of Figures

Chapter 1

Introduction

In this thesis, the study concentrates on biomimetic whisker sensors which are based on rats and pinnipeds such as harbor seals and California sea lions. The abilities of each species have extraordinary abilities of its own kind. Rats can sense features of an object such as size, shape and distance, while pinnipeds can sense subtle hydrodynamic trails generated by fish. Inspired from these animals' abilities, biomimetic whisker sensors were studied in this thesis.

1.1 Biomimetic Whisker Sensors : Inspired by Rats and Pinnipeds

Biomimetics has given the technology a breakthrough time to time. Looking into nature and unraveling the mysteries is a good way to find novel methods to do particular tasks. Rats and pinnipes also have great abilities of sensing their environment using their whisker sensors. It seems like rats have been studied more than pinnipeds, probably because they are common and small enough to fit inside a small cage where intensive examination could be held. On the other hand, pinnipeds are rare. There are many biomimetic whiskers which mimic rats, but not many mimic pinniped whiskers.The rarity of each species may be the main reason for this.

One of the main characteristics of the rat whisker sensors is that they actively whisk (active sensing). They actively move their whisker back and forth in a certain frequency range which allows them to avoid obstacles or follow a wall. Also more subtle tasks such as discriminate textures or radial distances are possible. Rat whiskers are tapered (which means it resembles a cone shape). Such tapered whiskers' advantage has given in (Williams and Kramer, 2010), which explains that the tapered whisker's natural frequency will not vary much even when the tip of its whisker will break. If the end of a cylindrical whisker breaks, the natural frequency will vary significantly compared to the tapered whisker.

On the other hand, pinnipeds have different whisker morphologies. Harbor seals and California sea lions are both classified as pinnipeds but their whisker morphology differs as will. While they both have an oval cross section, harbor seals have a bumpy profile while the California sea lion has a smooth profile. Harbor seal's abnormal whisker morphology is known to reduce the vortex induced vibration (a well known phenomenon; when a bluff body is exposed to a linear fluid flow, an oscillating vortex is generated when Reynolds number is big enough, and these vortices make the bluff body to vibrate. Also known as VIV). Even through computer simulation, this was proven (Hanke et al., 2010). The reduced VIV can increase the signal to noise ratio (SNR) where the wanted signal is the subtle hydrodyanmic trails generated by fish (or prey). Harbor seals and California sea lions are both capable for tracking hydrodynamic trails even when their eyes and ears are covered (giving only whiskers to be used) (Schulte-Pelkum et al., 2007; Gläser et al., 2011). However, harbor seals seem to have better abilities to track their prey.

The applications of 'biomimetic rat whisker sensors' can be classified into 'obstacle avoidance', 'radial distance estimation', and 'tactile discrimination'. Examples of such applications are given in (Kaneko, 1994; Ueno and Kaneko, 1994; Kaneko et al., 1996, 1998; Hartmann, 2001; Scholz and Rahn, 2004; Clements and Rahn, 2006; Solomon and Hartmann, 2006; Kim and Möller, 2006, 2007; Birdwell et al., 2007; Solomon and Hartmann, 2008, 2010; Towal and Hartmann, 2010; Lepora et al., 2010, 2011; Solomon and Hartmann, 2011; Towal et al., 2011).

Obstacle avoidance is the most simple method which uses whisker sensors to sense obstacles. Textile discrimination is using the whisker shaft's vibration in order to discriminate different textures. Such method could use the spectrogram or a naive Bayes filter for such task. Radial distance estimation, is one of the most sophisticated tasks which purpose is find the distance from whisker sensor base to whisker shaft - object contact point, which is why it is some times called 'contact distance estimation'.

On the other hand, there are very limited studies on 'biomimetic pinniped whiskers'. The several applications which mimic pinniped whiskers are in (Solomon and Hartmann, 2006; Chagnaud et al., 2008; Stocking et al., 2010; Yu et al., 2010; Eberhardt et al., 2011; Rooney et al., 2011), but none of them really mimics the pinniped whisker's morphology or structure. The attempts of these studies are concentrated on sensing hydrodynamic stimuli, but are merely prototypes. They do not yet mimic the core characteristics of the pinniped whiskers. The whisker morphology are rigid or wide, which differs from the actual pinniped whisker sensory systems.

In this thesis, we concentrate on 'radial distance estimation' methods and 'biomimetic pinniped whiskers' which can sense hydrodynamic stimuil. The motivation for such work is written in the following section.

1.2 Motivation and Ojectives

There are various types of sensors which are used to perceive the world. Examples are vision sensors, sonar sensors, lasor sensors, IMU and many other types of sensors. Therefore the question of 'Why should biomimetic whisker sensors be studied' may arise. This question may be answered in three ways.

First of all, there are cases where a certain system or robot needs to observe the nearby environment or object where visual sensing is difficult due to an insufficient light source. There can be several sensors which could be selected for this case, but the whisker sensors can be advantageous over others because it can select the direction in which it wants to sense by moving the sensor's direction. Also, using the mechanical characteristics of the whisker shaft, different types of information can be obtained. For example, the different whisker length can give different resonance frequencies, and different structures (such as cylindrical/tapered or smooth/bumpy) will results in different responses, where each may have its own advantages in different situations. Also, it is much simpler to implement sensors in an array. An array of whisker sensors with different whisker shaft lengths will easily give the system a heterogeneous sensory system.

Secondly, (this reason is constrained to the pinniped whiskers) there are many ways to examine the flow of fluids, but the whisker systems of pinnipeds have shown that it is possible to measure or observe a hydrodynamic trail or stimuli. By making a simple artificial whisker system, it could be implemented easily on under water robots, or possibly mounted on a frame immersed in fluids to examine flow speed and direction with ease.

Thirdly, the reason for studying biomimetic whiskers is not only for the engineering field but also for the biological field. Even though this study is concentrated on an engineering view, it could shed light on the biological view on whisker systems by giving them a new hypothesis for each animal type.

1.3 Organization of dissertation

The organization of this dissertation is as follows. In this chapter, the reason why whisker sensors are important (hence the motivation) has been described. The background for this research is described in Chapter 2, which introduces the abilities of rats and pinnipeds as well as the application issued of biomimetic whisker sensors.

Chapter 3 shows biomimetic whiskers based on rats. ’Radial distance estimation’ methods have been presented where one is a model using a cylindrical whisker for contact distance estimation proposed by Kim and Möller (Kim and Möller, 2007). Another is a tapered whisker model which is first proposed in this paper. The last model proposed in this chapter is a contact distance estimation method using two different deflection measurements.

Chapter 4 and 5 shows biomimetic whiskers based on pinnipeds. Chapter 4 concentrates on ’passive sensing’ while chapter 5 concentrates on ’active sensing’. Inspired from pinniped whisker systems, five microphone based whiskers were made where the vibration of the whisker could be sensed by the microphone sensor. The impulse-like response (in air and water) of the whisker sensors were first given to check the characteristics such as the natural frequency and the decaying rate of the impulse responses, while it also checked for any defects. Also, passively sensing hydrodynamic trails generated from a propeller have been shown

In chapter 5, active sensing and passive sensing have been compared via including more experimental results. Then, vortex induced vibration (VIV) sensed by the whisker sensors were also analyzed. The VIV frequency variation due to the change of the length and moving speed of the whisker sensors has been explained from the results. The results implied that the VIV frequency was increased as the whisker moving speed increased. Also, the results of sensing the hydrodynamic trial with the static and moving whisker was compared, which shows that active whisking under water could enhance sensing ability. Finally, the difference between a normal hydrodyanmic trail generated by a motor and with or without an artificial fin oscillating in front of it was compared.

Chapter 6 summarizes the whole dissertation and includes future works.

Chapter 2

Background

All animals need sensors to sense their environment. Generally many mammals, including humans, depend heavily on their visual sensors. Other animals that do not depend on visual cues use other sensors to explore their circumstances. Bats are well known for their ultrasonic waves. Weakly electric fish which live in turbid water (where visual cues are scarce) generate an electric discharge from their unique type of organ in order to catch their prey. The electric field is distorted by objects which have different electrical properties from water. Sand scorpions can find prey by sensing vibrations through sand.

While there are diverse sensory systems, rats are known to use their whiskers in order to explore their environment. Rats are not the only species which use whiskers. Harbor seals are known to use their whiskers to detect water trails generated by fish (their prey) (Dehnhardt et al., 2001; Schulte-Pelkum et al., 2007; Wieskotten et al., 2010a). One of the main differences between the harbor seal's whisker and the rat's whisker is that rats actively whisk their whiskers while the harbor seal does not (Towal and Hartmann, 2006, 2008; Szwed et al., 2003; Hartmann, 2009). In this chapter, the overview of rat whiskers, pinniped whiskers and the application issues are given.

2.1 Rat whiskers

2.1.1 Overview

Rats are known to use their whiskers for texture discrimination or feature extraction of nearby objects. Inspired by the ability of rat's whiskers, many engineers have attempted to apply the principle of whisking into engineering by making artificial whisker sensors which could discriminate different textures, estimate radial distances (Solomon and Hartmann, 2008; Clements and Rahn, 2006; Kaneko, 1994; Birdwell et al., 2007; Solomon and Hartmann, 2011),object feature extraction(Solomon and Hartmann, 2006, 2010) and other various types of applications (Schultz et al., 2005; Lepora et al., 2010, 2011).

2.1.2 Rat's ability

The large mystacial vibrissae of the rat's could be used to perform various types of tasks, such as tactile discriminations (A. Harvey, 2001; Ahl, 1986; Hartmann, 2001).

Individual whiskers could be regarded as a patch of skin on a single finger tip(Carvell and Simons, 1990). For instance, when a human uses his or her fingers to find a particular object in the dark, he or she will actively move the fingers in order to explore the environment and finally find the target object. The individual whiskers could act as an individual sensor, or it could have a distinct function for a larger functional unit. But Krupa suggests that each whisker would act as an equivalent sensor when it is doing a radial distance difference discrimination task,(Krupa et al., 2001). He shows that the rat can discriminate the radial distance difference of the left and right very accurately. Using an apparatus which can control the width using a computer controlled stepper motor. Measuring the difference between the variable width aperture, and making the rat poke the center nose poke as a reference point, the rat would go to the left or to the right and get its reward if it selects the correct answer. The paper suggests that even without whisking the whiskers actively, the rat can accurately distinguish or determine the radial distance difference even when the difference is small. When the long whiskers were cut, the accuracy for the correct answer became approximately 50% which means that it lost its ability for radial distance difference sensing. In a nutshell, individual whiskers can provide the ability to discriminate with great sensitivity

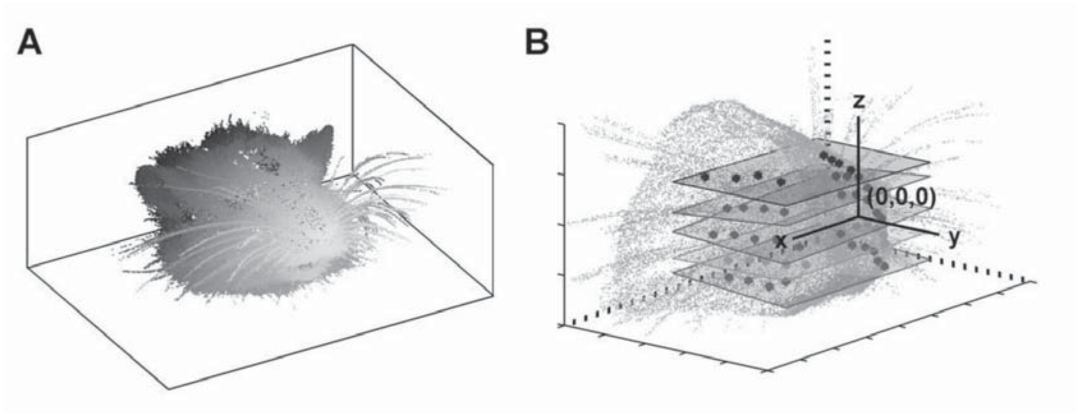

Figure 2.1: The 3D head reference frame of rat (a) Representative point cloud obtained from the 3D scanner. (b) Standard position and orientation for the head (Reprinted from Towal et al. (2011))

which could sense aperture width (Krupa et al., 2001).

2.2 Rat Whisker Morphology

The most recent study of morphology of rat vibrissal array was done by Towal et al. (2011). Neuroscience is needed in studying the relationship between the physical embodiment of the sensor array and the neural circuits underlying perception. In order to conduct such research, it is necessary for one to understand the morphology of the whisker array. Towal et al. was the first to attempt to quantify the array morphology in three dimensions. Towal et al. took 3-dimensional scans of 6 rats. 158 whiskers were scanned in a 3-D scanner while 196 whiskers were scanned in a 2-D scanner. The quantification of the rat whisker morphology was to make each whiskers shape into a function of 'row','column' and 'sideof the whisker. Assuming that the whiskers' bases were all on the surface of two independent mystacial pad, the parameters for the whisker and the mystacial pad were defined. The relationship between the length of the whisker and the row and column was first found. Also, through the 2-D scans, it was shown that the individual whiskers could be approximated as a quadratic function $w = ax^2$, where a is a parameter to be found. The mystacial pads could be approximated as an ellipse.

Based on the quantified equations, a MATLAB program has been made so that every whisker (approximately 60) could be simulated as the mystacial pad is assumed to

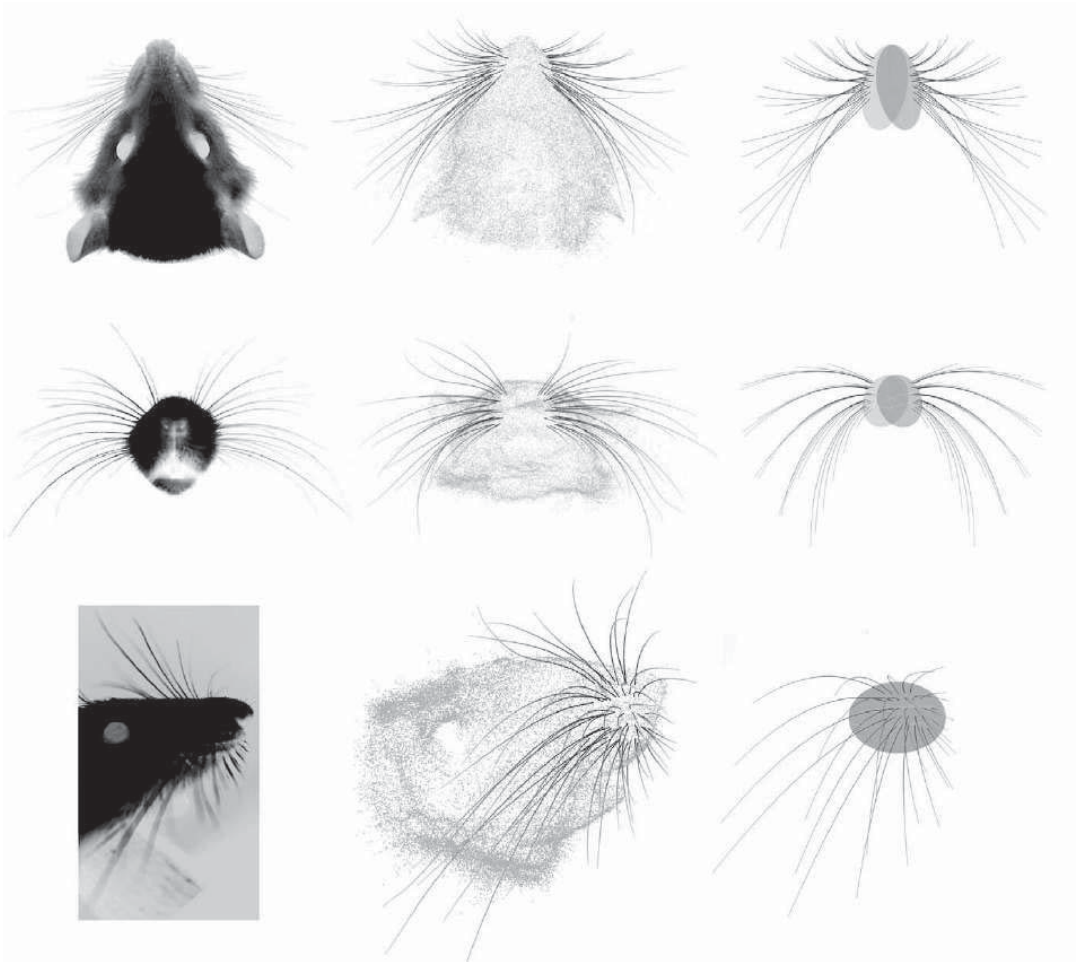

Figure 2.2: Comparison between photographs of the vibrissal array, 3D scans of the vibrissal array, and the model of the vibrissal array (Reprinted from Towal et al. (2011))

rotate. The final results of the whisker equations turned out to be a good match comparing them with the real whisker arrays. Using this model, the force or torque which is applied to every whisker base could be calculated when there is a contact with an object. Fixing the simulation parameters for the whisker array, it was also shown that the morphology directly affects the angle of contact of each signal. Therefore, the morphology of the whisker array could constrain the overall pattern of sensory inputTowal et al. (2011).

2.3 Whisker Structure

One of the most important characteristics of the rat whisker is that it is tapered. Of course, the rats are not the only types of animal which have tapered whiskers. Animals

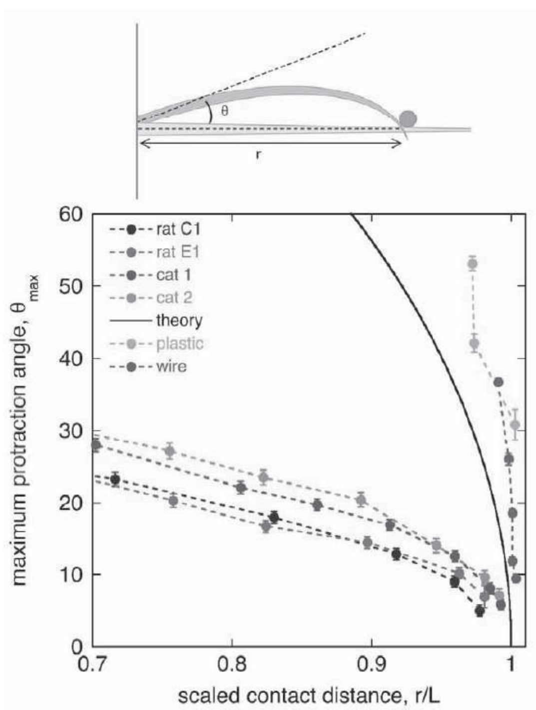

(a)

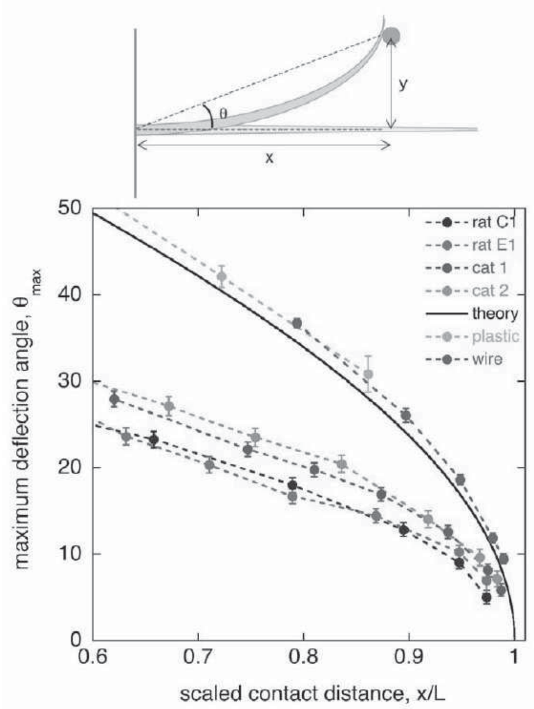

(b)

Figure 2.3: Maximal deflection and protraction angle (a) maximal whisker deflection (b) maximal whisker protraction ; both compared with tapered and cylinder type whiskers (Reprinted from Williams and Kramer (2010))

with tapered whiskers are found all around the world. When the term 'tapered' is used, it could be misunderstood as if the whisker at the end has zero radius. Even if a linearly tapered whisker did have zero radius at the end, it will be most likely to break. Hence, the end of the whisker will be thinner than the base, but it will not be zero. Williamns and Kramer (Williams and Kramer, 2010) have investigated 9 different types of animals and have summarized the taper ratio (R_B/R_T), whereR_B is the radius of the base, and R_T is the base of the tip. Three of the longest whiskers for each animal type was plucked. Some had low values of taper ratio, around 4 to 6, while some whiskers and high taper ratio values, around 20 to 24. The mouse and the rat had high ratio values both around 15, indicating the tip of the whisker to be 15 times smaller in radius compared to the base.

The maximal whisker deflection and maximal protraction angle were checked. Because the area moment of inertia is much smaller on the tip of the whisker compared to the base, it tends to flick. Hence, it would be easy for the rat to control the whisker position with the relatively rigid base, while the end will move very easily. This is the

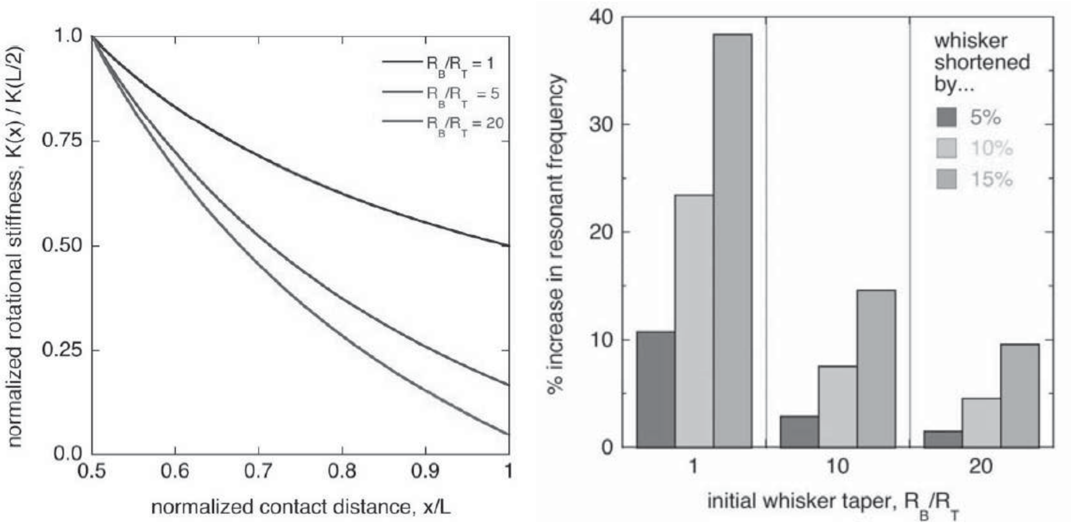

(a) (b)

Figure 2.4: Advantages of tapered whisker (a) Normalized rotational stiffness; the more it is tapered the more the rotational stiffness changes rapidly (b) Resonant frequency robustness; graph shows that the tapered whisker is more robust to whisker breakage. (Reprinted from Williams and Kramer (2010))

reason for flicking. Because of this characteristic, the maximum deflection angle of a tapered whisker is much smaller than that of the cylinder whisker. The maximum deflection angle or protraction angle does not rely on the Young's modulus but only on the structure of the whisker. .

Another advantage of the tapered whisker comes from the fact that the rotational compliance varies more severely compared to the cylinder type whisker(Williams and Kramer, 2010). Since the rotational compliance could be used to find the radial distance, it would be better for the rotational compliance to vary more along the radial distance. This would give a better estimation of radial distance, and it would be more robust to noise. .

In the perspective of resonant frequency robustness, the tapered whisker is again better than a cylinder shaped whisker. The resonant frequency is decided by several parameters. When a whisker is broken, the taper ratio and the whisker length changes and this affects the resonance frequency of this whisker. In figure 2.4, the increase of resonant frequency due to whisker shortening is shown. The whisker taper ratio was given 1, 10 and 20. The higher the taper ratio, the smaller the resonant frequency percent change. Compared to the case where the ratio is 1 (the cylinder type whisker), the whisker with ratio 20 only increased around 8 9% of resonant frequency, while almost 40% increased for the cylinder shaped whisker(Williams and Kramer, 2010).

The reason for inherent curvature of the rat's whisker could be a question. Much research has made analytical models based on the assumption that the whiskers are straight. However, this is not the case. Therefore studies on the effect of the inherent curvatures should be conducted. The whisker curvature or shape could be expressed as a quadratic equation. In Solomon and Hartmann (Solomon and Hartmann, 2006) supplementary information, using a numerical method which can accommodate the inherent curvature of a whisker, it was shown that the effect of the shape did not affect the radial distance estimation task. The test was done as the inherent curvature was assumed to be much more curved than that of a normal whisker.

Also, the numerical methods or linear models of the whisker is assumed to have constant Young's modulus across the whole whisker. However according to Quist et al. (Quist et al., 2011) showed that the average Youngs modulus across the segments was 3.34 ± 1.48GPa. The average modulus of a tip-segment was 3.96 ± 1.60GPa, and the average modulus of a base-segment was 2.90 ± 1.25GPa.Thus, on average, tip-segments had a higher Youngs modulus than base-segments. Such information could be accommodated into the numerical simulation model. The variation of the Young's modulus may have some effect on the radial distance estimation method. However, from Solomon and Hartmann (Solomon and Hartmann, 2006), the simulation and experimental results with a real whisker turned out to be very similar. In that perspective, perhaps the variation of the Youngs' modulus might not have significant effect.

2.4 Pinniped whiskers

2.4.1 Sensing ability of pinnipeds

The harbor seals have shown great sensibility in their whiskers. To test the ability of hydrodynamic stimuli tracking, a harbor seal was trained to follow a stimuli generated by a small submarine. First, the submarine was to move in the water to a random direction leaving a stimuli generated by the propeller. After a certain amount of time, the submarine was stopped. While the submarine's propeller was rotating, the seal eyes and ears were covered. Even though there were no auditory signals (since the propeller stopped to rotate) or visual signals (since the eyes were covered) available, only the hydrodynamic trails were available. The results showed that the seal could follow the hydrodynamic trails successfully. However since there is a possibility that the seals were sensing the trails by its skin, another type of experiment where the whiskers were sealed inside a mesh was conducted. The seal, for that case of experiment, could not find the submarine which reinforces the hypothesis that the seal's main sensory system to find their prey is their whiskers.

It was shown that the seals are able to hunt in dark and murky waters because they have a highly sensitive mystacial vibrissae (Hanke et al., 2011; Dehnhardt and Kaminski, 1995). Movements in the water generated by fish (hydrodynamic trials) or miniature submarines could be detected by the seals. Therefore, a seal could also track a trail generated by another harbor seal (a biogenic hydrodynamic trail). The structure of the trails generated from this experiment was measured using a particle image velocimetry (PIV) system. While one seal was trained to generate a trail by a predefined course, another seal was trained to search and follow the trail which was generated by the seal in front of it. The results showed that the trail-following seal could successfully follow the track of the trail-generating seal (Schulte-Pelkum et al., 2007). The trail-following seal could track a trail using either a linear tracking pattern or an undulating trail following pattern. From the results, it could be hypothesized that seals could 'relocate a lost trail or find a fleeing, zigzagging prey fish'.

In another experiment, it was tested how long after a harbor seal could sense a movement of an artificial fin. For this particular experiment, an artificial fin was made. After a single sweep of the artificial fin in still water and a certain amount of pause (5 50 seconds), the seal was able to sense the direction of the artificial fin sweeping direction within the experimental box. The longer the time is, the less accurate the choice will be. The results showed that the accuracy became under 70% as the delay time exceeded 35 seconds. The structure of the vortices generated from the artificial sweep were counter rotating which is the characteristics of the movement direction and could be sensed by the seal (Wieskotten et al., 2010a). Checking the hydrodynamic discrimination abilities have also been tested (Wieskotten et al., 2011). Pinnipeds are able to sense water movements (or hydrodynamic stimuli) using their whiskers. While pinnipeds can acquire visual information from their visual sensory systems (Hanke et al., 2009; Schusterman et al., 1972; Schusterman and Balliet, 2006; Hanke et al., 2011; Hanke and Dehnhardt, 2009), through experiments it was shown that harbor seals (*Phoca vit-*

ulina) and California sea lions (*Zalophus californianus*) are able follow hydrodynamic trails even when visual cues are absent by only using their whiskers (Dehnhardt et al., 2001; Gläser et al., 2011; Schulte-Pelkum et al., 2007). It was shown that the harbor seals and sea lions have extraordinary whiskers which could sense the hydrodynamic trails which were generated by the fish. The morphology of each of the species (which are significantly different) could answer the question of why the sensing ability differs for each species. While the harbor seal(*Phoca vitulina*) has an undulated profile which makes it look 'bumpy' when viewed closely, the California sea lions (*Zalophus californianus*) had a smooth profile. Both of the whiskers had ellipsoidal cross sections and both were tapered. However, the ellipsoid of the harbor seals whiskers is much more slender compared to those of the California sea lions.

2.4.2 Suppressing Vortex induced vibration due to whisker morphology

Because both of the species whiskers are sensitive enough to detect hydrodynamic trails, they can catch their prey such as fish by sensing the wakes generated by the prey. However, the whisker shapes differ significantly. While the harbor seals have an undulated shape with an ellipsoidal cross section along the shaft axis, the California sea lions whiskers have a smooth profile with an ellipsoidal cross section. The undulated structure of the harbor seal's whiskers are known to suppress vortex-induced vibrations, and was shown in (Hanke et al., 2010; Miersch et al., 2011; Hanke et al., 2012a). To understand the term vortex-induced vibration, one must first know what a vortex is. A vortex (plural: vortices) is any circular or rotary flow. Such a vortex can be generated when a bluff object such as a cylinder is exposed to a fluid flow. When a cylinder is exposed to a fluid flow, a von Karman vortex street will be generated. Such a vortex will make the bluff body to vibrate with a frequency determined by the Strouhal number, Reynolds number, fluid velocity and the characteristic length (diameter of the cylinder).

According to (Hanke et al., 2010, 2012a), the undulated structure of the harbor seal was to suppress the vortex induced vibration. Since the small pressure changes in the water which were made by the swimming fish must be sensed by the whiskers of the harbor seal, other signals should be suppressed. The vortex induced vibration is one of the major sources of whisker vibration which would corrupt the signal making the signal to noise ratio significantly lower. Through numerical simulations and experiments, it was shown that the Karman vortex street was not generated strongly behind the harbor seal whisker when it was compared to the circular and ellipsoidal cylinders. Since the vortex generation was suppressed, the vortex induced vibration (VIV) was also suppressed which made the SNR of the whisker higher than the other circular and ellipsoidal cylinders. However, the high SNR of the harbor seal whisker may explain why the harbor seals are so great at finding hydrodynamic trails, but it does not explain how California sea lions can forage swimming fish. Another experiment conducted by Miersch et al. (Miersch et al., 2011) was done by plucking 3 whiskers from a harbor seal and a California sea lion and submerging the isolated whisker into water to measure the VIV signal and Karman vortex street generated by a aluminum cylinder in front of the whisker sensor. The cylinder and whisker were both exposed to a linear flow (which was made by a rotating flume). The first purpose of the experiment was to check the SNR of the whiskers. The wanted signal was the Karman vortex street generated by the cylinder (this vortex shedding frequency can be pre known from the simple equation $St = \frac{f_d}{U} = 0.198(1 - \frac{19.7}{Re})$ where f_d, U, Re are the vortex shedding frequency, fluid velocity and Reynolds number ($Re = \frac{\rho U d}{\mu} = \frac{Ud}{\nu}$, where ρ, d, μ, ν is fluid density, characteristic length (cylinder width), viscosity, kinematic viscosity). The results of the experiment showed that the SNR of the whisker was much more higher for the harbor seals compared to the California sea lion whiskers (harbor seal whisker: 9dB, California sea lion whisker: -7dB). The morphology of the pinniped whiskers has been analyzed by Ginter et al., where various types of pinniped whiskers could be classified into two big groups with having either a bumpy or smooth profile. Since the bumpy profile has an undulatory characteristic, the characteristics measured by each whisker was 'total bumps', 'peak-to-peak distance', 'crest width' and 'trough width' as well as the 'overall length'. In (Ginter et al., 2010), three different species (harp, hooded, and grey seal) whiskers have been analyzed. The results showed the difference between the species. In (Ginter et al., 2012), eleven types of pinnipeds' whiskers have been analyzed. Two types of methods have been applied to see if the given features could classify the pinnipeds into several groups. One of the methods was the traditional method, and the second was the elliptic fourier analysis (geometric morphometrics) have been used to obtain such results.

For the biological understanding Dehnhardt et al. has answered the question if whether the temperature affects the sensitivity of the whiskers or not (Dehnhardt et al., 1998).

According to that paper, the whiskers sensitivity of the harbor seal may be affected by the water temperature just like the finger tip's sensitivity would drop in cold weather. The tactile discrimination task has been done in both winter and summer (where the water temperature was $1.2°C$ and $22°C$ for each season). The results showed that the tactile discriminating task had been done with identical abilities with the harbor seal. Using an infrared thermogram, it was shown that the temperature near the whisker follicles were higher than other regions. Mauck et al. claimed that each single vibrissal follicle may have a separate blood supply which makes the temperature near the follicles to be constant (Mauck et al., 2000). The Karman vortex street generated from the cylinder was to mimic the hydrodynamic trail made by a fish, though the vortex rotation direction was inverted. The experimental results were consisted with (Hanke et al., 2010), harbor seal whiskers VIV was significantly lower than that of the California sea lions whisker. The VIV amplitude for the California sea lion was approximately 10 times larger than the harbor seals case, hence the SNR was bigger for the harbor seals case. (Harbor seal 7dB, California sea lion 9dB in average) From the results, it was shown that the SNR was better for a harbor seal. However, a question arose since the California sea lion also was able follow hydrodynamic trails (Gläser et al., 2011) and yet the SNR for its whiskers were substantially lower than the harbor seals whiskers. In (Miersch et al., 2011), it was claimed that the California sea lion may use a different strategy. The VIV signal may not be just be mere noise but a carrier frequency. Such a mechanism may explain why the California sea lion is more affected by the hydrodynamic trail age (Gläser et al., 2011). Ginter et al. analyzed the morphology of the pinniped whiskers (Ginter et al., 2010, 2012). By measuring several characteristics such as overall length, total bumps, peak-to-peak distance, crest width and trough width of three different types of seals (harp, hooded and gray seal) vibrissae have been analyzed showing the difference between the species (Ginter et al., 2010).Not only the traditional method but also elliptic Fourier analysis (geometric morphometrics) have been used to analyze the morphology of various types of pinniped whiskers. Some whiskers had asmooth profile while others had a bumpy profile (Ginter et al., 2012).

According to simulations using computational fluid dynamics, the hypothesis that the undulated structure of the harbor seal whiskers are to suppress the vortex induced vibration (VIV). VIV is a well known phenomenon in fluid dynamics. When there is a fluid flowing towards a bluff body, in some conditions (such as high Reynolds number) the fluid flow will turn in to a Karman vortex street behind the bluff body. If the bluff body is constrained to not move, the vortex would obviously have no effect on the bluff body. However when the bluff body has a freedom in movement, it will move as the Karman vortex street will make the bluff body to vibrate. In the case for seal whiskers, the whisker shaft becomes the bluff body and an approximate linear fluid flow is generated when the seal swims. If the whisker shaft vibrates due to the Karman vortex street, hence even when there is no prey nearby, the whisker shaft would vibrate making it more difficult to capture the subtle movements of the fish which makes hydrodynamic stimuli (Hanke et al., 2010, 2012a,b). There has been many studies to understand and reduce the VIV (Assi et al., 2009; Govardhan and Ramesh, 2005; Hartlen and Currie, 1970; Gabbai and Benaroya, 2005; Jauvtis and Williamson, 2004; Blackburn et al., 2001; Vandiver, 1993; Yamamoto et al., 2004; Assi et al., 2009; Wu et al., 2012; Bearman and Branković, 2004; Gabbai and Benaroya, 2005; Matsumoto et al., 1992). According to the simulation results of (Hanke et al., 2010, 2012a), the general idealized undulated structure had the ability to suppress the vortex induced vibration. While cylindrical or ellipsoidal bluff body which had a uniform cross section was subject to a vortex induced vibration. On the other hand, the vortices did not formate in the way cylindrical and ellipsoidal bluff body did. Since the apparent vortex structure did not formate clearly, it was also shown that the force on the whisker was significantly lower. While the drag force or lift force on the other bluff bodies oscillated fervently, the forces on the whisker had a very small oscillation amplitude which indicates that the vibration would be much more smaller than the other bluff bodies. The obvious merit of the low VIV levels is that the signal to noise ratio (SNR) will become higher. Since the signal that the seal needs to sense is the hydrodynamic trails and the VIV signal would be regarded as noise. Reducing the VIV signal obviously increases the SNR.

It was mentioned before that the whisker shaft morphology of harbor seals and California sea lions were significantly different from each other. This difference would give a different SNR since the California sea lion's whisker shaft is ellipsoidal but not undulated. While the reduction of SNR in the harbor seal whiskers can explain the reason for its eccentric morphology, it does not still yet explain the result of how the California sea lions may forage for fish. The California sea lions turned out to be less sensitive to hydrodynamic trials (Gläser et al., 2011). By plucking three whiskers from each of the species (harbor seal and California sea lion) and then attaching it to a piezo sensor. The isolated whisker which was partially submerged into a water flow (made by a rotating flume with water inside), and the signals from the piezo sensor were recorded. The desirable result for an ideal whisker would have minimum vibration for this would mean the SNR would be very low. From the empirical results of the experiment, it was shown that the SNR for the harbor seal whisker was 9dB and -7dB for California sea lions(Miersch et al., 2011). The method for which was employed here was using a Karman vortex street generated by the cylinder submerged inside the flume. Assuming that the Strouhal number can be known which would be approximately around 0.2. From that, the vortex shedding frequency can be known by the simple equation $St = \frac{f_d}{U} = 0.198(1 - \frac{19.7}{Re})$ where f_d, U, Re are the vortex shedding frequency, fluid velocity and Reynolds number ($Re = \frac{\rho U d}{\mu} = \frac{Ud}{\nu}$, where ρ, d, μ, ν is fluid density, characteristic length (cylinder width), viscosity, kinematic viscosity). The high SNR for the harbor seal whisker can show why the harbor seals are better in tracking the hydrodynamic trails which are left by a miniature submarine (and the same will apply to the fish which they would forage). The morphology of the pinniped whiskers have been closely analyzed by Ginter et al. (Ginter et al., 2010), where the various types of the pinnipeds could be classified into two groups, where one has a bumpy profile and the others are classified into the smooth profile. The harbor seal whiskers are classified into the bumpy profile group and the California sea lion whiskers are classified in to the smooth profile group. The bumpy profile could be characteristics measured with the features 'total bumps', 'peak-to-peak distance', 'crest width' and 'trough width' as well as the 'overall length'. In (Ginter et al., 2012), eleven types of pinniped's whiskers in total have been analyzed. By using the traditional method which uses traditional characteristics or the elliptic Fourier analysis method which uses geometric morphometrics, the pinnipeds could be classified.

2.4.3 Strouhal Number in Hydrodynamic Trails

Strouhal number may have some importance in analyzing the hydrodynamic trails generated by fish. From the definition of (Triantafyllou and Triantafyllou, 1995), defined as the product of the frequency of tail flapping times the jet width divided by the fish's speed. Most of the fish swim which the Strouhal number becomes within 0.25 and 0.35. It is known to maximize the efficiency of a swimming fish or fish robot.

2.4.4 Other characteristics

There are studies that the tactile sensitivity of skin may decrease when it is cooled below normal temperature. The same logic may apply to the harbor seals since it is subject to both warm and cold water depending on the season, and the cold water could increase the tissue stiffness which would decrease the mobility of the whisker. Texture discriminating tasks have been withhold in winter and summer (water temperature $1.2°C$ and $22°C$) and the results showed that the water temperature did not affect the overall performance. The infrared thermogram which was taken in the winter showed that the regions where the majority of the vibrissal follicles were present, the temperature exceeded $18°C$. Since the surface temperature is over $18°C$, it is assumed that inside the follicle the temperature would be much more higher. Therefore, it was concluded that the energy loss from the high temperature region is a price to pay for the vibrissal sensing system to work properly (Dehnhardt et al., 1998). Mauck et al. showed that single vibrissal follicles might have separate blood supply (Mauck et al., 2000).

2.4.5 Hydrodynamic stimuli

The trails generated by fish has been study groups (Tytell and Lauder, 2008; Drucker and Lauder, 1999; Müller et al., 1997; Hanke et al., 2000; Hanke and Bleckmann, 2004)

In order to understand how the pinnipeds sense the hydrodynamic trails, it is also essential to understand the structures. From the work of Blickhan et al. (Blickhan et al., 1992), the structure of the generation of a vortex chain which comes from a subundulatory swimming fish was shown. Starting from the fact that a swimming fish needs to have bigger thrust force compared to the drag force it will experience, it estimates the thrust and efficiency based on the flow of the wake which is generated by a swimming rainbow trout (*Oncorhynchus mykiss Waldbaum*). In order to do such kind of calculation, the three-dimensional vortex pattern was required to be reconstructed. Since there were data gaps which needed to be filled, modern techniques were applied to fill them. From the reconstructed data, the chain of the vortex rings which were generated turned out to be 'slightly deformed'. This vortex street was generated by the pumping action of the undulating body movement. When the upper body bends, it

’sucks in’ the water in the lateral direction. As the fish undulates and when the water flow is shed from the end of the tail, the vortex is generated. This makes the pattern of the fluid flow to have periodic wakes. This kind of periodic vortices are the main source which predators sense to catch their prey. Thus, the thrust coefficient and the propulsive energy can be estimated.

Müller et al. had did a detailed analysis on the flow pattern made by a swimming mullet which is 12.6cm in length. The structure of the wake was analyzed by using a two-dimensional particle image velocimetry. By analyzing the flow pattern and the kinematics of the fish, the relative contributions of the fish’s body and the tail has been estimated. It was shown that the active propulsion make an alternating vortices which had a jet flow between the vortices. From this paper, the divergence, vorticity, and vortex circulation of the data allowed to estimate the costs of swimming under several assumptions. In order to capture a sequence of the fish to move within a layer (where the PIV measurements are taken), the water level of the tank was reduced to 10 cm (to increase the chance of the fish to move through the layer of laser) and the test lasted for 2 hours. The fish was not trained in any way. The vortices generated by the fish were similar in the structure of a Rankine vortex ring, which was compared to the empirical data. Parameters of the structure of the vortices were defined and quantified. Also the energy of the vortex ring momentum has been calculated. Apart from the data which may be hard to interpret, the overall concept of the kinematics and hydrodynamics was also given. The suction zone and the pressure zone with a moving fish has been drawn for conceptual understanding. Here, the middle lines of the fish while swimming have been captured to show the kinematics of the swimming fish.(Müller et al., 1997; Hanke et al., 2000).

Hanke et al. has analyzed the wakes which has been caused by swimming goldfish (*Carassius auratus*)(10cm and 6cm fish) and the aging effect of each of the fish. It was shown through the particle image velocimetry system that for a wake could be seen clearly for at least 30 seconds for the 10cm fish and 20 seconds for the 6cm fish. This paper also concludes that this kind of hydrodynamic trail can be the cue for the predators to catch the swimming fish even if they are few minutes away because the wakes generated by the fish did not quickly dissipate but lingered for a long time. It was assumed that the lateral-line might be able to measure the simultaneous velocity and estimate the vorticity of the fish generated wake. Also from the gradient of the wake, the swimming direction could be estimated (Hanke et al., 2000).

For the fish swimming thrust efficiency, the dimensionless Strouhal number is known to be important. According do Rohr et al., most of the fish (out of 248 measurements) have their Strouhal number between 0.2 and 0.4 (Rohr and Fish, 2004). The Strouhal number for fish was defined as $St = fD/U$, where f, D and U are frequency of tail flapping, peak to peak of tail (jet's width) and fish's speed. In (Triantafyllou and Triantafyllou, 1995), it was claimed that the optimal range of Strouhal number was 2.5 3.5 and many fish swim within this range. Flapping the fin to match the Strouhal number to be within 2.5 3.5, the efficiency has been optimized showing that the number is important.

From (Drucker and Lauder, 1999), the three-dimensional vortex wake dynamics have been quantified using digital PIV (DPIV). The swimming movement of the fish of a bluegill sunfish (*Lepomis macrochirus*). The three dimensional vortex ring velocity profiles were very close to the theoretically predicted profiles. Hanke and Bleckmann measured the hydrodynamic trails made by *Lepomis gibbosus*, *Colomesus psittacus* and *Thysochromis ansorgii* which turned out to make a trail which lasted 5 minutes, 30 seconds and 3 minutes respectively.

2.5 Active Whisking

It was mentioned that 'active whisking' is one of the unique characteristics of rat whiskers(Towal and Hartmann, 2010; Towal et al., 2011). The rat whisker system could be a good model for a biorobot for active sensing. The behavior of two rats in free exploratory behavior and during a texture discrimination task was examined by Hartmann (Hartmann, 2001). While the macro whiskers were well studied, which are the big whiskers which can move actively around 5 to 12 Hz (Carvell and Simons, 1990), the small whiskers near the rat's lip surface cannot be actively moved. While most of the studies done on rat whiskers are on macrovibrissae, the micro and macrovibrissae was assumed to be closely correlated. To see how the micro and macrovibrissae are used in free exploratory behavior and during a texture discrimination task was done, a simple experiment was done by Hartmann (Hartmann, 2001). A rat was put in cage where a metal bar is placed at the end of the cage. There are two types of metal bars, one having a rough surface on the left and a smooth surface on the right. The other metal bar had the opposite characteristics. Such metal bars were placed in the cage randomly. The rat is trained to go to the side where the rough part of the bar is. When

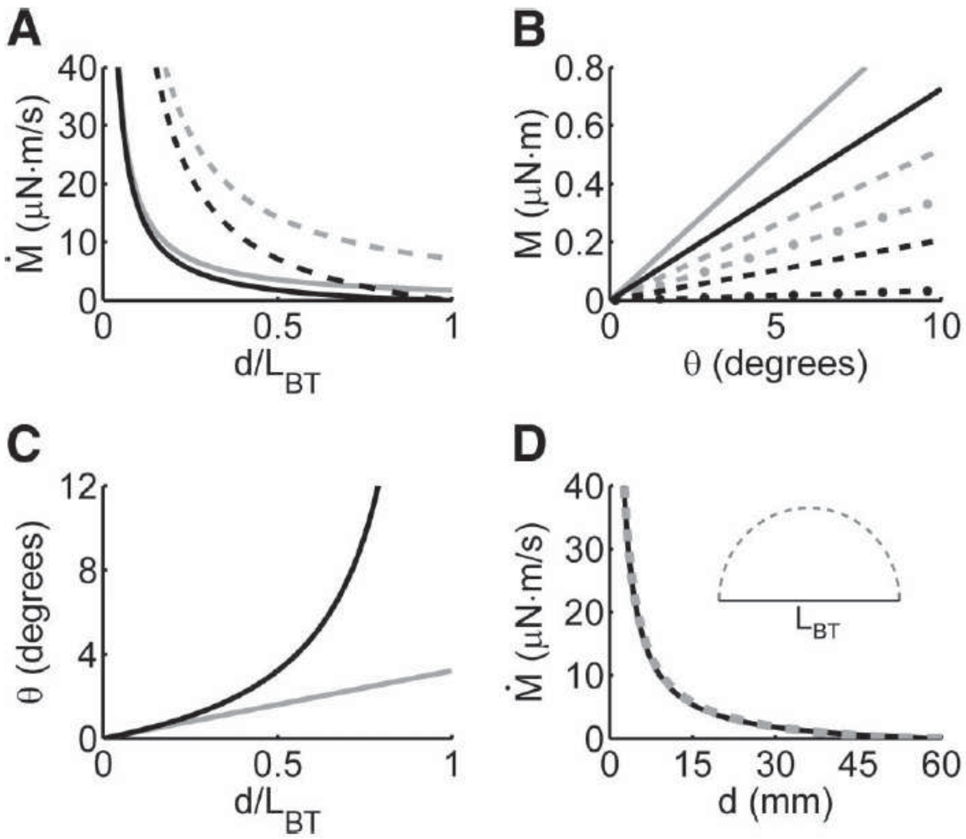

Figure 2.5: Simulation comparison with a tapered whisker (a) rate of change of moment vs. normalized radial distance for conical and cylindrical whiskers rotating at different velocities. Black curves represent relationship for a tapered whisker, whereas the gray curves are for a cylindrical whisker. Solid lines: velocity = 1 rad/s; Dashed lines: velocity = 4 rad/s. (b) moment as a function of whisker angle since contact with the object. It shows a linear relationship for moment and angle (c) whisker deflection as a function of normalized radial distance with an imposed moment (d) inherent whisker curvature has a negligible effect on rate of change of moment M. (Reprinted from Birdwell et al. (2007))

it does, it is rewarded with a drop of sugar water. There were two types of rats which participated in this experiment, and both of the rats showed different strategies for tactile discrimination. It turned out when the rat uses both the micro and macrovibrissae touching both sides of the metal bar, the tactile discrimination accuracy is high.

Passive sensing and Active sensing of an artificial whisker was compared by Kim(Kim and Möller, 2006). Passive sensing and active sensing were compared in the task of distance estimation. There are many animals which use whiskers, but dont use active

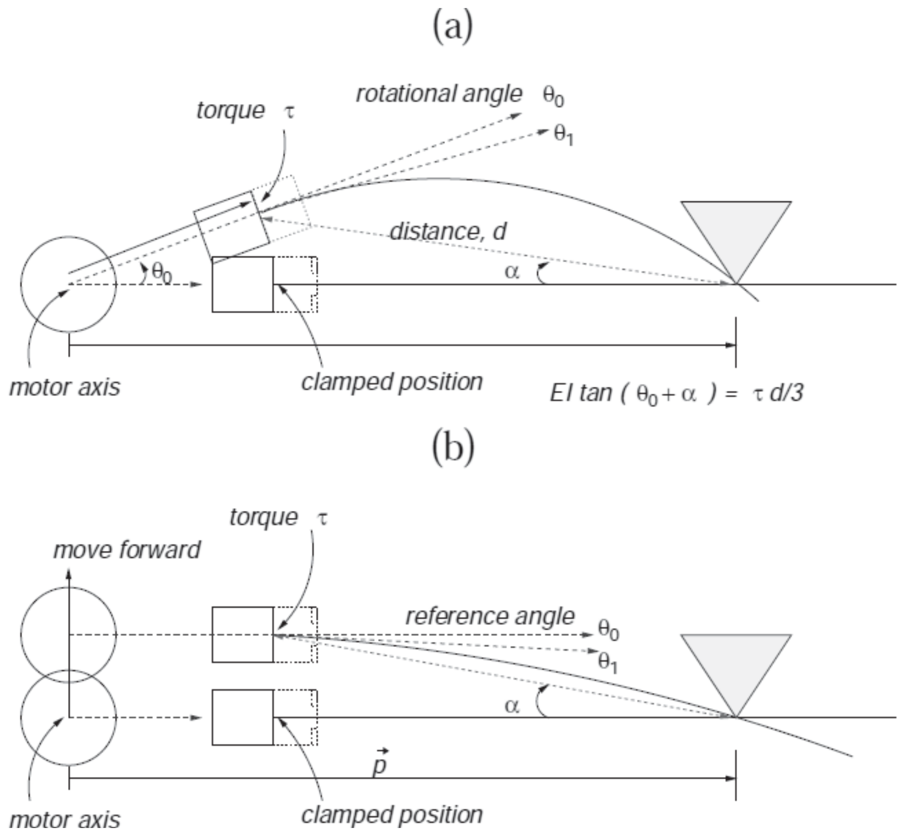

Figure 2.6: The concept of passive and active sensing (a) active sensing (b) passive sensing (Reprinted from Kim and Möller (2006))

sensing. Since the rats use active sensing, and one of their main tasks is to estimate the radial distance, this paper had compared the passive sensing and active sensing in the radial distance estimation point of view.

Active sensing is moving its whisker back and forth in order to explore the environment, while passive sensing is non moving whisker but feeling the forces from other external contacts. Through calculation, the final equation used in Kim and Möller (2006) is $tan\theta_1 = (\frac{3h^2}{2d^2} - \frac{3h}{d} + 1) \cdot tan\theta_0$. (explanation of the teriminology can be found in the Kim and Möller (2006)). Magnetic hall effect sensors were used for the deflection angle measurement.

2.6 Contact Distance Estimation

Estimating the radial distance with a whisker sensor is one of the most important functions. Estimating the distance could be done using several different strategies.

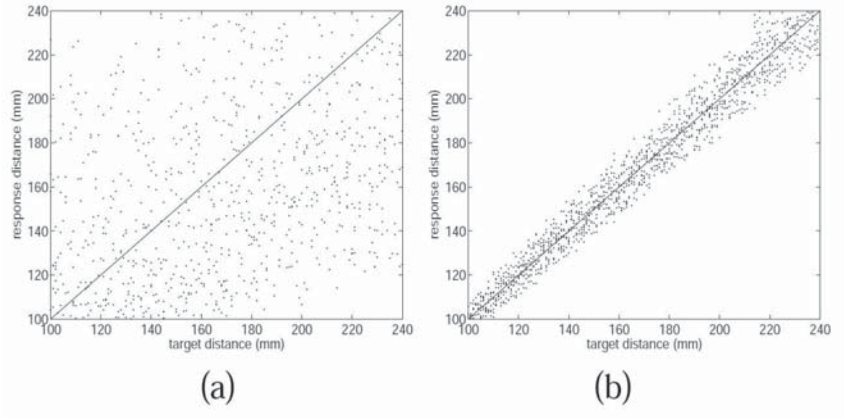

Figure 2.7: Contact estimation for passive case with noise (a) 0.1degree noise (b) 0.01 degree noise (Reprinted from Kim and Möller (2006))

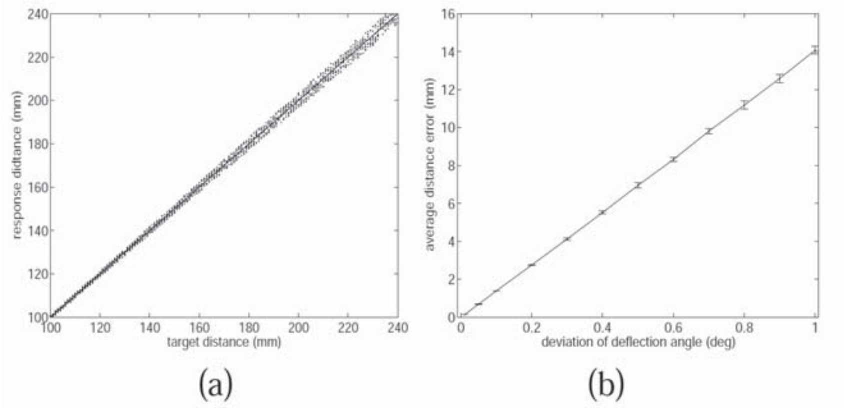

Figure 2.8: Contact estimation for active case with noise (a) 0.1degree noise (b) average distance estimation error base on the deviation of deflection angle where the protraction angle was 25 degrees.(Reprinted from Kim and Möller (2006))

2.6.1 Linear Models

If one is to extract a surface shape or a complex feature, it is necessary to estimate multiple contact points along the object surface. There are several linear models which models the whisker as a cylindrical or tapered straight beam under the small angle approximation assumption. While some models assume passive sensing, some assume active sensing.

The most basic linear model for radial distance estimation would be the case where the whisker has a constant radius from base to tip (cylinder whisker), and a motor is rotating the whisker at the base. Hence a cylinder whisker under active sensing. Since the cylindrical whisker will act as a torsional spring, under the small angle approximation, the radial distance can be estimated by $d = C\frac{\theta}{M}$ where $C = EI$. If a rat could measure the moment at the base of its whisker, and know the angle of protraction of its whisker, the rat could know the distance of the object. For a robot with an artificial whisker which has a torque sensor at the base, and an encoder at the motor, the required information for radial distance estimation would be given. In summary, it only requires one torque sensor and an encoder on the motor. However, this equation will estimate the radial distance accurately when the protraction is small (but not too small, since the moment sensor value should be big enough to be distinguished from noise). Also, that equation does not account for lateral slip. Finally, several methods of the linear/nonlinear modeling of whiskers and the engineering applications of artificial whiskers will be introduced.

Instead of actively moving the whisker in order to eliminate the lateral slip problem, the radial distance could be estimated using $d = C\frac{\theta}{|M|} \cdot cos\beta$ where $|M| = \sqrt{M_x^2 + M_y^2}$ and $\beta = tan^{-1}(M_y/M_x)$. The β is the slope of the surface. This is an equation which assumes that the plane has zero friction. As it can be known from the equation, this requires a two axis moment sensor instead of a one axis sensor. This will improve the radial distance estimation accuracy.

$$ \tag{2.1} $$

The linear models explained above use torque sensor(s) and an encoder. Kim and Mollor have proposed a method for radial distance estimation which does not require a torque sensor, but measures a deflection angle on a point of the whisker a little apart from the base. Assuming that a whisker is rotating actively, the contact point could be considered as a pin joint in the inertial frame of view.

In the paper of Kim and Moller, the artificial cylinder whisker was 45mm in length, and the hall-effect magnetic sensors were placed 14mm away from the base which measures the deflection angle. The models introduced above are based on cylinder shaped whiskers (constant radius throughout the whisker). While the cylinder shaped whiskers are easier to make, the tapered artificial whiskers are closer to the real rat whisker. Analytical equations for tapered whiskers were also derived Kaneko et al. (1998); Solomon and Hartmann (2006), simply by changing the area moment of inertia term. The cylinder shaped whisker obviously has a constant area moment of inertia while the tapered whiskers are moment of inertial could be expressed as $I = I_{base}(1 - \frac{x}{L})^4$ where $I_{base} = \pi/4 \cdot r_{base}^4$ and r_{base} is the radius of the whisker's base.

2.6.2 Nonlinear Models

While linear models are analytical equations which can give quick estimations of the radial distance, the results are subject to error since it is based on the small angle approximation. Nonlinear models can be considered to be the almost exact representation of the system.

Rahn has shown that solving nonlinear equations using sensor values, the whisker shape could be reconstructed even when the deflection angle is large. By checking where the reconstructed whisker shapes coincide, the contact points of the objects could be estimated. Solomon and Hartmann have used a numerical method for exact solutions. The method is to consider the beam as an assembly of numerous elements. The Euler equation, and calculating the curvature (κ_i) for each element, the whisker shape could be reconstructed. Knowing the curvature for each element, the deflection angle for each element could be known as well. This is represented as $d\kappa_i = \frac{\bar{r_i} \times \bar{F}}{EI_i}$.

Sufficient iterations are done until the result converges. The method is simple to implement and gives accurate results. The simulations done by Solomon, force of on the whisker was assumed to perpendicular to the whisker. In other words, the simulations assumed zero friction. However, the method can also simulate with forces applied to the whisker in a slanted manner. And because the I_i is the second moment of inertia for the i^{th} node, tapered whiskers could be simulated as well. The model is flexible for such parameters, and it could be used for verification of a derived model.

2.6.3 Other Strategies

One of the simplest strategies is to use the information of the length of all whiskers. Knowing each length of whiskers, there may be some whiskers which are in contact with an object and several which are not. Suppose that a long whisker was in contact with an object while a short one was not. Then one could assume that the object's distance is in between the length of the two whiskers. But this method is based on a strong assumption that if the radial distance is shorter than the whisker, that whisker would be in contact with the object. However, this may not always be true. There could

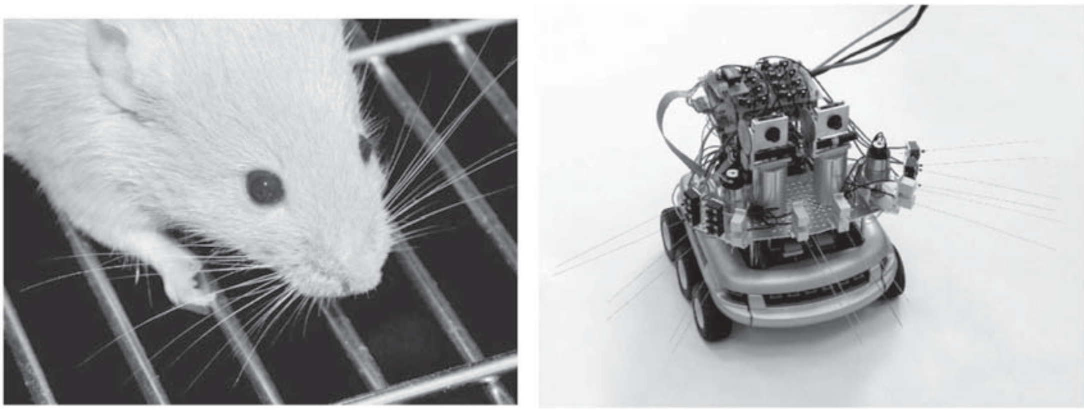

(a) (b)

Figure 2.9: Rat and a Koala robot with whisker arrays (a) a picture of a mouse with whiskers (photo: Wolfram Schenck) (b) artificial whisker arrays on a Koala robot (Reprinted from Kim and Möller (2007))

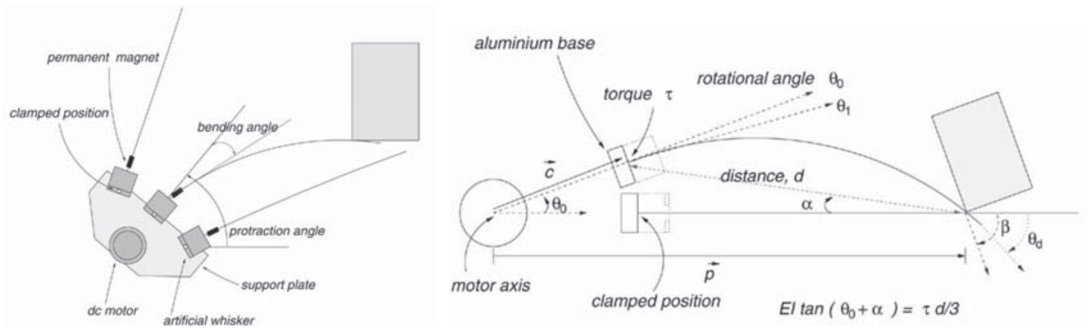

(a) (b)

Figure 2.10: Whisking system of Kim and Moller (a) robot with artificial whiskers rotated by a dc motor (b) the notations used for the system (Reprinted from Kim and Möller (2007))

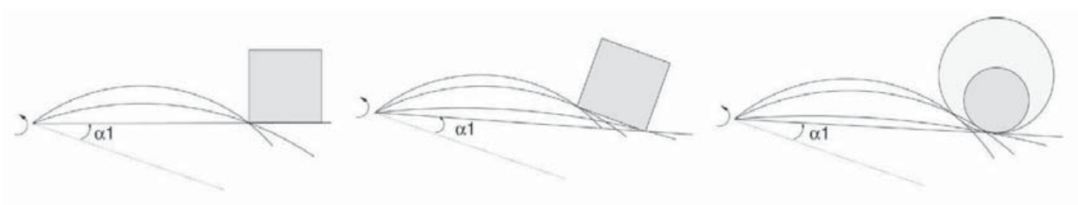

Figure 2.11: Artificial whisker in contact with various types of objects; this situation of active whisking lets this system to be modeled into a clamped-pinned-free condition beam. The contact point serves as the pin joint. (Reprinted from Kim and Möller (2007))

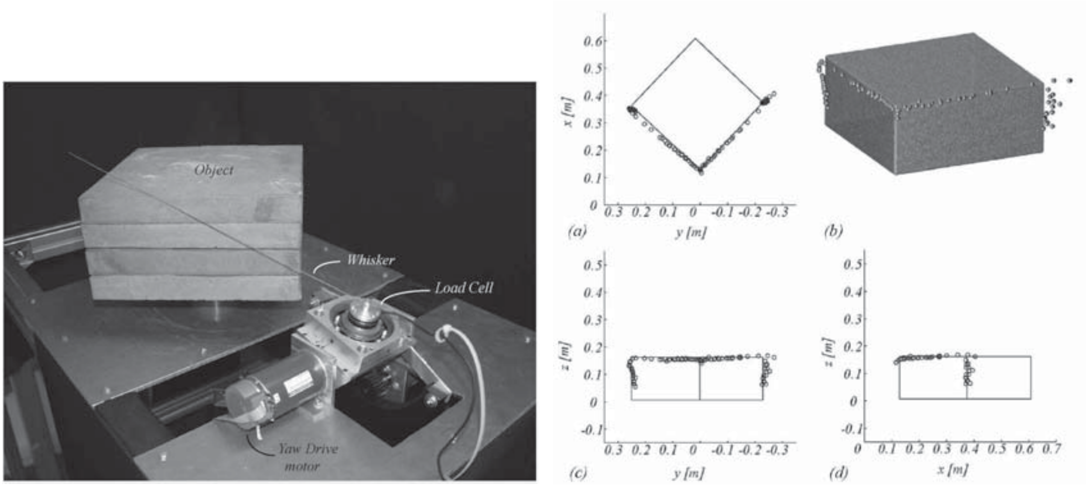

(a) (b)

Figure 2.12: Nonlinear 3D model for whisker shape reconstruction (a) Experimental setup of Rahn (b) The final results of extracting multiple contact points of a given object. (Reprinted from Clements and Rahn (2006))

be many situations where a shorter whisker would be in contact where the longer one is not. Therefore, this method could not be sufficient.

Another method is 'vibrissa length' method. (Solomon and Hartmann, 2011) This is another simple method which assumes that the length of the whiskers are known. Under the assumption that the object contact is done on the tip of the whisker, one could assume that if one of the whisker is in contact, the radial distance is equal (or a little less) to the length of the whisker. However, as Hartmann has explained, the whisker tips could be damaged. Since the whiskers are not straight cylinder types, but have tapered shape, the tip of the whisker could be easily broken. An easily broken whisker means that it is hard to know the length of the whisker. Also, according to Krupa et al., the rats can estimate the radial distance without touching the object through the vibrissa tip.

According to Williams (Williams and Kramer, 2010), the tapered whisker was shown to be robust to tip breaks in the perspective of resonance frequency, so the resonance frequency when contact with an object could provide information of the radial distance. It was also shown by [check advantages of tapered whiskers] that the rats react to certain frequencies of the whisker. Since, the resonance frequency will be decided by the length and shape and other parameters of the whisker itself, the frequency a whisker might have after contact would be the same. Hence, the whisker frequency

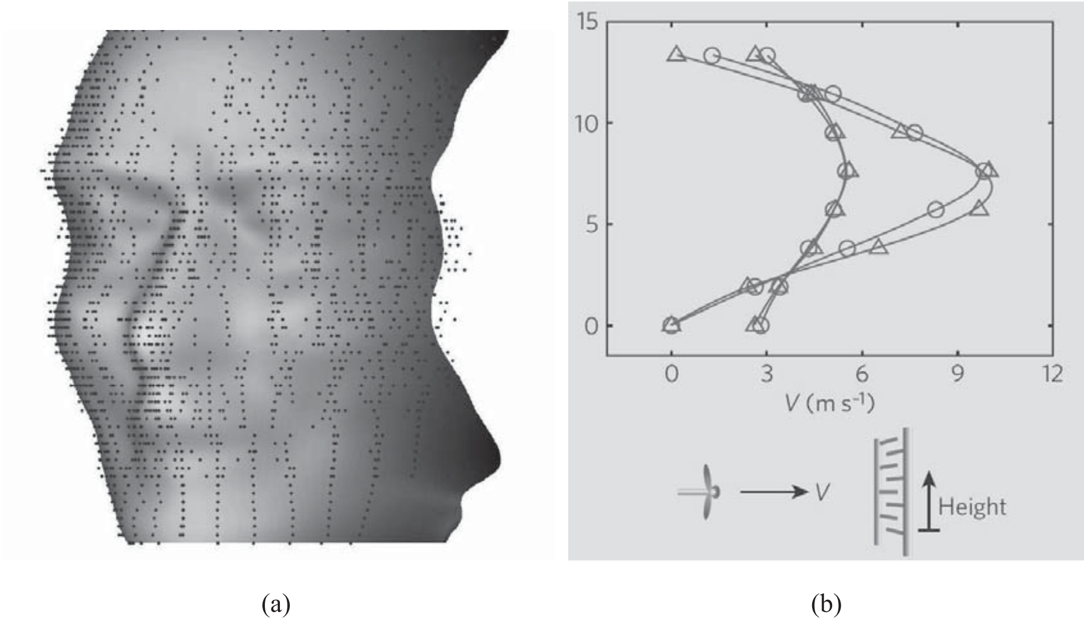

Figure 2.13: Whisker array in engineering application (a) Face feature extraction with multiple contact points (b) Fluid flow velocity estimation with whisker array. (Reprinted from Solomon and Hartmann (2006))

will be independent to the radial distance. However, since the amplitude of the whisker vibration might change dependent to the radial distance, this might be a cue to the radial distance. However, 'all preliminary results suggest that there is no simple unique spectral signature associated with a particular radial distance and that it would be difficult for the rat to extract radial distance from such a complicated spectral profile'. (Solomon and Hartmann, 2011)

Solomon and Hartmann have proposed two unique types of radial distance estimation methods. One of them is called 'balance of moments method'. The method is based on the idea that the rat could protract a whisker with only a certain amount of torque. This method is 'based on how radial distance relates to how much the vibrissa rotates beyond initial impact'. If the moment exerted by the muscle and the moment due to the deflection of vibrissa is balanced, the rat could estimate the radial distance. However, if the whisker 'flicks' through the object, or the moment balance was not achieved due to the limited range of whisking motion, the radial distance could not be estimated.

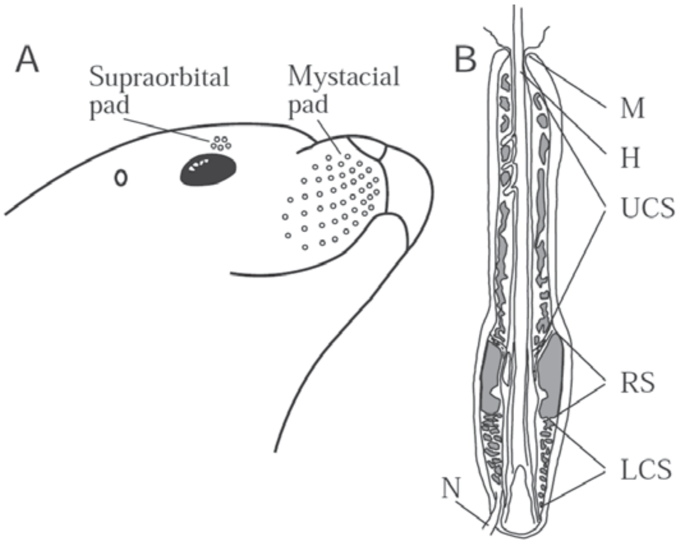

Figure 2.14: A detailed discription of pinniped whiskers.(Reprinted from Dehnhardt et al. (1998))

.

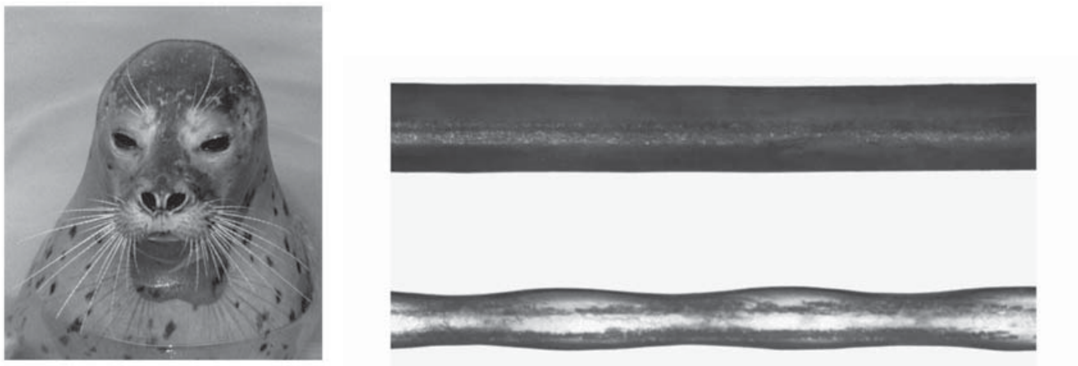

(a) (b)

Figure 2.15: Pinniped whiskers. (a) A typical pinniped (b) The surface pattern of vibrissal hair shafts of a California sea lion (top) and a harbour seal (lower) (Reprinted from Dehnhardt and Kaminski (1995))

2.7 Rat whiskers: Application issues

2.7.1 Contact distance estimation

Schultz et al. has proposed various types of applications which may be appropriate for a hovering robot in Mars, such as rover speed estimation, wheel slip detection, surface roughness measurement and etc (Schultz et al., 2005). Kaneko et al. have

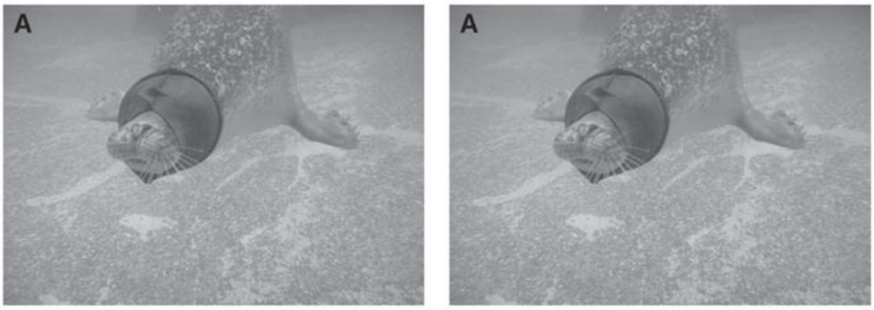

(a) (b)

Figure 2.16: A pinniped (harbour seal) tracking a hydrodynamic trail (Reprinted from Schulte-Pelkum et al. (2007))

mimicked the antenna of insects (which could also be a mimic of rat's whiskers) and made mathematical models (Kaneko, 1994; Ueno and Kaneko, 1994; Kaneko et al., 1996, 1998).

One of the most popular applications of the whisker sensor is radial distance estimation (or radial distance estimation), which is estimating the euclidean distance between the base of the whisker to the contact point (whisker - object contact). Birdwell et al. derived analytical equations of tapered whisker deflection and radial distance estimation method using moment and angular velocity of the whisker(Birdwell et al., 2007).

Contact point location estimation is relatively simple when the contact object has very high curvature (close to a point). However, objects which are not just a point could occur longitudinal slip or lateral slip. Solomon and Hartmann proposed a method to estimate contact point location, even in situations where lateral slip exists when a good estimation of the friction coefficient could be made (Solomon and Hartmann, 2008). They also have made an algorithm which could account for longitudinal slip by constantly updating the contact positions using torque information (Solomon and Hartmann, 2010).

Novel methods for estimating the radial distance was also made using the tapered whisker (Solomon and Hartmann, 2011). While many methods for contact point estimation are based on linearized models, methods that use the exact nonlinear equations exist. Using torque and force measurements, the exact shape of the whisker could be reconstructed. One study was implemented for 2-D (Scholz and Rahn, 2004), while another was for 3-D implementation (Clements and Rahn, 2006).

Instead of using torque or force measurements, by measuring a deflection angle at a point of the whisker sensor, the radial distance could be estimated even without knowing the rotational stiffness of the whisker (Kim and Möller, 2007, 2006). This paper's work is an extension of such work.

2.7.2 Texture discrimination

The rats are known for their ability to discriminate different types of textures(Arabzadeh et al., 2003, 2005; Von Heimendahl et al., 2007). In the attempt to mimic the ability of the rat's texture discrimination, Fend et al. used a whisker sensor attached to a mobile robot in order to perform texture discrimination(Fend, 2005). Kim and Moeller also performed a texture discrimination task using a biomimetic whisker sensor (Kim and Moeller, 2004). Lepora et al. put a whisker sensor on a Roomba robot and sweeped the floor surface and classified different types of surfaces using the whisker deflection measurement. The classification was based on Naive Bayes algorithm (Lepora et al., 2010, 2011).

2.8 Pinniped whisker: Application issues

Whisker sensors were also used in other applications, such as fluid flow measurements. Solomon and Hartmann have proposed that a wide and thin whisker array could accurately measure a stationary air flow (Solomon and Hartmann, 2006). Rooney et al. have implemented an active whisker on an underwater robot in order to guide the robot (Rooney et al., 2011).

Stocking et al. has designed a capacitance-based whisker-like artificial sensor inspired from the fact that harbor seals have extraordinary whiskers which can detect water movements. If one could develop a sensor which can navigate within a fluid environment without any other cues, such sensors could be applied for commercial, military and scientific purposes. This capacitance based whisker which looks like a cone has an underlying structure. The basic idea is that if the rigid whisker-like shaft is moved or tilted by drag force due to fluid movements, the capacitance values changes as the gap between the capacitor plates vary. In this paper, numerical simulations and actual experiments have been done in order to verify the feasibility of this sensor. The drag force was calculated with the equation $F_d = \frac{1}{2}\rho v^2 A C_d$ where is the fluid density, is fluid velocity, is the exposed whisker area, is the coefficient of drag. The drag force was assumed to act on the tip of the whisker shaft for simplification, and this configuration was used for numerical simulation using a commercial software, ANSYS. The capacitance due to the change in gap can be written like equation $C = \varepsilon\kappa\frac{A}{d}$.

Through the numerical simulation, the gap size for each quadrant of capacitor plates could be estimated, and show that the fluid speed can be measured by the capacitance variation. For empirical data, steady force and oscillating force were applied to see if the sensor responds well to the deflections. In order to see if it can actually estimate the fluid flow, the whisker like sensor was submerged in fluid flow. The results showed that the change of capacitance increased as the flow speed increased (not a linear relationship). Though the whisker-like sensor did not resemble much of the real whiskers, it showed that it could estimate the fluid flow speed based on its drag force. This sensor can also estimate the direction of the fluid flow (Stocking et al., 2010; Eberhardt et al., 2011). Yu et al. developed a bio-inspired flow sensor which can measure turbulent flow while not disturbing the original flow. In order to minimize the fluid flow disturbance, the sensors were in micro or nano scales. The sensor is consisted with micro-pillars or nano-pillars, where the sensor element is based on piezoelectric fiber (Yu et al., 2010; Chagnaud et al., 2008).

Another example of fluid flow sensing artificial whisker-like sensors have been presented in (Solomon and Hartmann, 2006). In this paper, the artificial whiskers were not actually similar to the real whiskers of animals in shape. The artificial whiskers looked like a slender beam which was 0.5 cm wide and 11 cm long. 8 of these sensors were used. Two 4×1 array of these whisker sensors were placed on the opposite direction. A constant air flow was given to see if the whisker array could extract the velocity profile of the air flow. The results showed that the whisker array could extract the velocity profile very accurately. However, because the whiskers were made of highly flexible plastic strips, it may not be used for fluids such as water. Also, because the whisker sensor used in this paper is wide and thin, it would only bend in one direction. Such kind of structure would only be able to measure a flow in one direction. If the purpose of the artificial whisker is to sense the vortex structures like harbor seals, a wide and thin structure would not be adequate.

Recent applications using artificial whisker-like sensors include Valdivia et al. (2012), Hans et al. (2012), Beem et al. (2012) and Beem et al. (2013). Valdivia et al. (2012)

and Hans et al. (2012) designed an artificial seal whisker-like sensor in order to evaluate the sensitivity for underwater wake detection. Both evaluate the sensitivity by sensing von Karman wakes. It was concluded that the seal whisker-like sensor was suitable for underwater detection by observing the fact that the whisker shafts vibration frequency was close to the von Karman street frequency. The whisker morphology closely resembled the harbor seal's undulated shape.

Valdivia et al. (2012), the whisker was modeled while considering the follicle sinus complex (FSC) as a part of it. The model was modeled with a torsional spring, torsional damper, linear spring and a linear damper, and describes the angular oscillations of the whisker shaft when external force is present. They claim that by changing the linear spring and damper parameters, a desired (or required) sensor natural frequency can be determined. However, this model does not put the damping effect of water into account. The sensor's natural frequency determined by the model may be true when the whisker is exposed in air but not in water.

Beem et al. (2012) and Beem et al. (2013) also designed an artificial whisker sensor. The whisker model had similar morphology with the actual harbor seal whisker and was scaled up 30 times. By using 4 bending sensors, the drag direction and vibration amplitudes in two axis could be determined. Experimental results were shown in detail in Beem et al. (2013) which shows that when the flow direction is parallel to the whisker direction (angle of attack being 0 degrees), VIV was minimized. When the angle of attack increased, the VIV amplitude increased dramatically. Such whisker sensor showed that it could sense von Karman street with high accuracy.

2.9 Summary of Chapter 2

In this chapter, the ability of animals (rats and pinnipeds) which use whisker sensors as their primary sensory system and the biomimetic application issues have been presented. First, the rat whiskers ability to discriminate textures and object locations were explained. Also, several models which modeled the whisker sweeping motion or the mechanical characteristics were shown.

For the pinnipeds, it was shown that by using only their extremely sensitive whisker sensory systems, they could follow trails after a fish or mini submarine has moved in water. One of the reasons for this extraordinary sensibility comes from the morphology

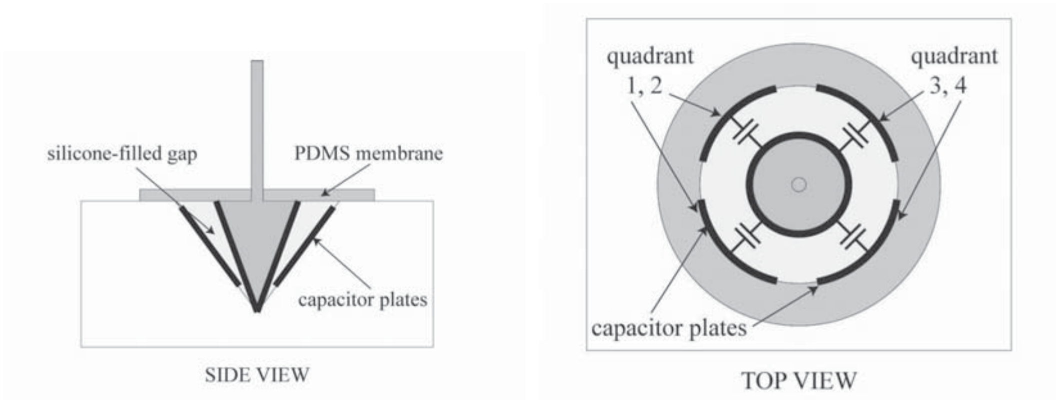

(a) (b)

Figure 2.17: The capacitance based whisker sensor. It is not very sensitve to the fluctuations, but can sense the direction of a flow and its intensity. (Reprinted from Stocking et al. (2010))

of the whisker shafts. Harbor seals have an undulary (or bumpy) profile which is known to suppress the vortex induced vibration (VIV), so that it could sense the actual hydrodynamic stimuli or trails which increases the SNR. On the other hand, California sea lions have a smooth profile. Both pinniped whisker shafts have oval cross sections, but the harbor seal's whiskers had higher SNR compared to California sea lions.

Another proof that the pinnipeds' are highly relying on their whiskers is that the temperature near their whiskers are constant despite the weather by possibly pumping blood to their mystacial whisker. Since the structure of the hydrodynamic trails are important, detailed studies on the trails generated by fish has been summarized.

Finally, the applications of rat whiskers were summarized. The first and main application of biomimetic rat whisker sensors was 'radial distance estimation'. There were various types of sensors used in order do such task. For hydrodynamic stimuli sensing applications, there was a capacitance based whisker sensor and an array of small sensors which could measure the water flow without disturbing it.

Inspired from the existing work and also from the lack of it, the following works concentrate on biomimetic whisker sensors.

Chapter 3

Feasibility Test for Radial Distance Estimation with Artificial Whisker Sensors

Rats use their whiskers to sense their environment by actively moving them back and forth continuously. Rats are able to discriminate different textures or extract features of a nearby object (such as size, shape and distance). Inspired by the ability of rats, engineers have derived mathematical models for whiskers and also made artificial whiskers. Many methods for radial distance estimation (the distance between the base of the whisker to the object - whisker contact point) has been proposed based on the numerical or analytical models of the whiskers. These methods could be classified with 'the shape of whiskers (cylinder or tapered)', 'sensors used at the base' and 'sensing strategy, active or passive'. In this paper, we first analyze the linear cylinder whisker model proposed by Kim and Möller. Under an active sensing situation, this model only measures the protraction angle and a single deflection angle a little away from the base. With the information of the two angles, the model can estimate the radial distance without knowing the whisker's property or the moment at base. We analyze this linear model in the perspective of robustness to noise. Also, how accurately this model estimates the radial distance in large deflection is analyzed by comparing linear simulation results with numerical nonlinear results. Extending this model, we propose a linear tapered whisker model. It is shown that the radial distance can be estimated using only two angles (protraction angle and a deflection angle on the whisker) as well. The same analysis has been done on the tapered model. Using the real data measured

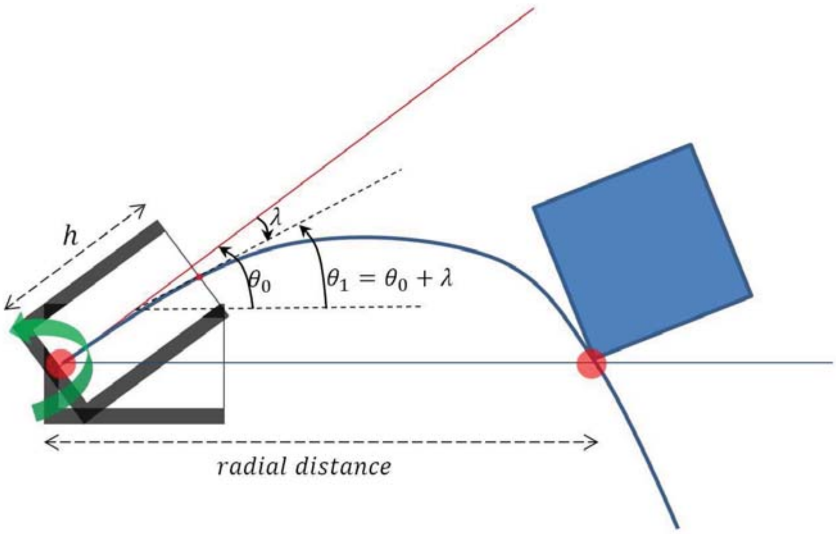

Figure 3.1: The schematic of the active whisker sensor system. Radial distance is defined as 'distance between whisker sensor's pivot point to whikser-object contact point. θ_0 denotes the protraction angle, λ is the deflection angle measured by sensors at position h, and the tangential angle at sensor θ_1 is calculated as $\theta_1 = \theta_0 + \lambda$.

from various animals' whiskers, we attempt to show what kind of advantages or disadvantages for each case may have. Finally, it is shown that knowing two deflections, the radial distance can be estimated. Using the real data measured from various animals' whiskers, we attempt to show what kind of advantages or disadvantages for each case may have. Finally, it is shown that knowing two deflections, the radial distance can be estimated. This section is to be prepared for submission as a scientific paper (Ahn and Kim, 2013b).

3.1 Results

3.1.1 Linear Cylinder-Type Whisker

Using the protraction angle and deflection angle at the location of the sensor on the whisker, the radial distance can be estimated Kim and Moeller (2004); Kim and Möller (2006, 2007). This analytical model assumes that the whisker is under active sensing, which means it rotates the whisker for contact. The distance from the base of the whisker to the contact point of object is called 'radial distance'. The relationship with the tangential angle at an arbitrary location x of the whisker or radial distance can be

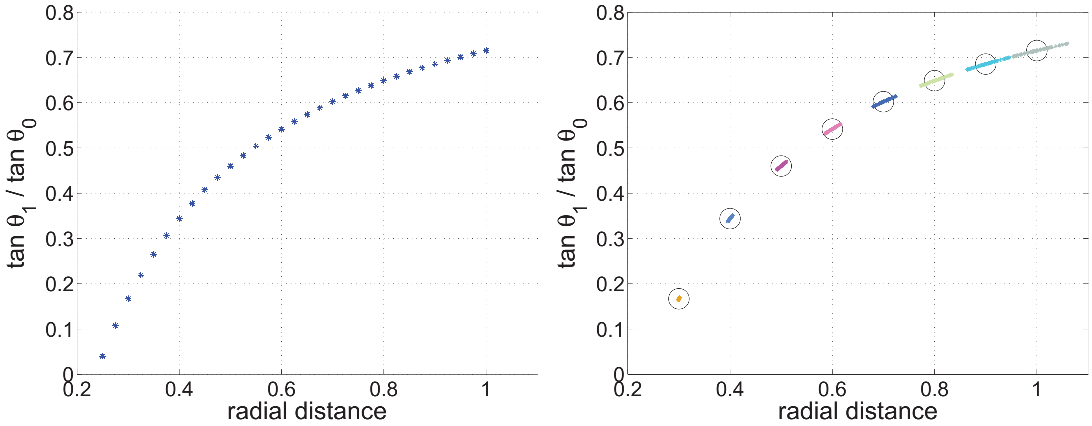

(a) (b)

Figure 3.2: Torque invariance characteristic of analytical model (a) x-axis: $tan\theta_1/tan\theta_0$, y-axis: radial distance, z-axis: τ(moment) (b) The variation of radial distance estimation with noise applied relative to the size of each angle, θ_0 and θ_1. Using the given analytic equation, radial distance d can be estimated with $tan(\theta_1+\varepsilon)/tan(\theta_0+\varepsilon)$, where ε is gaussian noise. (Sensor position $h = 0.1$)

expressed as

$$EItan\theta = \frac{\tau}{2d}x^2 - \tau x + \frac{1}{3}\tau d \tag{3.1}$$

where E is the Young's modulus, I is the moment of inertia, θ is the tangential angle at x and τ is the torque at whisker base.

We denote the protraction angle as θ_0 and the tangential angle at sensor position $x = h$ as θ_1 (where $\theta_1 = \theta_0 + \lambda$, and λ is deflection angle at position h) and obtain the equation 3.2.

$$\frac{tan\theta_1}{tan\theta_0} = (\frac{3h^2}{2d^2} - \frac{3h}{d} + 1) \tag{3.2}$$

The robustness to noise using the linear model is shown in Figure 3.2(b). It is shown in equation 3.2 that the information of two angles is sufficient to estimate the radial distance. When the measurements of these angles are noisy, the tangential ratio will vary, giving an estimate with error.

Surprisingly, equation (3.2) shows that without the torque information, the radial distance can be estimated.

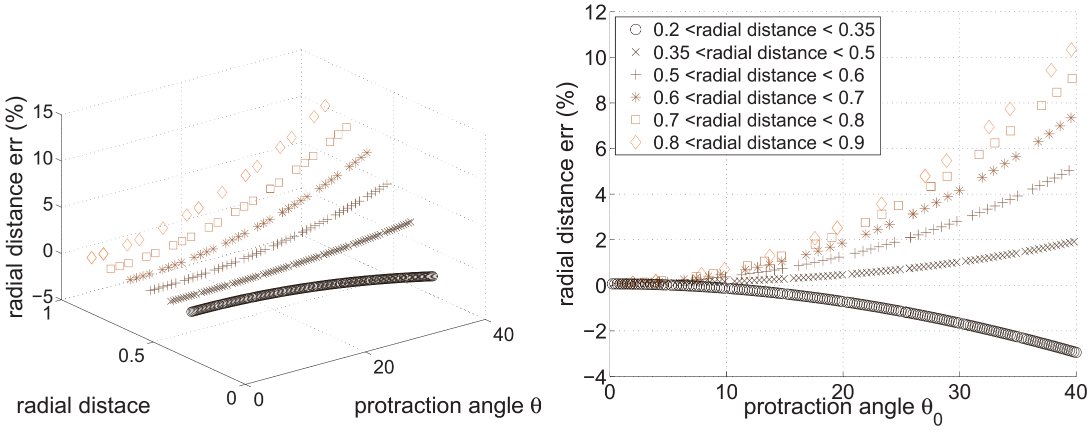

(a) (b)

Figure 3.3: Linear model of cylindrical whisker's estimation error analysis. The radial distance estimation error (a) shown with protraction angle θ_0 and radial distance, and (b) shown with only protraction angle θ_0. The larger the protraction angle, a larger error is expected. The data points are discriminated with 'range of actual radial distances'.

However, the torque invariance characteristic may only be valid because the system is linearized. To see if the torque invariance characteristic holds even for cases where large deflection occurs, the numerical method was used. For the analytical equation, the two parameters to decide the tangential angle θ_1 are torque τ and radial distance d. On the other hand, the numerical method needs a force at the point load P, and the point where the contact is held on the whisker (This is different from radial distance. Identical when the protraction angle is very small after contact).

Therefore, first the numerical simulation was conducted, by varying the position of point load and the magnitude of load. For every point load magnitude and position, a deflected whisker will be given. From that deflected whisker, we can extract the 'actual radial distance', 'protraction angle' and 'deflection angle'. Hence, we can increase the point load magnitude and change the protraction angle. It should be noted that the 'actual radial distance' will generally become smaller as the point load magnitude becomes larger.

From the simulation results, we can extract the 'actual' protraction angle and deflection angle. Since it is assumed that the whisker sensor will only be given these two values, the 'estimated radial distance' was given by using these two information plugged into the linear model expressed in equation 3.2. The 'estimated radial distance' could be compared with the 'actual radial distance' and the 'radial distance estimation error' could be calculated. The ’radial distance estimation error’ is defined as

$$err(\%) = \frac{d_{actual} - d_{est}}{d_{actual}} \times 100 \tag{3.3}$$

where d_{actual} denotes ’actual radial distance’ and d_{est} denotes ’estimated radial distance’. In Figure 3.3, the error relationship with protraction angle and the actual radial distance is shown. Because the radial distance cannot be controlled to be constant, the data is discriminated with radial distance ranges.

As expected, when the protraction angle is small, the radial distance estimation error is close to zero. When the protraction angle increases, the magnitude of error will always increase.

From the simulation results, it could be seen that the radial distance will be overestimated for most of the cases. However, when the actual radial distance is small, it would underestimated. Regardless, the linear model will be quite accurate as long as the protraction angle is under approximately 15 degrees regardless of actual radial distance.

3.1.2 Linear Tapered Type Whisker

3.1.2.1 Why tapered whiskers?

Most animals’ whiskers are tapered Williams and Kramer (2010). There were several advantageous shown in Williams et al. (2010), and in order to explore if there were any other reasons for tapered whiskers to be a universal standard among animals, simulations based on a tapered whisker model were conducted.

Tapered whiskers may be found in many animals due to biological reasons which are not shown in this paper. The focus of this paper is the advantages coming from such structures.

3.1.2.2 Simulation results of tapered whiskers

The analytical linear model Kim and Möller (2007) is based on a cylinder shaped whisker. To extend the idea of KimKim and Möller (2007), we derived an equation using the same idea for a tapered whisker. The linear equation of deflection of a tapered

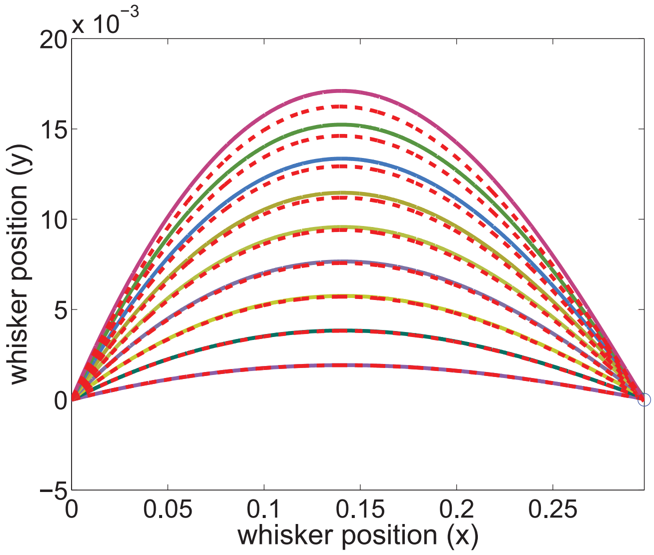

Figure 3.4: Bending tapered whiskers. Comparison with numerical methods and linear methods. Several cases with different torque values when radial distance is 0.3 are shown. The red dashed lines are the result of linear simulation while the other colored solid lines are the results of the numerical method. It is shown that for small protraction angle, the results are closely matched.

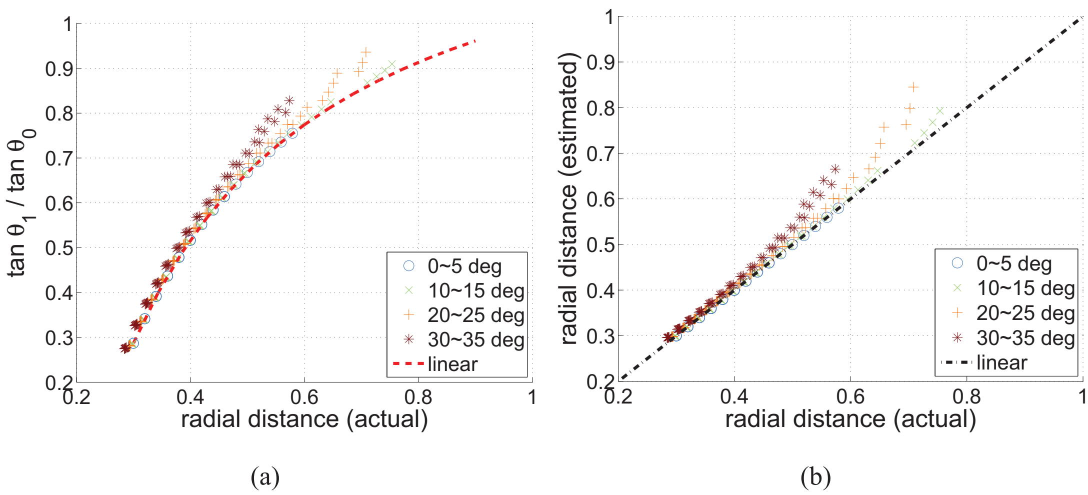

Figure 3.5: Comparison of results of linear model and numerical method for tapered whisker. (a) radial distance (actual) - tangential ratio (b) radial distance (actual) - radial distance (estimated).

whisker was given by Birdwell et al.Birdwell et al. (2007). The relationship of 'torque at base', 'radial distance' and 'tangential angle' is

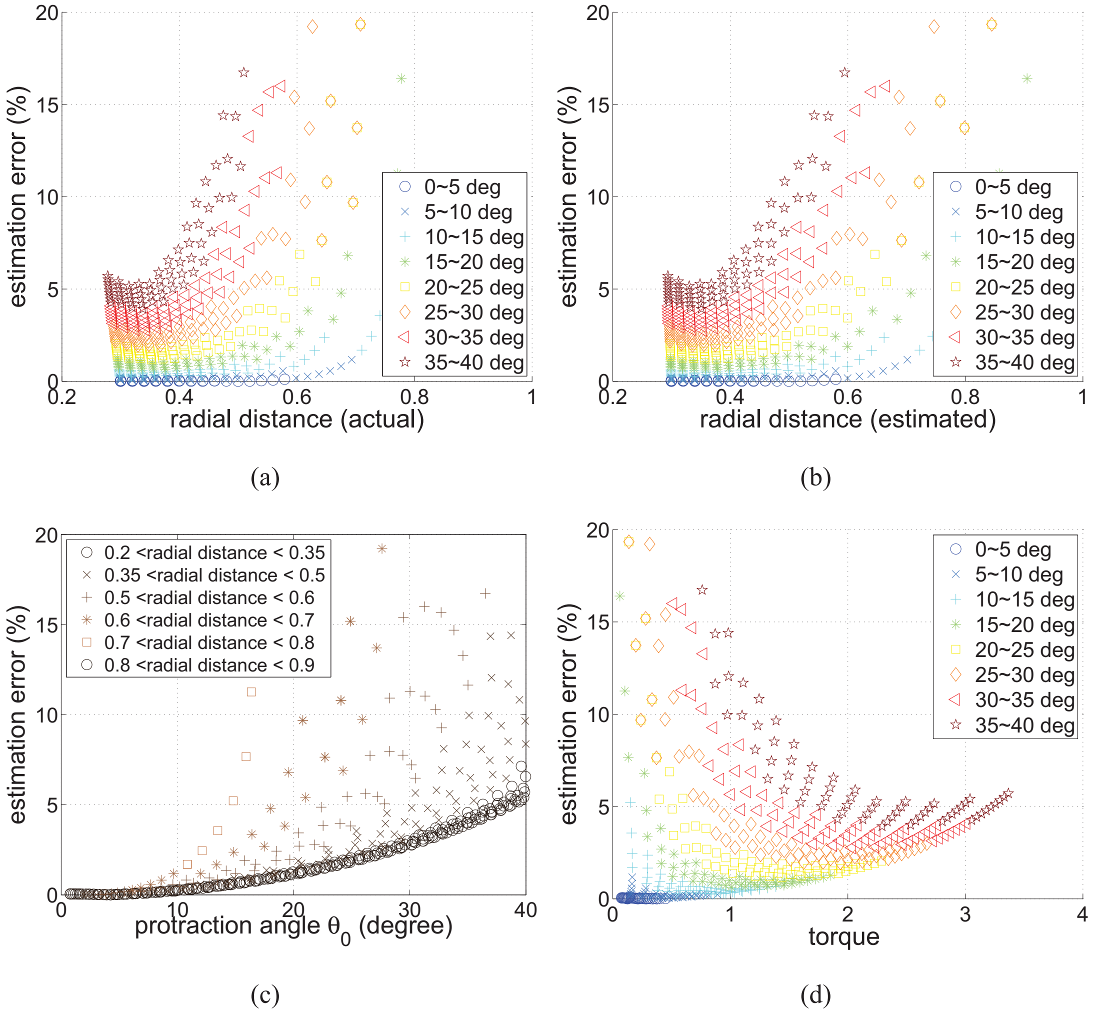

Figure 3.6: Linear model of tapered whisker's estimation error analysis. Radial distance estimation error shown with (a) radial distance (actual) (b) radial distance (estimated) (c) protraction angle and (d) torque.

$$E\alpha\frac{dy}{dx}|_{x=0} = E\alpha tan\theta_0 = \left(\frac{L+2d}{6L^3} + \frac{1}{d}\left(\frac{d+2L}{6L^2} - \frac{1}{3(L-d)}\right)\right)\frac{\tau}{d} \tag{3.4}$$

$$E\alpha\frac{dy}{dx}|_{x=h} = E\alpha tan\theta_1 = \left(\frac{L+2d-3h}{6(L-h)^3} + \frac{1}{d}\left(\frac{d+2L}{6L^2} - \frac{1}{3(L-d)}\right)\right)\frac{\tau}{d} \tag{3.5}$$

where $\alpha = \pi/4(r_{base}/4)^4$, L is the length of whisker, d is the radial distance, τ is the moment at base and h is the sensor position from the base. Dividing equation (3.4) by equation (3.5), we remove τ and α. The tangential ratio equation is derived as

$$\frac{tan\theta_1}{tan\theta_0} = \frac{L+2d-3h/6(L-h)^3+\frac{1}{d}(d+2L/6L^2-1/3(L-d))}{L+2d/6L^3+\frac{1}{d}(d+2L/6L^2-1/3(L-d))} \tag{3.6}$$

$$d = \frac{-B-\sqrt{B^2-4AC}}{2A} \tag{3.7}$$

where the A, B and C are the coefficients which are defined below:

$$A = \frac{tan\theta_1/tan\theta_0}{3L^3} - \frac{1}{3(L-h)^3} \tag{3.8}$$

$$B = \frac{L+3h}{6(L-h)^3} - \frac{1}{6L^2} \tag{3.9}$$

$$C = \frac{L^2-3hL}{6(L-h)^3} - \frac{1}{6L} \tag{3.10}$$

Hence, using the same information, θ_0 and θ_1, the radial distance can be estimated even with a tapered whisker. To verify if the derived linear equation is correct, simulation results of the linear equation and with numerical simulations were compared. Such validation is shown in Figure 3.4. By first conducting a numerical simulation for a given position of point load and magnitude, the deflection of a tapered whisker is shown. After a numerical simulation, the torque at base $\tau$and actual radial distance d can be extracted. Using these two parameters, the deflection of a tapered whisker based on the linear model could be given. The simulation results are compared and it is clearly seen that when the protraction angle is small, the results closely match but the difference increases as the protraction angle increases (or as point load magnitude increases). This simulation result is a validation for the linear tapered model.

While Figure 3.4 gives a glimpse of how the numerical method and linear model differ for a tapered whisker, Figure 3.5 and Figure 3.6 gives a more thorough comparative analysis. In Figure 3.5(a,b), it is clearly seen that the estimated radial distance is always overestimated regardless of protraction angle and radial distance. Also, if the protraction angle and/or radial distance are small, the estimation error will be small as expected.

The relationships between absolute radial estimation error and parameters such as 'actual radial distance', 'estimated radial distance', 'protraction angle', and 'torque' are shown in Figure 3.6. The estimation error could not be known with a single variable, Figure 3.6 (a) (d) can reveal main characteristics. Figure 3.6(a),(b) give similar results

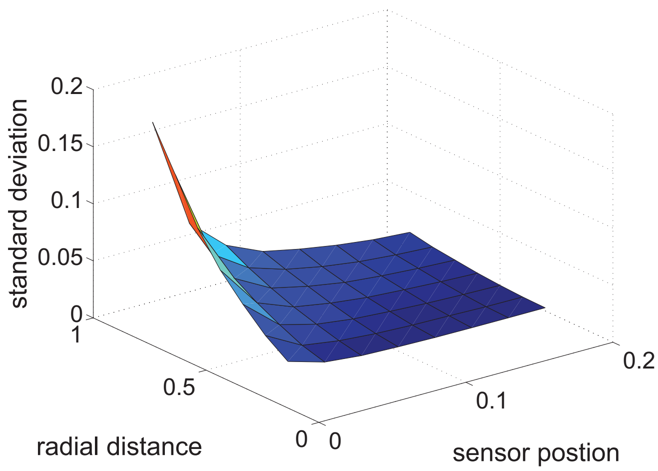

Figure 3.7: Error standard deviation as a function of radial distance and sensor position with tapered whisker. All the simulations were conducted when protraction angle $\theta_0 = 15degree$.

since the actual radial distance and estimated radial distance are somewhat similar. From these Figures, the fact that small angle protraction and small radial distance will result in small estimation error, while the opposite case will result in high error can be deducted. It should be noted that for the tapered whisker case, as the point load or radial distance gets closer to 1 (or tip), the error will greatly increase. This is due to the fact that when the point load is near the tip, the tip will bend significantly since it has low moment of inertia value which will make the difference between the linear model and numerical method large.

Figure 3.6 (c) shows interesting results. 'Most' of the radial distance estimation error could be known with only the protraction angle. However, the estimation error will quickly escalate for large radial distances. This result is consistent with Figure 3.6 (a,b). On the other hand, Figure 3.6 (d), the relationship between torque and estimation error, shows that the increase of torque generally decreases the estimation error. Generally, for the same protraction angle, the larger the radial distance, the smaller the torque will be. The high error cases are where the radial distance is close to the tip. For such cases, the torque (at base) would be small.

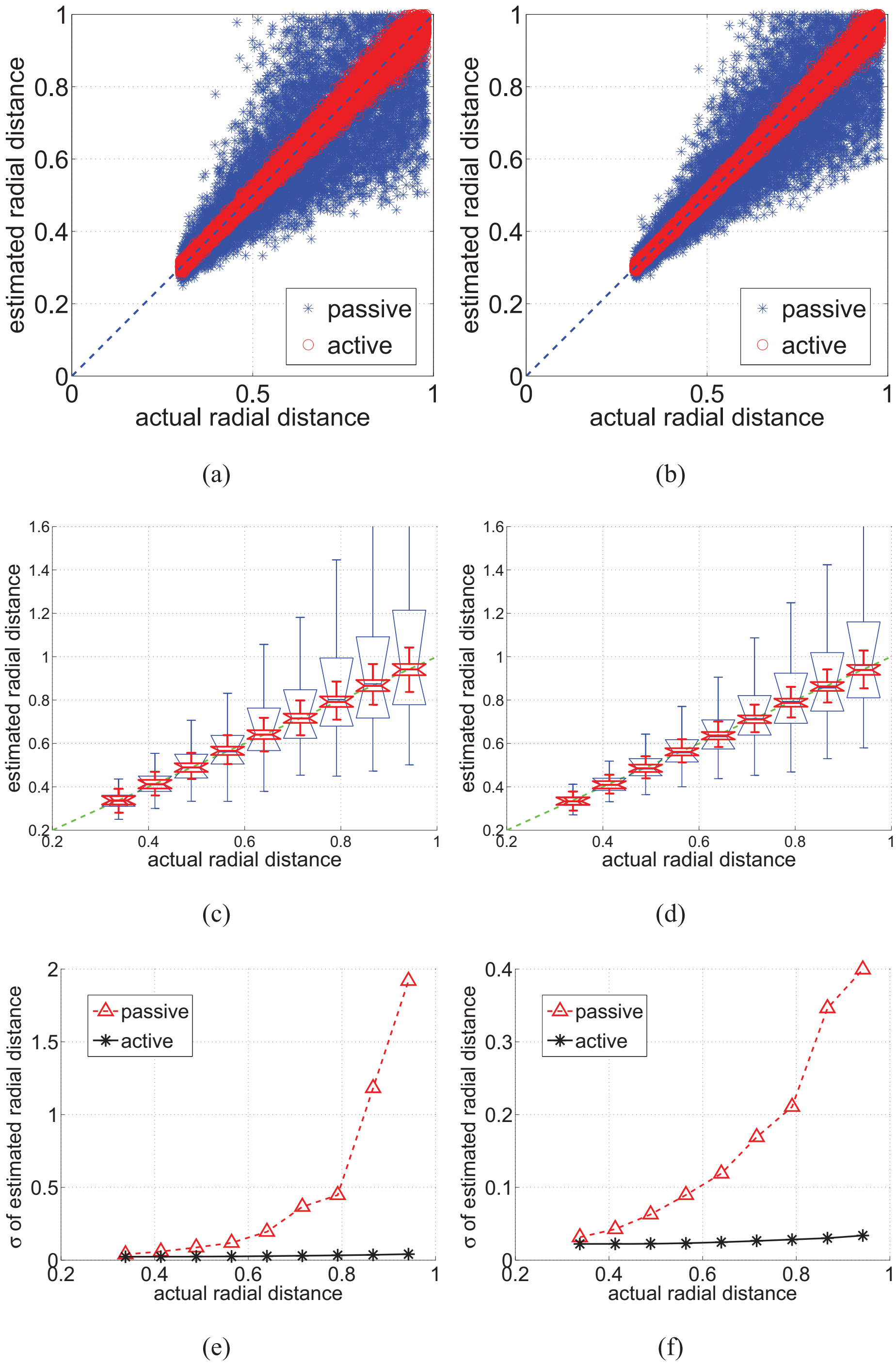

Figure 3.8: Comparing radial distance estimation using the cylindrical and tapered analytical model for active and passive sensing (a) tapered whisker: absolute noise [0.25degree] (b) cylindrical whisker: absolute noise [0.25degree] (c,d) The mean and variance of the results of (a) and (b). (e,f) are graphs of the standard deviation of the radial distance estimation results.

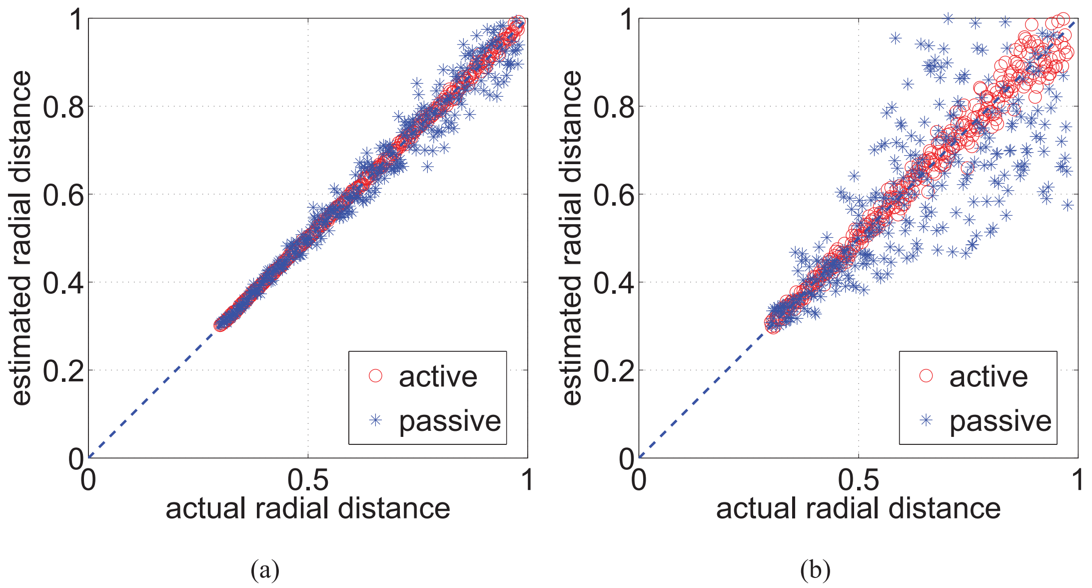

Figure 3.9: Radial distance estimation using analytical models of active and passive sensing (a) tapered case; absolute noise [0.1degree] applied (b) tapered case; absolute noise, 0.5 [degree]

3.1.3 Noise Robustness Comparison of Cylindrical and Tapered Whisker

In the previous sections, the inaccuracy occurrence due to large deflection has been quantified for cylindrical and tapered whisker sensor system. For real implementation, it is also very important for whisker sensor systems to be robust to noise. In order to test such robustness for each whisker types, Gaussian noise was added to both protraction angle θ_0 and tangential angle θ_1. Using the information of the two noisy angles, the radial distance was re-estimated. All the simulations were based on linear models. In order to assume that the simulation results are close to the actual system, the protraction angles for all cases were fixed to 15 degrees. Such an angle would be small enough except for the cases for tapered whiskers when the radial distance is close to the tip.

For previous simulations, the sensor position was fixed. However, to see the effect of sensor position as well as the radial distance, both parameters were varied. 300 simulations have been conducted for each 'radial distance - sensor position' case and the standard deviation was calculated for each case.

From Figure 3.7, it is shown that as the radial distance increases, the estimation error increases for both cases. It can be intuitively understood that a closer object could be estimated more correctly compared to an object far away.

Also, for both cases, the uncertainty or standard deviation will decrease as the sensor position (distance from base) increases. This can be understood intuitively as well since if the sensor is very close to the base, the protraction angle and tangential angle will be almost identical, not giving additional information. However, the sensor position should not be too far or it would become impractical. The difference between the tapered whisker and cylindrical whisker seems to be small in the perspective of standard deviation, but the magnitude of the standard deviation of the tapered whisker sensor is always smaller than the cylindrical sensor, which means the tapered whisker is more robust to noise compared to the cylindrical sensor.

In Figure 3.9 (a) and (b), different levels of noises were applied. For Figure 3.9 (a), Gaussian noise $N(0,0.1^2)$ degree and for (b) Gaussian noise $N(0,0.5^2)$. The estimates for both methods regarding small noise seem to be usable, while the passive sensing strategy with larger noise seems to be unreliable, unless an appropriate estimation algorithm is employed with multiple measurements.

The comparison between passive sensing and active sensing using a cylindrical whisker sensor was conducted by Kim and Möller (2006). As an extension of that work, an analytical model of a tapered whisker was derived. The model for the active tapered whisker was shown from the previous section, while the passive model is shown in this section. Both passive and active sensing models need the information of at least two different angles in order to estimate the radial distance without knowing 'torque', 'rotational stiffness' or 'force'.

For the active sensing case, only one deflection angle sensor on the whisker is required if the DC motor has an encoder attached (Encoder can measure protraction angle). However, since there is no protraction angle in passive sensing case, at least two deflection angle sensors are required. Putting the two sensor locations as h_1 and h_2, and the corresponding tangential angles (which are identical with deflection angles in this case) as θ_1 and θ_2, the radial distance d can be estimated through the following equation.

$$d = \frac{(L-h_2)^3(L^4-3h_1L^3-(L-h_1)^3L)-k(L-h_1)^3(L^4-3h_2L^3-(L-h_2)^3L)}{k(L-h_1)^3(2L^3-2(L-h_2)^3)-(L-h_2)^3(2L^3-2(L-h_1)^3)} \tag{3.11}$$

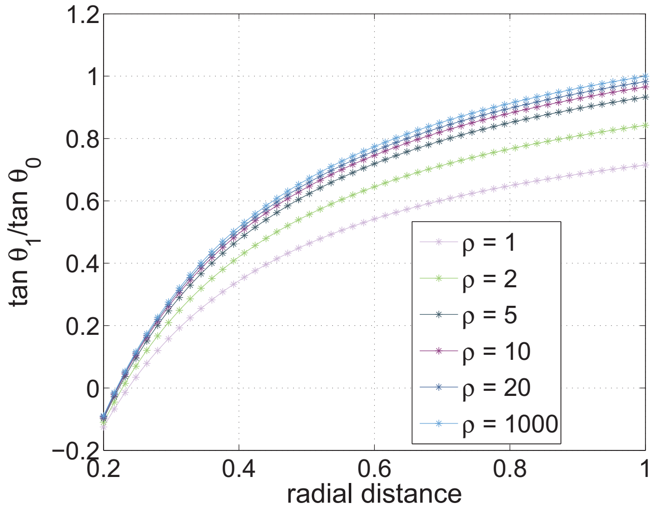

Figure 3.10: Simulations with different types of taper ratio. Taper ratio, defined as $\rho = r_{base}/r_{tip}$ varies from 1 to 1000. Taper ratio 1 means that it is a cylinder type whisker, and taper ratio 1000 means it is almost a perfect tapered whisker (tip radius being close to zero). Rat whiskers' tapered ratio is approximately in the range of 10 to 22 Williams and Kramer (2010).

where $k = tan\theta_2/tan\theta_1$, the tangential ratio with θ_2 and θ_1.

Figure 3.8 (a) compare the active and passive sensing using a cylindrical whisker sensor and Figure 3.8 (b) compare the active and passive sensing using a tapered whisker sensor. Figure 3.8 (c) and (d) summarizes the statistical characteristics of the cylindrical and tapered whisker for 9 intervals of radial distances by drawing multiple boxplots. Since each boxplot is a summarization of an interval of estimated radial distances, it is bound to have at least a small value even if the estimated radial distances are exactly the same as the actual radial distances. Nevertheless, the boxplots can be a good tool for comparing the statistical characteristics for active, passive sensing.

From the results of Figure 3.8, the obvious conclusions are that the active sensing strategy is better than the passive sensing strategy regardless of sensor type (cylindrical or tapered). Also, the active tapered whisker is slightly better than the active cylindrical whisker and the passive tapered whisker is better than the passive cylindrical whisker.

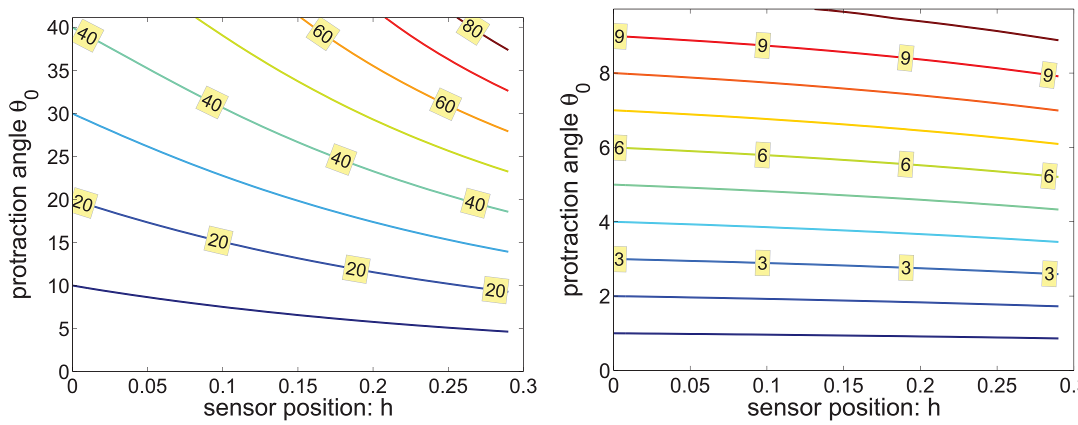

(a) (b)

Figure 3.11: The tangential angle when protraction angle and sensor position is varied. (a) radial distance fixed to 0.5, (b) radial distance fixed to 0.9. The tangential angle shown in (a) monotonically increases when protraction angle increases case. On the other hand, the tangential angle decreases at a certain point for the case of (b).

3.1.4 Practical Considerations

While all the analytical models and numerical methods for tapered whiskers assumed that the whisker is an ideal cone, either for actual animals and sensor manufacturing, such an ideal shape cannot exist. Even if one attempts to create one, the tip will break with great ease. Williams et al. Williams and Kramer (2010) measured the tapered ratio of eleven types of different animals' whiskers, three whiskers for each animal and found that some animals have small taper ratio whiskers (4 9) while some animals, including the rat and the mouse, had larger tapered ratio (10 24), where the taper ratio is defined as $ratio = r_{tip}/r_{base}$. Hence, the ideal tapered whisker's ratio would become infinity.

In Figure 3.10, the relationship of radial distance - tangential ratio for various cases with different taper ratio is shown. It can be seen that while the taper ratio 1 (cylindrical whisker) to 5 differ greatly, 5 to 10 has a relatively small difference, and 10 to 1000 has a smaller difference. Hence, if the taper ratio is approximately around 10, it could be regarded as a very close approximate of an ideal tapered whisker. Another assumption that the overall moment of inertia is similar also should hold for such approximation.

In Figure 3.11, the tangential angle θ_1 is given as a function of sensor position h and protraction angle θ_0. While Figure 3.11 (a), where radial distance is 0.5, the protraction angle could be extended to approximately 45 degrees, and Figure 3.11 (b) had radial distance 0.9 and the protraction angle could be extended to approximately 10 degrees. From the simulation, we saved only the data when the deflected whisker's tip had the largest distance in the x-axis. When the radial distance was large, the tip bent severely making the tip bend inside. Hence, Figure 3.11 (b) only showed data for protraction angle within 10 degrees.

From Figure 3.11, two conclusions could be made. First, tapered whiskers touching objects with its tip would 'flick' due to its small rotational stiffness. This result is consistent with the results of Williams and Kramer (2010). Second, since the difference between protraction angle and tangential angle is very similar when the radial distance is large, it would be more difficult to discriminate radial distances. In other words, it is more vulnerable to noise.

3.1.5 Radial Distance Estimation Based on Deflection

The radial distance estimation methods are shown from the previous sections were based on two different angle information, protraction angle and deflection angle (or tangential angle). One was a model of cylindrical whisker Kim and Moeller (2004); Kim and Möller (2006, 2007), and the other model was base on a tapered whisker which was proposed in this paper.

Instead of using the information of two different angles, one could estimate the radial distance with the information of two different deflections (assuming the whisker is cylindrical shape).

Since the deflection of an arbitrary point's deflection and moment's relationship could be expressed as

$$EIy(x = h_1) = \frac{-\tau h_1 (h_1^2 - 3dh_1 + 2d^2)}{6d} \tag{3.12}$$

$$EIy(x = h_1) = \frac{-\tau h_2 (h_2^2 - 3dh_2 + 2d^2)}{6d} \tag{3.13}$$

where h_1 and h_2 are an arbitrary point on the whisker, d is the radial distance, $y(x = h)$ is the deflection at $x = h$ and τ is the torque sensed at base. Using equation 3.12 and 3.13, the radial distance could be estimated from the following equation.

$$\frac{y(x=h_1)}{y(x=h_2)} = \frac{h_1(h_1^2 - 3dh_1 + 2d^2)}{h_2(h_2^2 - 3dh_2 + 2d^2)} \tag{3.14}$$

Like the other methods, using deflection information could also cancel the torque term. For this method, there should be two sensors along the whisker sensor for radial distance estimation.

3.2 Discussion

There are three methods described in this paper. One is a model using a cylindrical whisker for radial distance estimation proposed by Kim and Möller (2007) , one is a model tapered whisker proposed in this paper. Both of these models use the information of two different angles. Another model proposed in this paper is a radial distance estimation method using two different deflection measurements.

The contribution of this paper is proposing a method which can evaluate the accuracy of linear models in large deflection angles. Also, extending the model of Kim and Möller (2007) , two new methods for radial distance estimation have been proposed. Finally, through simulations which compare ’active / passive sensing’ and ’cylindrical / tapered whisker’, it could be concluded that active sensing is better than passive sensing, and a tapered whisker was better than a cylindrical whisker in radial distance estimation.

3.2.1 Tapered whisker

Tapered whiskers are known to be widely spread, and such tapered structure have many advantages such as ’small diameter at whisker tip’ which allows the whisker to probe small surface features, ’a smaller deflection angle’ when whisker is passively sensing a moving object compared to a cylindrical whisker which lets the whisker to not have a large curvature, and a robustness in resonant frequency when the tip of the whisker breaks Williams and Kramer (2010). The paper by Williams and Kramer (2010) gives great insight in the advantages of tapered whiskers.

In our paper, we attempted to observe other advantages of a tapered whisker sensor in an engineering perspective. Extending the model of Kim and Moeller (2004), a new tapered whisker model was shown. A similar derivation of this analytical model was also shown in Birdwell et al. (2007), but the model given here estimates the radial distance by measuring the torque or the derivative of torque at base while our model uses the protraction angle and a single deflection angle on whisker shaft as in Kim and Moeller (2004).

This model is based on a linearized Bernoulli-Euler equation, which means that the accuracy will drop when the 'small angle approximation' assumption breaks. In order to see how well this linear equation holds for large angles, a numerical method was used to compare its results with the linear model's results. The results showed that even when there is a difference between the linear model and numerical model, it was shown that the error could be accurately known by only knowing the radial distance. In other words, even if the rodents do not use the exact mathematical model proposed in this paper, it is highly possible that it could use the protraction angle and deflection angle in order to estimate radial distances.

3.2.2 Active and Passive sensing

Through linear models, the active and passive sensing for cylindrical whiskers and tapered whiskers were compared. Though the simulations are based on linear models, it still would give insight in active and passive sensing. The results showed that active sensing is more robust to noise for both of the whisker types. Also, it showed that tapered whiskers are better than cylindrical whiskers in both cases. Hence, this simulation results not only supports the fact that tapered whiskers are better, but also supports the fact that active sensing is beneficial in radial distance estimation. This kind of results may explain why rats actively move their whiskers.

One may argue that rats sense the change deflection angle rather than the deflection angle itself, similar to the claim of Solomon and Hartmann (2006) that rats would sense the change of torque rather than the torque itself. The active tapered whisker model could be differentiated with time in order to make a model based on 'change of deflection angle'.

$$
\begin{aligned}
\frac{\frac{\partial}{\partial t}(tan\theta_1)}{\frac{\partial}{\partial t}(tan\theta_0)} &= \frac{(\frac{L+2d-3h}{6(L-h)^3}+\frac{1}{d}(\frac{d+2L}{6L^2}-\frac{1}{3(L-d)}))}{(\frac{L+2d}{6L^3}+\frac{1}{d}(\frac{d+2L}{6L^2}-\frac{1}{3(L-d)}))}\cdot\frac{\frac{\partial}{\partial t}\tau\cdot\frac{1}{d}}{\frac{\partial}{\partial t}\tau\cdot\frac{1}{d}} \\
&= \frac{(\frac{L+2d-3h}{6(L-h)^3}+\frac{1}{d}(\frac{d+2L}{6L^2}-\frac{1}{3(L-d)}))}{(\frac{L+2d}{6L^3}+\frac{1}{d}(\frac{d+2L}{6L^2}-\frac{1}{3(L-d)}))} \\
&= \frac{sec^2\theta_1\cdot\dot{\theta}_1}{sec^2\theta_0\cdot\dot{\theta}_0} \\
&\approx \frac{\dot{\theta}_1}{\dot{\theta}_0}
\end{aligned}
\tag{3.15}
$$

From equation 3.15, it is shown that given the protraction angle, deflection angle, and the change of them, the radial distance could be estimated. It should be noted that the above equation is based on the assumption that the radial distance does not vary with time.

3.2.3 Retuning for Whisker Length and Thickness Change

If the length and thickness of the whiskers do not change, rats would be able to acquire information from its whiskers in a consistent way. However, there will be cases when short whiskers will grow longer due to whisker breakage or perhaps because the rat is not fully grown. For either case, the whisker length and possibly the thickness of the whisker will constantly change in this whisker growing process. Hence, if the rats actually use radial distance estimation methods based on either torque, change in torque Solomon and Hartmann (2006), deflection angle or change in deflection angle, then the rats will need to re-tune its brain due to the characteristics change of the whisker.

Assuming that the growth of rat whisker will change only the length, or length and radius of the base, the robustness to such change could be analyzed using the existing equations for tapered whiskers' radial distance estimation. If the rats used radial distance estimation methods based on torque or change in torque information, the variation will exist for both cases of variation (length only or length and whisker base radius). For this method, if the length changes (but not the base radius), the torque term will become more dominant but since the whisker will become more slender, the torque or change of torque at base will fall. Therefore, the retuning process would differ for case by case. On the other hand, if both the whisker length and base of radius will change as well, the torque term will become less dominant, but for this case as well, the whisker will become more thicker which will make the torque value higher. For this method, all the variables are intertwined making it inconclusive.

If the whisker used deflection angle information, and only the whisker's length grew, than for that case the tapered whisker will become more like a cylindrical whisker since the previous tip part would become thicker. If the radius of the base changes as well as the length (in the same ratio), then the normalized results for both case will be identical. For deeper analysis, the actual whisker growth data (of length and base of diameter) would be acquired as well as the actual whisker's mechanical characteristics for numerical validation of the proposed hypothesis.

3.2.4 Radial Distance Estimation with only Deflection Angle

The radial distance method for tapered whiskers used protraction angle and a tangential angle, assuming that the rat will be able to know both. However, it could be assumed that the rat could sense tangential angles from the follicle, but not the protraction angle. If this is the case, a simple modification of the original tapered whisker model can be shown. Assuming that the follicle can measure at least two tangential angles inside the follicle at location h_1 and h_2, the radial distance can be estimated as

$$\frac{tan\theta_2}{tan\theta_1} = \frac{(\frac{L+2d-3h_2}{6(L-h_2)^3} + \frac{1}{d}(\frac{d+2L}{6L^2} - \frac{1}{3(L-d)}))}{(\frac{L+2d-3h_1}{6(L-h_1)^3} + \frac{1}{d}(\frac{d+2L}{6L^2} - \frac{1}{3(L-d)}))} \tag{3.16}$$

3.2.5 The Numerical Method

The linearized Bernoulli-Euler equation is $\frac{M}{EI} = \frac{d\phi}{ds} = -d^2y/dx^2$ where the actual Bernoulli-Euler equation can be written as equation 3.17.

$$\frac{1}{r} = \frac{M}{EI} = \frac{d\phi}{ds} = -\frac{d^2y/dx^2}{[1+(dy/dx)^2]^{3/2}} \tag{3.17}$$

Since it is difficult to solve equation 3.17, a numerical method is used. For this, the whisker can be divided into N elements. In order to know how the whisker shaft will deflect, M_i/EI_i for each i_{th} element must be known.

When a force and its location is given, the M for each point on the whisker can be known, since $M_i = r_i \times F$ where M_i is the moment on the i_{th} element, r_i is the distance between the force and the element, and I_i is the moment of inertia of the i_{th} element.

After knowing M_i/EI_i for $i = 1, \ldots, N$, ϕ can be obtained as well by integrating $\frac{M}{EI}$ by ds. Since ϕ is known, the x, y position for every element can be known. Hence, the whole deflection can be reconstructed.

However it should be noted that when the x, y position for each element changes, so will r_i and ultimately M_i/EI_i will change. Hence, this calculation must be done iteratively until the results converge.

The results was validated by inserting x and y in $-\frac{d^2y/dx^2}{[1+(dy/dx)^2]^{3/2}}$ to see if it is identical to $\frac{M}{EI}$.

3.3 Summary of Chapter 3

There are three methods described in this paper. One is a model using a cylindrical whisker for radial distance estimation proposed by Kim and Möller (Kim and Möller, 2007), one is a model tapered whisker proposed in this paper. Both of these models use the information of two different angles. Another model proposed in this paper is a radial distance estimation method using two different deflection measurements.

The contribution of this paper is proposing a method which can evaluate the accuracy of linear models in large deflection angles. Also, extending the model of Kim (Kim and Möller, 2007), two new methods for radial distance estimation has been proposed. Since there are three different types of radial distance estimation methods, each method could be chosen for user specific needs. While the cylindrical whisker would be easier to make than a tapered whisker, it might be better to use a tapered whisker for more accurate results. There may be a case where deflection measurement is easier than deflection angle. In such case, the third model in this paper could be used and vice versa.

Using a tapered whisker sensor, there is a possibility that the tip will break, leaving the remaining whisker damaged. However, since there is a curvature change only within the radial point, it is irrelevant whether the tip is broken or not. Even though a tapered whisker sensor with a broken tip will no longer be able to measure the radial distance as far as before, the radial distance estimation method does not change. The same can be said about the cylindrical whisker sensor, but it is quite clear that the tapered whisker is more likely to break.

Chapter 4

Passive sensing of Hydrodynamic Stimuli

Many types of animals such as rats and pinnipeds use their whiskers as their primary sensor in order to perceive their environment. Pinnipeds such as the harbor seal and the California sea lion are known to have highly sensitive whisker sensors which can detect hydrodynamic trails generated by prey such as swimming fish. While rats move their whiskers back and forth doing ’active whisking’ or ’active sensing’, pinnipeds do not ’whisk’ their whiskers but only protract them. Hence, they can be using a ’passive sensing strategy’.

Inspired from such a whisker system, a five microphone based whiskers were made. The artificial whisker shafts were made of optical fiber and attached to the microphone sensor via glue. The deflection of the whisker could be sensed by the microphone sensor. In this paper, the impulse-like response (in air and water) of the whisker sensors were first given to check the characteristics such as the decaying rate and the resonance frequency of the impulse-like response. Using these experimental results of ’in air’ impulse-like responses, a simple ’torsional spring and damper’ model could be made. By adding a nonlinear damper term, we could also model the whisker sensor ’in water’. The simulation results are similar with the experimental results.

To know more about passive sensing in water using whisker sensors, we did additional experiments such as ’sensing hydrodynamic stimuli generated by a underwater propeller while varying distances’. Instead of merely looking at the amplitude of the voltage measurements, the FFT results were compared. All FFT results were fitted to a Gaussian distribution in order to see the main characteristics more clearly. The results imply that 'passive sensing' may not be enough to sense far away hydrodynamic stimuli.

Another experiment was to see if a 'fin movement' would make hydrodynamic stimuli easier to sense. The hypothesis that was tested here is 'the structure of vortice affect the sensibility of the hydrodynamic stimuli'. In order to do that, an artificial fin was made and was swiped in front of the propeller, making the vortex structure to change. The results do not strongly support the hypothesis but may give a glimpse of such a concept.

The last experiment was to see 'why a whisker shaft is needed at all'. Instead of using microphone sensor based whisker sensor, a microphone sensor might as well be used without attaching a whisker shaft to it. To see the importance of the whisker shaft, experiments comparing a microphone sensor and a whisker sensing hydrodynamic stimuli are presented. This content is prepared to be published in a journal (Ahn and Kim, 2013a).

4.1 Artificial whiskers

4.1.1 Microphone sensor based artificial whisker sensor

The artificial whisker sensors were made with microphone sensors. The microphone sensors were designed to sense the change of air pressure due to sound. Inside the microphone sensor, there is a thin and flexible membrane which is responsible for the change in capacitance. Using circuits to bias and amplify the signals of the microphone sensor, the change in capacitance is converted into an electric signal which is read by a DAQ card (NI-DAQ USB 6008).

Our objective was to make an artificial whisker sensor which gives signals when the whisker shaft is deflected. For this, we first tore off the sponge like layer on top of the whisker sensor (used to protect the membrane). We used thin optical fiber approximately 1mm thick as a whisker shaft. A little amount of glue (from a glue gun) was applied to the end of the fiber. Before the hot glue could stiffen, it was attached to the top of the microphone sensor. Extra care was given so that the whisker shaft would not rip the membrane of the sensor which would make it useless.

The whisker shaft is plugged inside the small amount of glue, and the glue is attached to the microphone sensor's membrane. Hence, the displacement of the whisker shaft can be transmitted to the membrane via stiffened glue. Each whisker sensor was tested to check if they worked properly. Through several tests, it could be known that the amount of glue applied, curvature of the whisker, thickness and length of the whisker shaft made the whisker's characteristics vary.

If a small amount of glue is applied, the whisker shaft is able to move more freely making it more sensitive to small deflections. When the glue is applied in an asymmetric way, this will make the whisker to bend one way easily while hard the other way. Such asymmetry would give non consistent results, hence it was undesired.

The inherent curvature also affected the results. The whisker shaft was inherently curved. To see if the signals gave consistent results regardless of moving direction, the artificial whiskers were moved within the water tank with varying directions. If the whisker shaft was straight, it would ideally give consistent signals, but that was not the case. The signals differed when the direction changed. This may be due to the fact that the drag force is different for each direction. Also, the Karman vortex street formation structure would be different, making the signal due to VIV differ.

The thickness and length of whisker would obviously affect the overall results. When the whisker shaft is thick the stiffer it will be, making it insensitive to small changes in the water flow. However, if the whisker shaft is too thin (lacking stiffness), the whisker would not be able to sense trails consistently because it will deflect itself and would not be able to maintain its basic straight shape. Length will change the whiskers natural frequency as well as the overall drag force. Also, the longer the whisker is, the more curved the whisker will be.

As it is shown in figure (4.1), five different whisker sensors have been made. The whisker length could be classified into two groups. The first two whiskers were short whiskers (approximately 7cm in length) and the other three whiskers were called long whiskers (approximately 10cm in length). Each of the whisker was named as whisker number 1,2,3,4,5. The characteristics of the five whiskers including length and sensitivity could be summarized in the following table.

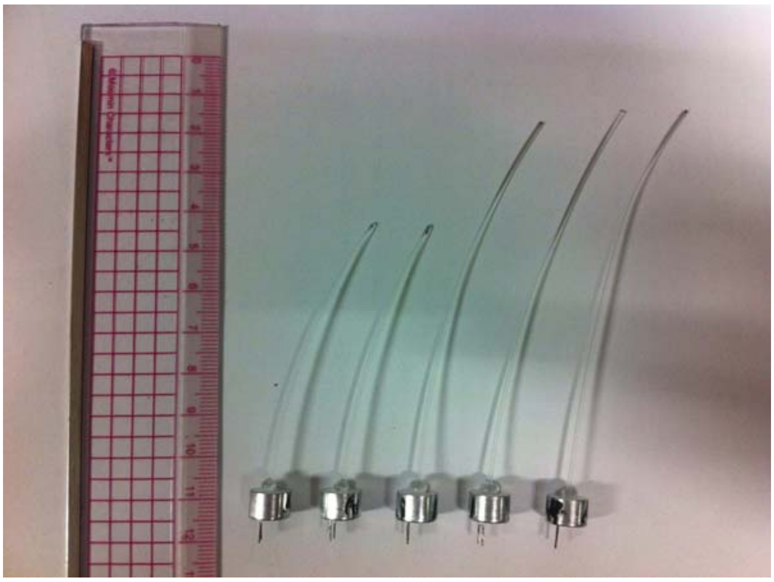

Figure 4.1: Microphone sensor based artificial whisker. The microphone sensor is attached to a frame which is used to hold the sensor still when needed. We use five different whiskers which can be classified into two groups, short and long.

Whisker name	length(approx.)	sensitivity
#1	7cm	middle
#2	7cm	middle
#3	10cm	middle
#4	10cm	low
#5	10cm	high

The number of each sensor will be used throughout the paper.

In this chapter, the experiments can be classified into four different groups. The first is impulse-like response (within air and water), the second is VIV sensing of whisker sensors and the third is hydrodynamic trail (which are generated by an underwater propeller) perception (passive and active), and the last is comparing the results when there is an artificial fin in front of the motor or not.

4.2 Impulse-like response of Whisker

All the movements have been conducted manually (which makes this paper's work less scientific. However, this paper is to show preliminary results). For the impulse-

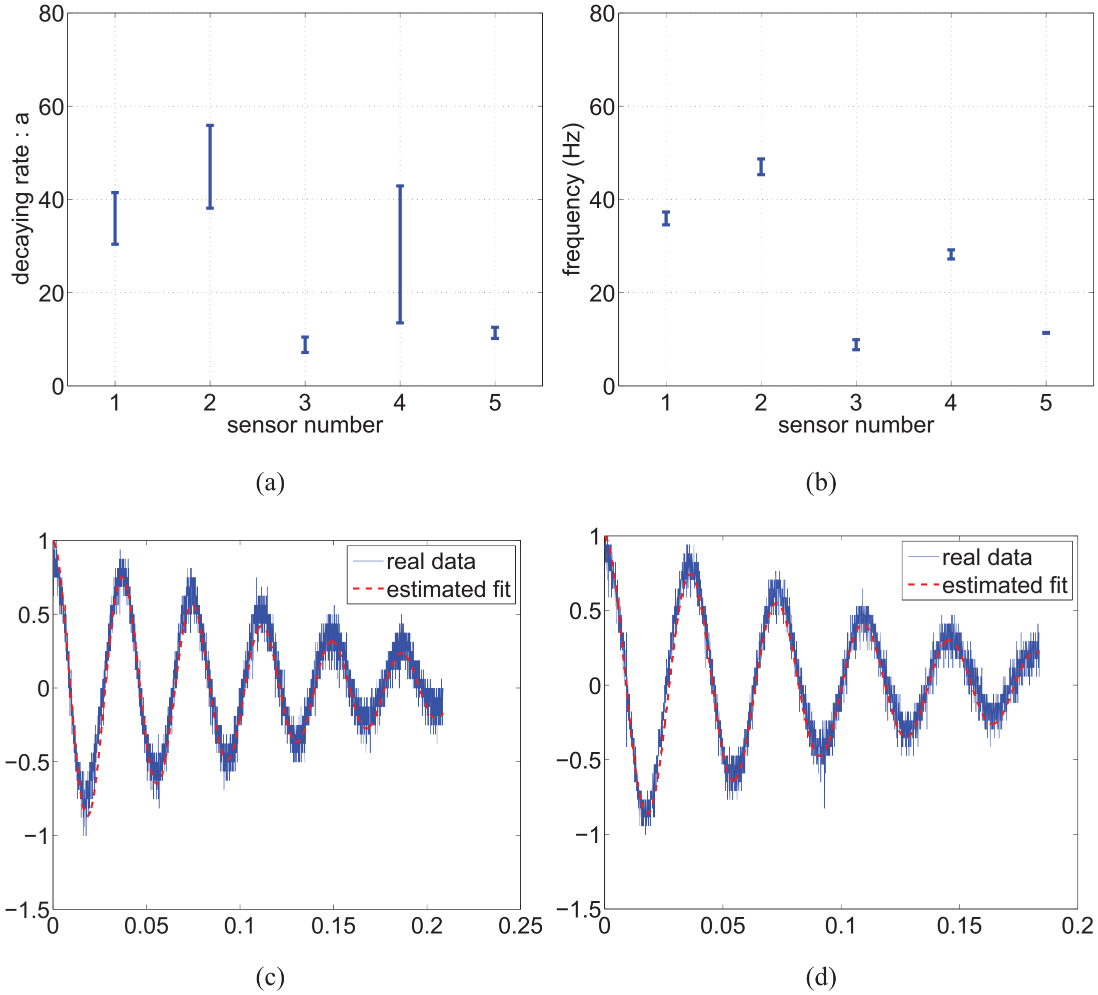

Figure 4.2: Impulse-like response parameter estimation for each whisker sensors. Impulse-like responses are assumed to fit $e^{-at}cos(2\pi\omega t)$ (a) decaying rate a and (b) ω for the five sensors. (c,d) Examples of the estimated impulse-like responses.

like response in air, an impulse-like force (by finger tip) was applied to the whisker shafts' end. The impulse-like response of a whisker within water was done in a similar way. The whisker was submerged in the water tank and the shaft's end was hit by the finger tip. The last experiment was conducted by using a propeller in water. For several whiskers, the whisker was placed 'far', 'moderate distance', 'close' to the motor (which is all passive sensing) and the last was to move the whisker towards and backwards to the motor.

The impulse-like input of each whisker has been given in order to compare the frequency response of each whisker. The impulse-like response for whisker sensors which have similar whisker shaft length were assumed to have similar impulse-like responses.

For the 5 sensors, multiple impulse-like responses were measured. All the impulse-like responses were assumed to fit $e^{-at}cos(2\pi\omega t)$. Hence, there were two parameters which we estimated. The parameter estimation results for each sensor is shown in Figure 4.2 (a,b), and two examples of impulse-like responses and its estimated results are shown. For each sensor, 5 impulse-like responses were used to calculate the mean and standard deviation of each parameter.

Figure 4.2 (a), it is shown that there is no strong correlation between whisker shaft length and parameter a. Also, some sensors have a large standard deviation while others have a small deviation. Sensor 4 had an exceptionally large standard deviation. This is most likely due to the fact that its SNR is the lowest of all sensors. Hence, the parameter estimation results might have been most poor for this sensor.

On the other hand, from Figure 4.2 (b), a very strong correlation between the whiskers shaft length and parameter ω is shown. Recall that the whisker shaft length of sensor 1 and 2 are approximately 7cm, and for sensor 3 to 5, 10cm. For the short whiskers, ω was near 56.1 Hz, and 24.7 Hz for the long whiskers. The small standard deviation for each case shows that ω is a parameter which does not vary compared to parameter a. Figure 4.2 (c) and (d) show the examples of the impulse-like responses. While the estimated impulse-like response does not exactly match the actual impulse-like responses, it gives a close approximation.

From the impulse-like responses, and the parameters estimated, the basic characteristics could be revealed. While these are characteristics when the whisker shafts are not exposed to water, but to air, the actual goal should be to know the whisker sensors' characteristics when it is submerged in water.

Since the sensors are made in order to sense the hydrodynamic stimuli, the impulse-like response of the whisker should be tested within water. There were some difficulties in conducting the impulse-like response in the water since there are many factors which make the experiment far from ideal. First of all, the water is a non linear damper which makes the whisker to not oscillate compared to the case of the impulse-like response in water. Because of that, the impulse (which was given by a finger) did not make the whisker shaft to deflect much but it lingered. This effect made the whisker and finger contact longer than expected. Also the finger moving fast within the water would also have made some non-linear effects.

From Figure (4.3), the FFT results have been shown. For this experiment, sensor

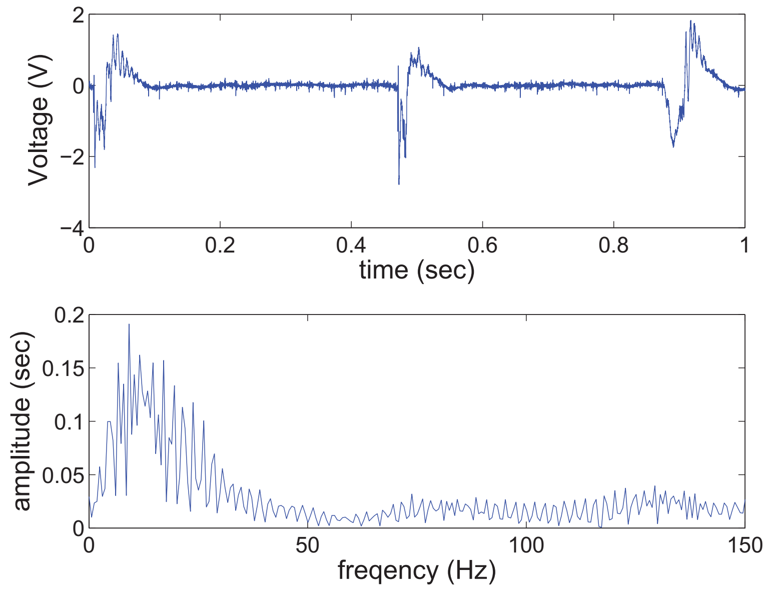

Figure 4.3: Impulse-like response of whisker number 5 within water.

number 5 was used. The impulse-like response is far from the looks of the other impulse-like responses (in air) but it does show some sort of oscillation. However, the damping effect is very clear. The dominant frequency turns out to show within the range of 10 20Hz. This is a damped response compared to the same sensor within air. The first dominant frequency being approximately around 15Hz, and second around 75Hz, third around 130Hz it seems as if the interval between the dominant frequency is approximately 55 60Hz. The other natural frequencies could be estimated with this pattern.

4.3 Modeling whisker sensors

4.3.1 Modeling whisker sensors in air

In the previous section, the impulse-like responses of the whisker sensors were given. Using the estimated parameters, such as decaying rate a and resonance frequency ω, a simple model of a whisker sensor could be made. Under the assumption that the whisker sensor (in air) could be modeled with a torsional spring and a torsional damper, the model could be represented like the following equation.

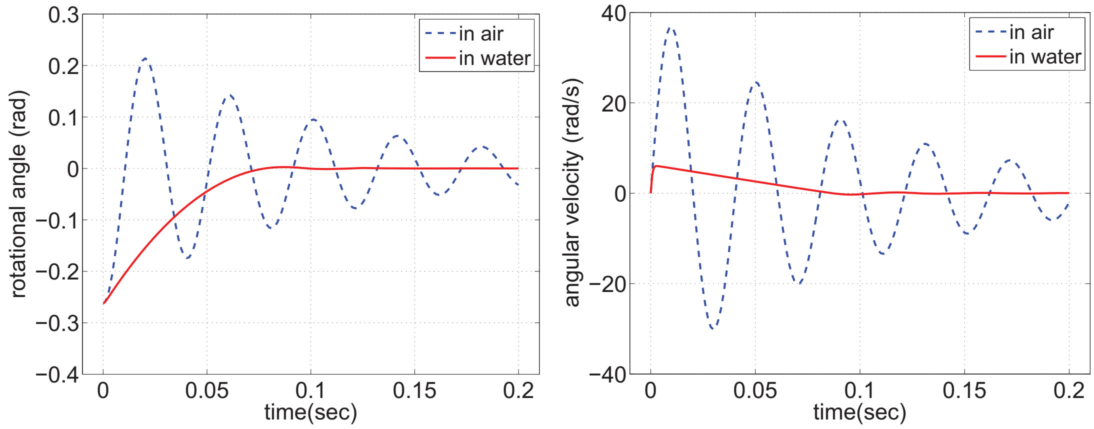

(a) (b)

Figure 4.4: Impulse response simulation for 'in air' and 'in water' whisker sensors. (a) Rotational angle and (b) angular velocity.

$$\sum T = J\ddot{\theta} + b_t\dot{\theta} + k_t\theta = 0 \tag{4.1}$$

where T is torque, J is the moment of inertia, b_t is the torsional damping coefficient, k_t is the torsional spring coefficient and θ is the angular position of the whisker shaft ($\theta = 0$ when shaft is at resting position).

Through Laplace transform, equation (4.1) can be transformed in to

$$\Theta(s) = \theta(0) \times \frac{s+a}{s^2+as+b} \tag{4.2}$$

where $a = b_t/J$ and $b = k_t/J$.

The inverse Laplace transform of equation (4.2), which gives the rotation angle of the whisker shaft in the time axis, is like the following equation.

$$\theta(t) = exp(-At)(cos\sqrt{B}t + \frac{A}{\sqrt{B}}sin\sqrt{B}t) \tag{4.3}$$

where $A = b_t/(2J)$ and $\sqrt{B} = \sqrt{k_t/J - b_t^2/(4J^2)}$.

To see how accurately this model can estimate the results of impulse responses, all the unknown constants were calculated for the case when the whisker shaft length is 10cm. First of all, the moment of inertia J is calulated.

$$J = \int x^2 dm = \int_{x=0}^{L} x^2(\pi r^2 \rho)dx = 3.1416 \times 10^{-7}[Kg \cdot m^2] \tag{4.4}$$

where x is the whisker shaft position ($x = 0$ being the base of the shaft and $x = L$ being the tip of the whisker), $r = 0.5[mm]$ is the radius of the whisker shaft and $\rho \cong 1200[Kg/m^3]$ is the approximate mass density of the whisker shaft material.

Using the average of the decaying rate ($a \cong 10$) of long whiskers and the average resonance frequency ($\omega \cong 24.7Hz$), the other unknown constants could be estimated ($b_t = 6.283e-6$ and $k_t = 0.0076$). The differential equation (equation (4.1)) was solved using the MATLAB function, ODE45, and the results are shown in Figure 4.4 (dotted lines). The results are very similar with the experimental results shown in the previous section.

4.3.2 Modeling whisker sensors in water

Since 'whisker sensors immersed in water' are basically the same with 'whisker sensors in air', except for the fact that the water will act as a damper. Therefore, a new 'torque' term which can represent the 'water damping effect' should be modeled and be included in equation (4.1). (The proposed model should only be regarded as a rough approximation.)

For this, we used the equation which calculates the drag force on cylindrical objects.

$$F_D = \frac{C_D A \rho v^2}{2g} = \frac{C_D (w \cdot h) \rho v^2}{2g} \tag{4.5}$$

where F_D is drag force on a cylindrical object, C_D is the drag coefficient, $A = w \cdot h$ being exposed area, width and height, and g is the gravitational acceleration constant.

The 'torque' term which was needed can be calculated as the following equation.

$$T = \int x dF_D \tag{4.6}$$

The dF_D term can is

$$dF_D = \frac{C_D (w \cdot dx) \rho (x\dot{\theta})^2}{2g} \tag{4.7}$$

Hence, T can be expressed as

$$T = \int x dF_D = \int_{x=0}^{L} \frac{C_D w \rho \dot{\theta}^2}{2g} x^2 dx = (\frac{C_D w \rho L^3}{2g}) \times \dot{\theta}^2 = D_T \times \dot{\theta}^2 \tag{4.8}$$

Adding the term in equation (4.8) in to equation (4.1), we can get

$$\sum T = J\ddot{\theta} + b_t\dot{\theta} + D_T\dot{\theta}^2 + k_t\theta = 0 \tag{4.9}$$

which is a nonlinear differential equation (where $D_T = 6.12e-5$). The results of solving equation (4.9) using ODE45 are shown in Figure 4.4 (solid line).

From the results, it is shown that the simulation results using equation 4.9 are much more damped. Experimental results are voltage measurements from microphone sensors, which mean that the voltage measurements are more likely to be proportional to the angular velocity rather than the rotational angle. Hence, experimental results should be compared with the angular velocities.

The resemblance of the in air results is obvious. The 'in water' results are similar in a way that they are both severely damped. They both have a sudden peak at the beginning but decay slowly at first. After the whisker shaft is almost at a resting position, they oscillate with very small amplitude. Hence, the overall pattern can regarded to be very similar.

It should be noted that the 'in water' impulse-like response and the simulation of the 'in water' impulse is slightly different. While the impulse-like experiment was done by 'striking' the whisker tip in water, the impulse simulation was calculated by setting the initial rotation angle value to a non zero constant ($\pi/12$ in this case). This is why there is a sudden down surge in Figure 4.3 while Figure 4.4 does not.

The conclusion is that the proposed model is quite an accurate way to estimate the experimental results. However, it should be noted that this model would only apply to cases where the Reynolds number is sufficiently small. If the Reynolds number is large, the whisker will oscillate due to the vortex induced vibration and this is not considered in this particular model.

4.4 Sensing hydrodynamic stimuli while distance varies

To see how the whisker sensors respond to a given hydrodynamic stimuli, it was mounted on different positions to vary the distance between the stimuli source and the whisker sensor. For this experiment, three whiskers were used which were mounted on a frame (sensor 1 to sensor 3). Between the sensors, there were equal intervals which was approximately 3cm. Sensor 1 was the shortest and sensor 3 was the longest.

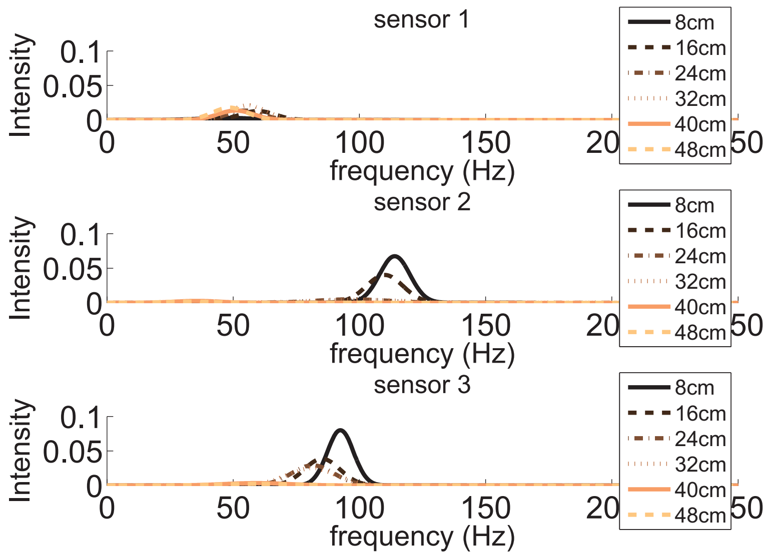

Figure 4.5: Sensing hydrodynamic stimuli from 8cm to 48cm with an 8cm interval. The graph shows the FFT results fitted as a Gaussian distribution. Results of sensor 1 (top), sensor 2 (middle) and sensor 3 (bottom).

The frame to source distance was varied from 8cm to 48cm with an 8cm interval. The FFT results are given in Figure 4.5. It should be noted that the FFT results were fitted as a Gaussian distribution in order to see more clearly what kind of characteristics each result has.

From the results, it shows that sensor 1 barely gives any signal at all. On the other hand, sensor 2 and 3 gives an acknowledgeable response for cases where the source was sufficiently near. (8 16 cm for sensor 2 and 8 24cm for sensor 3). Another characteristic that can be found is that the main frequency becomes smaller as the source gets farther, until it eventually fades out.

Even though this kind of tendency may alter as the type of stimuli source may vary, it still seems as if 'passive sensing' itself might not be sufficient to sense stimuli coming from a far distance. Another hypothesis is that the structure of the stimuli might be the main factor for such sensibility. The next section gives the experimental results of changing the stimuli structure using an artificial fin.

4.5 Sensing The Effect of Artificial Fin

Using an artificial fin to make a hydrodynamic trail was first done by (Wieskotten et al., 2010a) in order to see if the harbor seal can recognize the direction of the fin sweeping direction. The artificial fin is assumed to generate a trail more similar to the trail generated by a swimming fish while a mini-submarine or an underwater motor would just give a streaming jet.

Because the hydrodynamic trail was generated by moving the artificial trail in still water, the structure may have some difference when compared to the actual fish trail (Tytell and Lauder, 2008; Drucker and Lauder, 1999; Müller et al., 1997; Hanke et al., 2000; Hanke and Bleckmann, 2004), it will still have some similarities with the real biological trail having a three dimensional structure.

The artificial fin was made almost identical to the one shown in (Wieskotten et al., 2010a) while the size and material differed. The size was slightly smaller, and the material of the artificial whisker was flexible plastic.

Another experiment which has been done is using a propeller which is rotated under water and an artificial fin for another type of hydrodynamic trail making device as it is shown in Figure 4.6. A single whisker sensor (12cm in length) was used for this experiment.

5 different points were marked inside the water pool, where all five points all go through a same line, and it had a 20cm interval for each point. In order to see the effect of the artificial fin, we varied the location of sensor and artificial fin. 9 different experiments have been conducted. The variables are 'distance between motor and sensor' and 'distance between fin and sensor'. For readability, the variables are named as d_{m2s} and d_{f2s}.

The 9 experiments are like the following.

(1) $d_{m2s} = 80cm$ (no fin) (2) $d_{m2s} = 80cm$ and $d_{f2s} = 20cm$ (3) $d_{m2s} = 80cm$ and $d_{f2s} = 40cm$ (4) $d_{m2s} = 80cm$ and $d_{f2s} = 60cm$ (5) $d_{m2s} = 60cm$ (no fin) (6) $d_{m2s} = 60cm$ and $d_{f2s} = 20cm$ (7) $d_{m2s} = 60cm$ and $d_{f2s} = 40cm$ (8) $d_{m2s} = 40cm$ (no fin) (9) $d_{m2s} = 40cm$ and $d_{f2s} = 20cm$

Since the goal was not just to measure what the sensors sense when the propeller is on, but to see what kind of effect the artificial fin might have when all the other flow

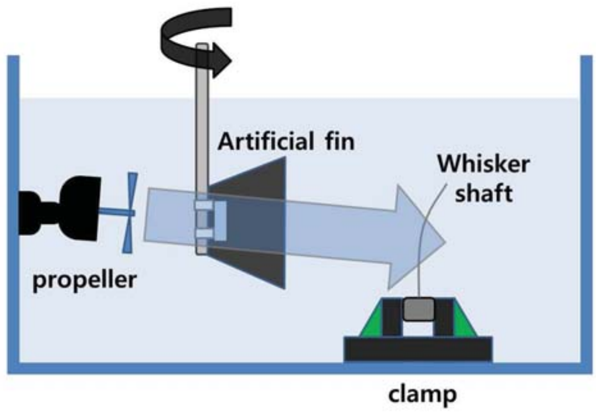

Figure 4.6: Diagram of experimenting with propeller under water with an artificial fin for sweeping in front of the whisker sensor.

conditions are equal. The case where only a propeller is rotating within water, and when there is an additional artificial fin rotating in front of the motor was compared in Figure 4.7. From the results shown in Figure 4.7, it was shown that for cases when the artificial was near (20cm), the standard deviation value of the voltage will slightly increase, but when the artificial fin is too far (over 40cm), the value will decrease.

It seems as when d_{f2s} increases too much (or d_{m2s} decreases), the artificial fin sweeping will disperse the (somewhat) linear flow generated from the propeller which would make the standard deviation value to decrease. For the case when the artificial fin is quite close, the standard deviation increases, which is either because of the additional jet stream or because of the vortex structure has changed. The results given here may not be sufficient to conclude what kind of effect the artificial fin may have. However, it may give a preliminary result that the fin may increase the signal when the sensor is close, but will disperse the flow when it is too far.

4.6 Summary of Chapter 4

In this chapter, a simple but effective microphone based sensor has been designed and manufactured inspired by the pinniped whisker systems. This chapter was concentrated on the passive sensing.

Five different microphone sensors were made which had either a short (approx. 7cm) whisker shaft or a long (approx. 10cm) whisker shaft. Two of the sensors had a short

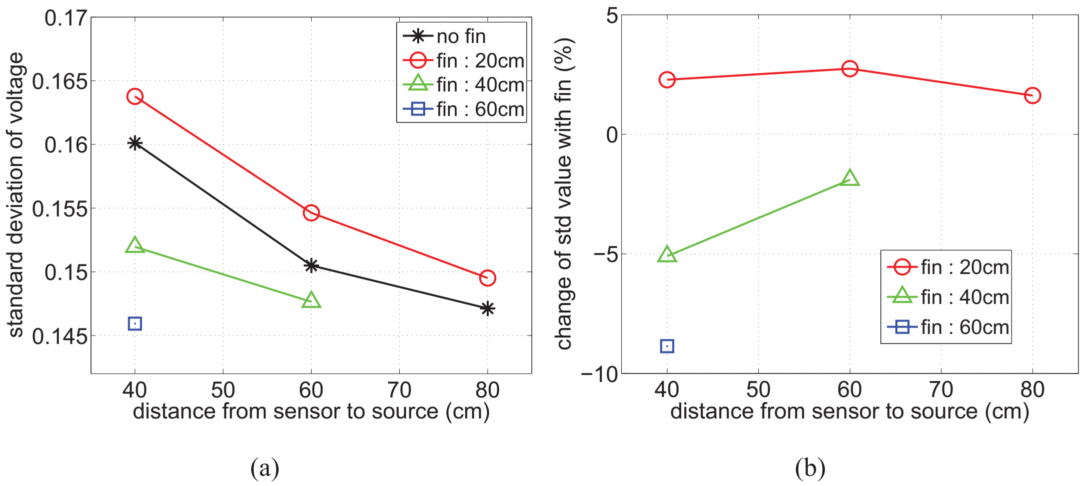

Figure 4.7: The standard deviation for 9 cases of experiments with and without an artificial fin. (a) Standard deviation of each case (b) The change of standard deviation compared with the case when there is no artificial fin.

whisker shaft and the other three had a long whisker shaft. Five of these sensors have been conducted under several experiments. First, all of them were tested with an impulse-like response to check if any defects were present, and if the length and natural frequency relationship was well shown from the results. For the fifth sensor, the impulse-like response within water was conducted.

Also a successful modeling of the whisker sensor has been completed, which mimics the main key features shown in the experimental impulse-like response. For passive experiments, a whisker sensor was sensing hydrodynamic stimuli while varying the source's location. The results showed that passive sensing may not be enough for sensing hydrodynamic trails.

Chapter 5

Active sensing of Hydrodynamic Stimuli

From the previous chapter, ’passive sensing’ of hydrodynamic stimuli using whisker sensors was shown. However, there were some limitations in such sensing strategy. It was shown in Schulte-Pelkum et al. (2007) and Gläser et al. (2011) that pinnipeds utilize undulatory patterns to track its target. This could be regarded as an ’active sensing’ strategy to acquire more information. Also, since the pinnipeds swim ’towards’ the hydrodynamic stimuli generating source, this could be regarded as active sensing.

In this chapter, the advantages that the ’active sensing strategy’ may have are presented. To show this, we first conducted a simple experiment where a whisker sensor senses the hydrodynamic stimuli generated by a motor using either a ”passive sensing strategy’ or an ’active sensing strategy’. For the ’passive sensing strategy’, the whisker sensor was located in 3 different distances (far, middle, close). For the ’active sensing strategy’, the whisker was either moving towards the stimuli source or away from the source.

Another important characteristic of artificial whisker sensors (which have circular cross sections, like the ones used in this theses) or whiskers or California sea lions (but not harbor seals (Hanke et al., 2010)) is that whiskers vibrate when moving in water, or when water is flowing perpendicular to the whisker sensors. This phenomenon is called vortex induced vibration (VIV).

This important characteristic has been intensively analyzed by varying ’whisker length’, ’whisker moving speed’, and measured the corresponding VIV frequencies. This was done in order to see what kinds of relationships these parameters may have. It was shown that the longer the whisker, the lower the frequency it will have compared to shorter whiskers (with the same speed) but will increase its frequency faster as speed increases. Also, the longer the whisker, the VIV frequency will appear more clearly, which resulted in a smaller ’dispersion value (defined in this chapter)’ than the others. This content is prepared to be published in a journal (Ahn and Kim, 2013a).

5.1 Comparing Active and Passive Sensing

In order to mimic the hydrodynamic trails which were generated by a mini-submarine in (Dehnhardt et al., 2001; Wieskotten et al., 2010b; Gläser et al., 2011), we used an underwater motor which had a small propeller attached to the shaft. According to (Schulte-Pelkum et al., 2007), the trail generated by a submarine was mainly consisted of a ”rapidly decaying backward streaming jet” which is different from the biological trails generated by swimming fish. Nevertheless, because many papers showed that pinnipeds are able to track such trails, we used the artificial whiskers to sense the trails.

The motor which we used to make a hydrodynamic trail was a motor initially designed to make a water flow within a water tank where fish live. The product which we had ordered had two distinct motors with propellers on each of them. The motor used 220V/60Hz. Since we wanted to mimic the hydrodynamic trails made by a mini submarine which were used in the experiments of (Dehnhardt et al., 2001; Wieskotten et al., 2010b; Gläser et al., 2011), the product which had a propeller which looked similar to a mini submarines was chosen.

The water flow due to the propeller was sufficient to make the motor move in the water when it is not attached to the wall (but held by the power cable). In this section, two different types of experiments have been conducted. One was passively sensing the hydrodynamic movement of the water from a fixed distance from the water propeller. The distance between the whisker and the propeller was varied. The other experiment was conducted by moving the whisker from ’far’ to ’near’ with a relatively constant speed.

There were practically 4 types of experiments done in Figure 5.1. Passively sensing the stimuli from ’far (approximately 40cm)’, ’middle(approximately 20cm’ and ’close(approximately 5cm)’ and actively sensing by moving the whisker back and

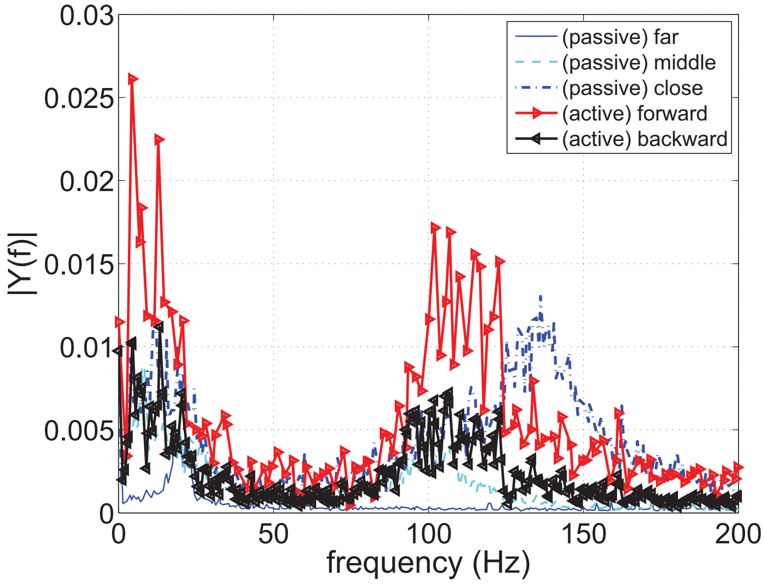

Figure 5.1: Modified (shows the max value in each small interval) FFT results for five cases. Three passive sensing and two active sensing.

forth. Moving 'back (away from source)' and moving 'forth (towards the source)' were regarded as two distinctive strategies, giving 5 different FFT results. We modified the FFT results in order to be able to catch the key features.

While 'passive - far' case has almost no response, 'passive - close' has a large response with frequency near 140Hz. Active sensing does go towards the source, but it will not go closer than 5cm, which means if the moving speed was slow enough, the intensity from active sensing would never exceed the response of 'passive - close'. However this is not the case. The whisker moves approximately $20cm/sec$ in average (sensing range approximately 5 - 40cm) and the overall response turns out to be larger than 'passive - close'. It should be noted that the whisker movement is not moving in a constant speed. Rather, the average speed is $20cm/s$ where the velocity increases and decreases in time. The frequency shift to approximately 110Hz should also be noted. 'Active - forward' and 'active - backward' both have a similar frequency distribution but differ in intensity.

From the results of Figure 5.1, it can be safely said that active sensing could be a good strategy to sense or track a particular stimuli source such as a fish. Even if a pinniped does not actively move its whiskers or head, the relative distance between source and whiskers will become smaller, and this could be regarded as active sensing.

5.2 Vortex induced vibration on artificial whisker

5.2.1 Vortex induced vibration

The well known phenomenon called Karman vortex street generated behind a bluff body has been observed for a long time (von Kármán and Edson, 1967; Govardhan and Ramesh, 2005). When a stationary circular cylinder is exposed to linear fluid flow, the vortex shedding frequency can be estimated by the equation the equation $St = \frac{fd}{U} = 0.198(1 - \frac{19.7}{Re})$, where St is the Strouhal number, f is the vortex shedding frequency, d is the characteristic length (the diameter of the circular cylinder), U is the flow velocity. and Re is the Reynolds number ($Re = \frac{\rho U d}{\mu} = \frac{vd}{\nu}$). When d, U, Re is known, the Strouhal number and the Karman vortex shedding frequency can be known.

The vortex shedding frequency is calculated when the bluff body is stationary. However, the generated vortex makes the bluff body to oscillate (usually perpendicular to the fluid flow). The vibration that is made by these shedding vortices is called vortex-induced vibration (VIV). VIV is mostly an undesirable effect in the industrial field, such as pipes in deep water, bridges or tall buildings and chimneys.

Because it is crucial to understand the phenomenon, many studies have been done to understand VIV (Hartlen and Currie, 1970; Gabbai and Benaroya, 2005; Jauvtis and Williamson, 2004; Blackburn et al., 2001; Vandiver, 1993; Yamamoto et al., 2004), and many studies have been done in order to reduce VIV (Assi et al., 2009; Fischer et al., 2004; Wu et al., 2012; Bearman and Branković, 2004; Gabbai and Benaroya, 2005; Matsumoto et al., 1992).

Pinniped whiskers are also under the influence of VIV. Since the harbor seal whiskers need to sense the deflection due to the hydrodynamic trail generated by a swimming fish (which is only a small pressure change), other signals which are not from the trail such as VIV should be suppressed as much as possible. In (Hanke et al., 2010), numerical simulations have shown that the harbor seal's bumpy profile can suppress VIV compared to circular or ellipsoidal cylinders.

In (Miersch et al., 2011), isolated whiskers of harbor seals and California sea lions have been compared in the sound-noise ration perspective and showed that the harbor seal vibrissa had a higher SNR than the California sea lions. It was concluded that the California sea lion may use some other strategy. While it was not the main point of

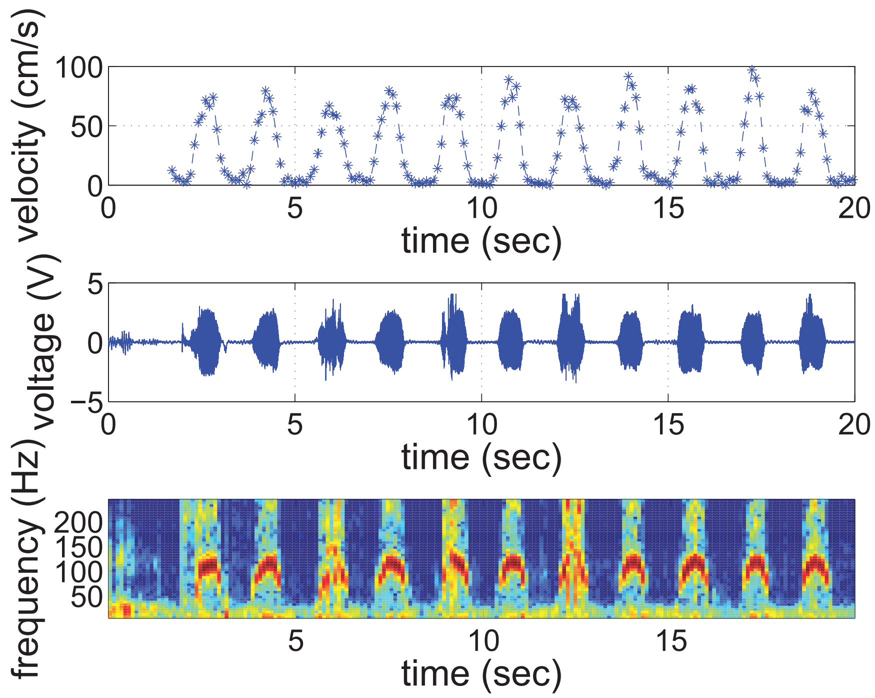

Figure 5.2: Velocity of whisker sensor (top), voltage measurement due to VIV(middle) and the corresponding spectrogram (bottom) with whisker 12cm long.

the paper, regardless of the shape of the whisker shaft (bumpy or smooth), the VIV frequency had a quasi-linear relationship with the speed of water. Hence when the whisker moves faster, the frequency of the VIV increases.

In a nut shell, when a cylinder-like object (the bluff body) is exposed to a linear fluid flow with a high Reynold's number, a 'Karman vortex street' will form behind the bluff body. These vortices will change the nearby pressure which makes the bluff body to experience oscillating force. If the bluff body is not fastened, it will vibrate. This is the 'vortex induced vibration(VIV)'.

Either a bluff body could be exposed to a fluid flow, or the bluff body could actively move in still water. Vortex induced vibration on the artificial whisker, which will be shown in the next section, corresponds to the latter case. The whisker shaft is the bluff body, and since the shaft is not fastened, it will vibrate under certain conditions. The results of this subject are explained in the next section.

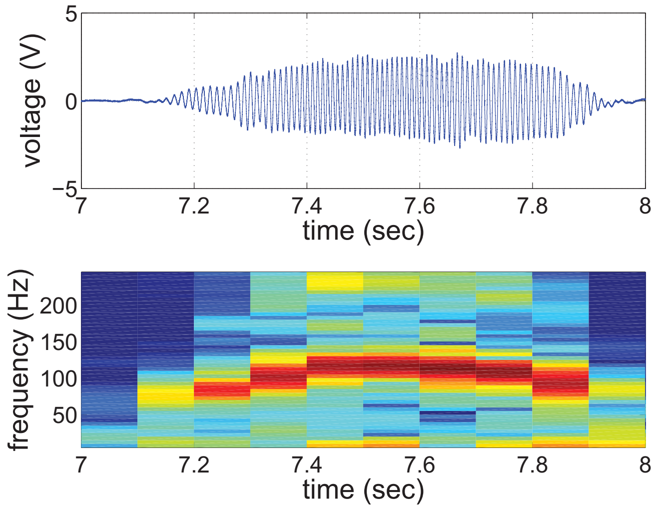

Figure 5.3: Magnified voltage measurements shown in Figure 5.2(top) and the corresponding spectrogram (bottom). The oscillation in the voltage measurements can be clearly seen. Also, the frequency increase and decrease can be seen from both the voltage measurements and (more clearly in) the spectrogram.

5.2.2 Sensing vortex induced vibration in static water

In this section, the relationship between 'whisker sensor moving speed', 'whisker shaft length' and the 'VIV frequencies' have been analyzed. To do such an analysis, it was essential to acquire multiple data points of (speed, frequency) for different types of whisker lengths.

To do this, a whisker sensor was immersed in water and was moved side to side with slightly varying speeds. An iPhone4 was used to record the whole experiment process from above. The resolution of the video was 1280×720 with $29.651 \pm 0.3[frames/sec]$. These videos were used to find the exact trajectory of the sensor movement. The sensor position was tracked manually by using a MATLAB function called 'ginput' (which returns the figure's X-Y information where the mouse clicks) every three frames for each video. From the manually tracked trajectory, the absolute velocity of the whisker sensor could be calculated as $|\vec{V}| = \sqrt{(dx/dt)^2 + (dy/dt)^2}$.

Hence, after the trajectory tracking, we have two types of data. The absolute velocity of the sensor and the voltage measurements. Using the voltage measurements, a spectrogram could be obtained. An example of 'velocity', 'voltage measurements' and 'spectrogram' is shown in Figure 5.2.

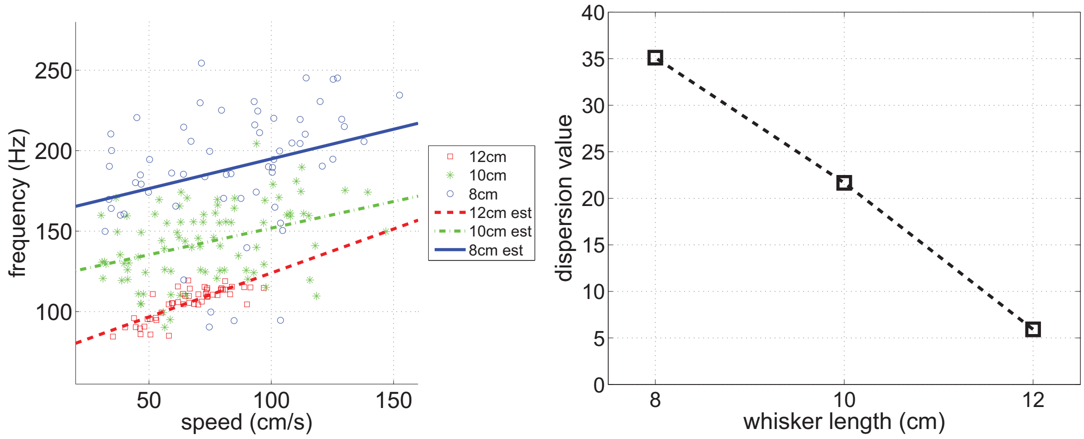

(a) (b)

Figure 5.4: Whisker length and VIV frequency. (a) The scatter plot to show the relationship between 'speed' - 'length' - 'frequency'. From the results, it is clearly seen that the longer the whisker, the lower VIV frequency at same speed values. (b) The dispersion value (defined in equation (5.4) is smaller for the longer whiskers and larger for the shorter whiskers.

To match the VIV frequency to its corresponding speed values, four steps had to be taken. First, the frequency component which has the maximum value for each time interval was selected. The second step is to discriminate the VIV frequencies from non-VIV frequencies by using different thresholds or selecting only from a certain range or frequencies. From this step, only a partial of the 'frequency candidates' will survive. The third step is to synchronize the 'velocity time' and 'voltage measurement time'. The synchronization was done manually. Finally, the VIV frequencies were matched to the appropriate velocity values. Since the time value for the VIV frequencies and the velocities can almost never be exactly matched, the closest was chosen.

Since for every translation movement, the speed is not constant but varies, various speed values could be acquired. We did this same experiment using a whisker sensor with its shaft length being 12cm, 10cm or 8cm. From the experiments, numerous data points have been obtained for each whisker length. The results of doing simple linear regression for each case are shown in the following equations. The results is shown in Figure 5.4.

$$frequency\ for\ 12cm = 0.5460 \times speed + 69.4213 \tag{5.1}$$

$$frequency\, for\, 10cm = 0.3307 \times speed + 118.7822 \tag{5.2}$$

$$frequency\, for\, 8cm = 0.3685 \times speed + 58.0387 \tag{5.3}$$

From the equations and from Figure 5.4, it can be clearly shown that the longer the whisker, the lower the VIV frequency at same speed, and the longer the whisker, the higher the VIV frequency it has. Although because of the high dispersion data for short whiskers, it still could be said that the longer the whisker, the VIV frequency will increase faster as speed increases and the shorter it is, the increase of VIV frequency value will be slower as speed increases. The dispersion is smaller for the longer whiskers and larger for the shorter whiskers.

The dispersion of the data points is calculated as

$$J = \frac{\sum_{i=1}^{N}(freq_{est} - freq_{real})^2}{N} \tag{5.4}$$

where $freq_{est}$ is the estimated frequency value from equations (5.1 - 5.3) and $freq_{real}$ is the actual frequency values of the data points. The dispersion value for whisker length 12cm, 10cm and 8cm is 35.0, 469.2 and 1232.9. The dispersion value shows a sharp increase as the whisker length gets shorter. This is mostly due to the fact that the longer whisker sensor gives a more clear VIV frequency (bigger amplitude) than the shorter, hence making the VIV frequency tracking less noisier. Also note that VIV frequency only appears when the whisker moving speed exceeds a certain value.

There are several conclusions which could be made from this particular section.

(1) Whisker sensors can sense VIV frequencies.

(2) The longer the whisker, the lower the VIV frequency (at same speed) it will have.

(3) The longer the whisker, the faster the VIV frequency will increase as speed increases.

(4) The longer the whisker, the dispersion value (defined in equation (5.4) will be lower.

(5) VIV frequency can be sensed by whisker sensors only when the whisker is moving fast enough (or when water is flowing through it fast enough)

(6) VIV frequency changes with negligible time lag when the whisker sensor speed changes.

To the author's knowledge, this is the first time to find characteristics for a whisker sensor. It is assumed that these kinds of characteristics of this whisker sensor could be used for various engineering applications.

5.2.3 Sensing vortex induced vibration with hydrodynamic stimuli

While the previous section showed the effect of VIV on whiskers when the whisker sensors moved in static water, this section will show how the response will change when there is an external stimuli. The external stimulus is the water flow generated by a propeller. The whisker sensor was swept back and forth in front of the water flow. There are four different types of sweep motion used in this experiment. Either by moving forward towards the propeller directly (and backwards), moving diagonally towards the propeller directly (with 45 degrees to the left or right), and moving perpendicular to the water flow.

In Figure 5.5, the four motions' results are shown. For all figures in Figure 5.5, a black solid line is given which represents the speed-frequency relationship when water is static. If the flow coming from the motor was a perfectly ideal linear flow which the flow velocity is uniform throughout the whole region, the expected results for Figure 5.5 (a) would be 'forward fit' slightly higher than 'static case' and 'backward fit' slightly lower than 'static case'. The same logic could be applied to Figure 5.5 (b,c). For the case shown in Figure 5.5 (d), it was expected that 'forward fit' and 'backward fit' would have no significant distinction even if the external fluid flow was not ideal.

The clearest results were shown in Figure 5.5 (b) and (d). Figure 5.5 (b) is similar with the expected result but Figure 5.5 (d) was completely different from expectation. The reason for this clear distinction probably comes from the fact that the motor generated water flow does not just go straight but rotates in the direction the propeller rotates, hence making a fluid flow even in the perpendicular direction of the motor.

The results shown in Figure 5.5 (a) and (c) are somewhat ambiguous, due to the fact that it has too little data points or the data points are cluttered, but the most probable explanation would be that the fluid flow is far from 'ideally linear and homogeneous flow velocity throughout the whole region'. Such flow could not be obtained by motors

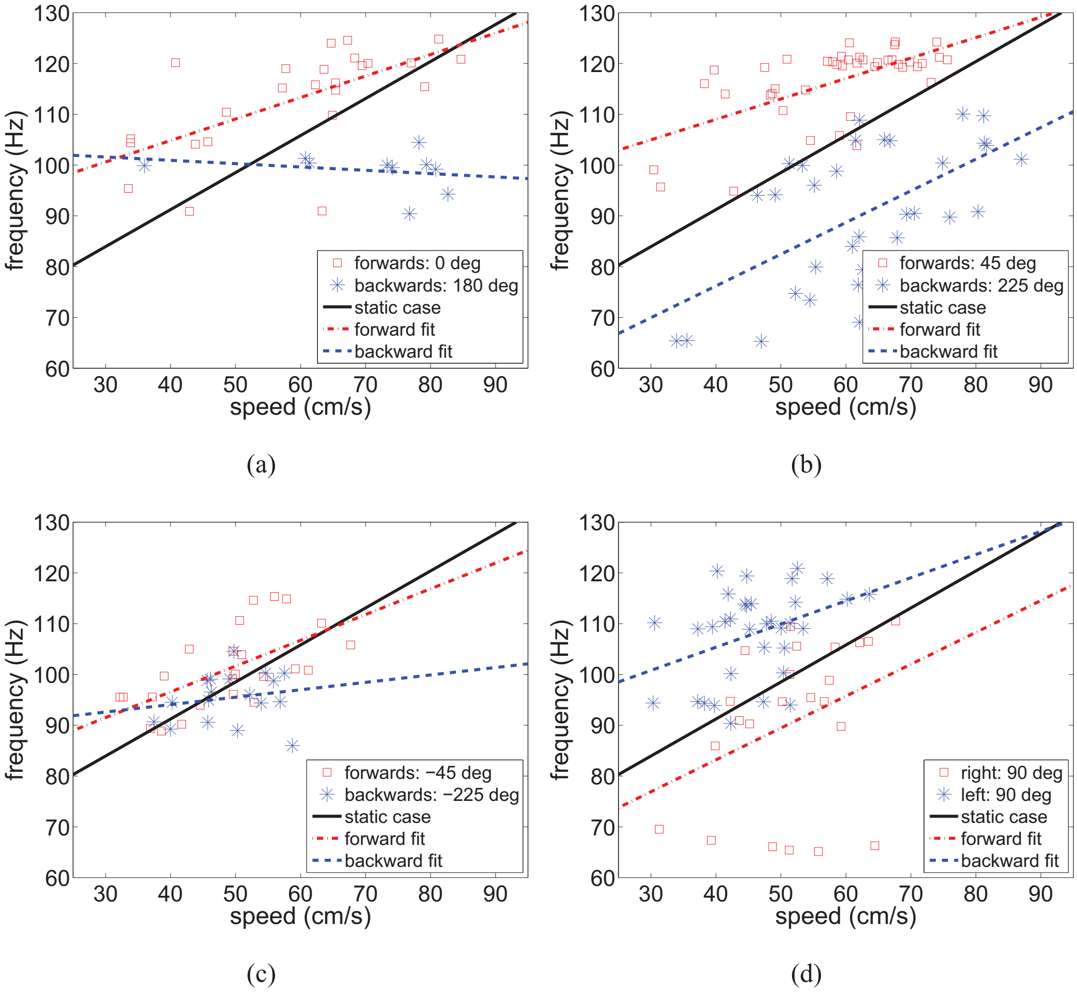

Figure 5.5: Sensing the VIV frequency when hydrodynamic stimuli is present (stimuli source: propeller). (a) Moving directly toward or backward from source (b) moving diagonally : forward (45 degrees to the left) or backward (135 degrees to the right) (c) moving diagonally : forward (45 degrees to the right) or backward (135 degrees to the left) (d) Moving perpendicular to the water flow. (Black solid line indicates the VIV frequency in static water case. Note that for this experiment, a different sensor was used compared to the previous section)

with propellers. However, from this experiment, it was shown that external stimuli will change the 'speed - frequency' relationship of a given whisker sensor. If the fluid flow was linear, and the whisker sensor moving speed is known, the fluid flow velocity could be estimated from the VIV frequency shift. The results for particular speeds are shown in Figure 5.6.

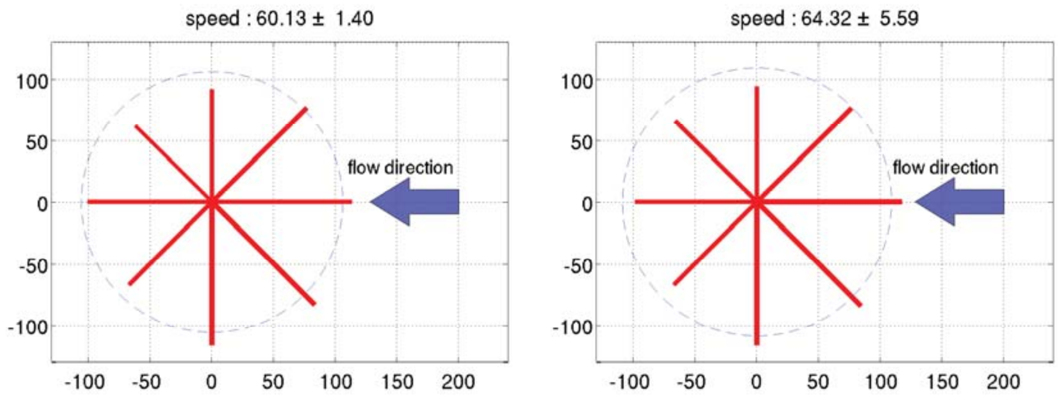

(a) (b)

Figure 5.6: Results of Figure 5.5 show in polar coordinates. Arrow represents the flow direction and the red line length indicates the average VIV frequency when moved in that direction when (a) speed is around 60cm/s and (b) around 70cm/s. Blue dotted line circle indicates the estimated VIV frequency (in static water) with the corresponding mean speed.

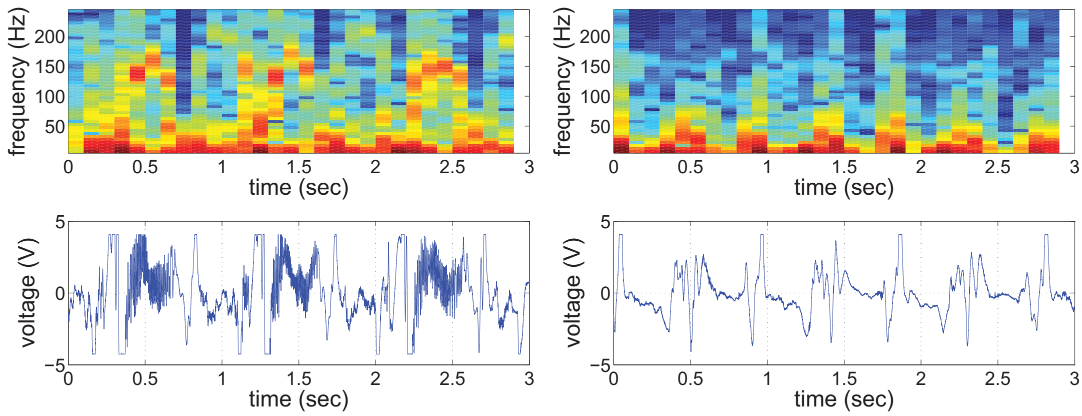

(a) (b)

Figure 5.7: Tapered and cylindrical whisker sensing VIV. (a) Tapered whisker (b) Cylindrical whisker.

5.2.4 Tapered whiskers sensing VIV

In order to see what kind of effect whisker shape may have, the tapered whisker and cylindrical whisker were compared. To make the tapered whisker, a 3-D printer (makerbot replicator 2) was used. Since the previous cylindrical whisker sensors were made out of different materials, both tapered and cylindrical whisker shafts were made (both were designed to have identical base diameter, approximately 2.75mm).

Both whiskers were moved back and forth with similar speed, and the results are shown in Figure 5.7. The obvious difference can be seen in the frequency domain. It is assumed that the tapered whisker has less drag force compared to the cylindrical whisker with equal base diameter. Therefore, while the cylindrical whisker just 'sways' in the way of the flow, the tapered whisker vibrates due to VIV. This may also serve as further evidence which makes the VIV effect stronger than just cylindrical whisker.

5.3 Summary of Chapter 5

The hydrodynamic trail which was generated by the motor was sensed by the whisker sensors either passively or actively. It was shown in the results that the relatively slow movements of the whisker sensor (moving towards the motor) can make the trail be sensed with higher sensitivity. However for the case where the whisker was moving too fast, the movement induced VIV effect becomes dominant (data not shown). Keeping in mind that the relative velocity of the predator and the prey cannot be extremely high, the slowly moving whisker (approx. $20cm/s$) may be a strategy pinnipeds might use.

Also, the VIV (vortex induced vibration) effect was measured from the results. Because the whisker shafts were all approximately similar to a circular cylinder, unlike the harbor seal's bumpy whisker, it did not suppress any VIV. The evident relation between the VIV and the moving velocity, the relationship between the length and VIV frequency has been shown from the results. Such differences of whisker length could be a cue for the use of various whiskers with different length.

Regarding the relationships between 'whisker length', 'whisker moving speed', and 'the corresponding VIV frequencies', it was shown that the longer the whisker, the lower the frequency it will have compared to shorter whiskers (with same speed) but will increase its frequency faster as speed increases. Also, the longer the whisker, the VIV frequency will appear more clearly, which resulted in a smaller 'dispersion value' than the others. Another experiment was to measure the VIV frequency when external stimuli or fluid flow exists. Though the experiment used stimuli generated by a propeller which is far from linear, it could be concluded that if there is an external linear flow, the flow velocity could be estimated using the characteristics of a whisker sensor.

Chapter 6

Conclusions

In this dissertation, studies of biomimetic whisker sensors have been presented. The work could be classified into two groups where the first one is 'biomimetic rat whiskers' and the other part is about 'biomimetic pinniped whiskers'. The 'biomimetic rat whiskers' part concentrates on 'contact distance estimation' methods using simulation via MATLAB, while the 'biomimetic pinniped whiskers' concentrates on making actual whisker sensors which can sense hydrodynamic stimuli from propellers or linear flow by moving the whisker itself. The detailed conclusions are described in the following subsections.

6.1 Rat whiskers

In chapter 3, biomimetic whiskers based on rats have been shown. Inspired from the ability of their 'contact distance estimation', three methods have been described. One is a model using a cylindrical whisker for contact distance estimation proposed by Kim and Möller (Kim and Möller, 2007), one is a model tapered whisker proposed in this paper. Both of these models use two different angle informations. Another model proposed in this paper is a contact distance estimation method using two different deflection measurements.

The contribution of this chapter is proposing a method which can evaluate the accuracy of linear models in large deflection angles. Also, extending the model of Kim (Kim and Möller, 2007), two new methods for contact distance estimation have been proposed. Since there are three different types of contact distance estimation methods, each method could be chosen for user specific needs. While the cylindrical whisker would be easier to make than a tapered whisker, it might be better to use a tapered whisker for more accurate results. There may be a case where deflection measurement is easier than deflection angle. In such a case, the third model in this paper could be used and vice versa.

Using a tapered whisker sensor, there is a possibility that the tip will break, leaving the remaining whisker damaged. However, since there is a curvature change only within the contact point, it is irrelevant whether the tip is broken or not. Even though a tapered whisker sensor with a broken tip will no longer be able to measure the contact distance as far as before, the contact distance estimation method does not change. The same can be said about the cylindrical whisker sensor, but it is quite clear that the tapered whisker is more likely to break.

6.2 Passive Hydrodynamic Stimuli sensing with whisker sensors

In this chapter 4, a simple but effective microphone based sensor has been designed and manufactured to see if they can measure the VIV effect and the hydrodynamic trails. The hydrodynamic trail has been made by a motor with a propeller. In order to make an artificial whisker sensor, a plastic wire (optic fiber) was used to make the whisker shaft. This whisker shaft was attached to the microphone sensor via glue. The thin membrane which was within the microphone sensor is the sensor component which is responsible for the capacitance change (or voltage change). Since all of the whisker sensors were made manually and the sensitivity highly depended on how much glue was applied and how deep the shaft has been penetrated into the microphone sensor, all sensors were tested accordingly before use.

Five different microphone sensors were made which had either a short (approx. 7cm) whisker shaft or a long (approx. 10cm) whisker shaft. Two of the sensors had a short whisker shaft and the other three had a long whisker shaft. Five of these sensors have been conducted under several experiments. First, all of them were tested with an impulse response to check if any defects were present, and if the length and natural frequency relationship was well shown from the results. For the fifth sensor, the impulse response within water was conducted.

A model of the whisker sensors was also constructed which could be used for future studies. This model turned out to be fairly accurate. Also, several experiments have been done in order to show that passive sensing could be insufficient for sensing hydrodynamic stimuli.

6.3 VIV sensing compared with Doppler effect

The VIV sensing of via whisker sensors is similar with the Doppler effect in several aspects. The Doppler effect can be expressed as the following equation.

$$f = (\frac{c+v_r}{c+v_s}) f_0 \tag{6.1}$$

where f is the measured frequency, c is the velocity of waves in the medium, v_r and v_s are the velocity of the receiver and velocity of source and f_0 is the source frequency.

It should be noted that 'VIV sensing via whisker sensors' and 'Doppler effect' are similar in the sense that when 'some kind of' velocity changes, so will 'some kind of' frequency. Since for the whisker case, there is no 'source velocity'. Hence, v_s in equation 6.1 will be zero. Modifying equation 6.1, it can turn into

$$f = \frac{v_r}{c} f_0 + f_0 \tag{6.2}$$

which can also be represented in the form of $f = av + b$.

While the comparison of 'VIV sensing via whisker sensor' and 'Doppler effect' using equations could be somewhat misleading, a somewhat crude understanding of 'VIV sensing via whisker sensor' could be done by putting two principles in mind. The faster the fluid velocity, the higher the Karman vortex street frequency will be. The shorter the whisker shaft, the higher the natural frequency will be. This phenomenon will need more complex explanations, but this is not covered in this thesis.

6.4 Active Hydrodynamic Stimuli sensing with whisker sensors

A simple active sensing (moving back and forth in front of stimuli source) has been shown and was concluded that active sensing could enhance the sensing abilities of whisker sensors. The hydrodynamic trail which was generated by the motor was sensed by the whisker sensors either passively or actively. It was shown in the results that the relatively slow movements of the whisker sensor (moving towards the motor) can make the trail be sensed with higher sensitivity. However for the case where the whisker was moving too fast, the movement induced VIV effect becomes dominan. Putting in mind that the relative velocity of the predator and the prey cannot be extremely high, the slowly moving whisker (approx. $20cm/s$) may be a strategy pinnipeds might use.

Also, the VIV (vortex induced vibration) effect was measured from the results. Because the whisker shafts were all approximately similar to a circular cylinder, unlike the harbor seal's bumpy whisker, it did not suppress any VIV. The evident relation between the VIV and the moving velocity, the relationship between the length and VIV frequency has been shown from the results. Such differences of whisker length could be a cue for the use of various whiskers with different length. As an extension of this exploration, the VIV frequency was measured. The results showed that there is a high possibility by using the characteristics of the whisker sensors, a linear fluid flow velocity could be estimated.

6.5 How do sea lions sense hydrodynamic trails?

According to Glaser et al. (2011), harbor seals and California sea lions have different kind of sensing mechanisms. Harbor seal whiskers reduce the VIV frequency which is due to its extraordinary whisker shaft morphology. On the other hand, sea lions, which have smooth tapered whisker with an oval cross section, were shown to have a basic carrier signal instead of suppressing VIV. It was claimed that the modulation of this signal by external stimuli could be measured, and information of the hydrodynamic stimuli could be extracted.

The experimental results would shed light more on the sea lion's sensing mechanism rather than the harbor seal's sensing mechanism due to the fact that the whisker shaft is smooth shaped. The smooth shape of the sea lion whiskers and the cylindrical artificial plastic whisker shaft are similar in the sense that they both do not reduce VIV.

According to the experimental results, it was shown that the whisker length is a main factor when it comes to VIV frequency sensing. As the whisker length increase the relationship between 'relative speed' and 'VIV frequency', which can be fitted with a linear equation, differs. The longer the whisker length, the lower the VIV frequency will be and with a smaller dispersion value. Also it should be noted that, the VIV frequency is sensed for only a certain range of relative speed.

Since the whisker length impacts the characteristics severely, whiskers with different length can be regarded as different sensors. Hence, a whisker array with varying lengths should be regarded as a heterogeneous sensor system. While a homogeneous sensor system, in this case a whisker array with same length will be advantageous in the sense that a few sensor failures (or breakage) will not affect the overall results. On the other hand, a heterogeneous sensor system will be able to sense a large range of interest.

Different length will give different sensing range of relative speed. For instance, short whiskers will vibrate in high speed, while long whiskers will vibrate even in low speed. It is known that there are cells which respond to a certain frequencies (cite here). Therefore it is plausible that VIV frequencies can be used to measure different types of speed.

In a scenario where a sea lion is swimming in water in low speed, the long whisker will vibrate due to VIV. When the sea lion increases its speed, the short whiskers will start to vibrate. The sea lion might have pre-learned that for a certain speed, which whisker shafts will vibrate, hence being able to estimate the speed. How sea lions sense hydrodynamic trails may not be known yet, but the results do show how speed may be estimated.

6.6 Future studies

In this dissertation, the biomimetic rat whiskers are based on simulations with no experimental data to verify the proposed validity. Therefore for actual implementation in the engineering field, it is essential to test the feasibility of such models in actual robot implementation. On the other hand, the biomimetic pinniped whisker sensors are based on actual simulations, but it lacks a theoretical model.

Apart from these weaknesses, the biomimetic whiskers could be used in applications such as feature extraction or sensing flows or trails in fluids. Using these sensors could expand the view of the human race in the unexplored world.

The active head movement for sensing is an issue that could be resolved through engineering. As future work, having better whisker sensors (higher sensitivity and similar physical characteristics as the real seal whisker including shape and stiffness), a moving head which resembles the real seal head and whisker sensors plucked inside the artificial head according to the seal whisker array morphology, this test could reveal how the seals may sense the hydrodynamic trail. Many hypotheses could be tested using such artificial seal head with whiskers.

Using the active strategy instead of passive strategy, it seemed as if there would be many disadvantages as well. First of all, since the whiskers will deflect very much as the head moves side to side, the small deflection due to the hydrodynamic trails generated by the swimming fish might be hard to detect. If the harbor seal could estimate what kind of signal it will receive (since it knows how it will move) and subtract such signal from the measured signal exactly, subtle movements of the water may be perceived with high accuracy by the harbor seal. Therefore, the SNR (hydrodynamic trail signal to movement induced signal) will highly depend on 'how well the harbor seal can predict the signals it will receive due to its movement'.

Another reason the head movement might be disadvantageous is that the movement of the head could disturb the fluid flow near the whiskers. Therefore this might as well corrupt the wanted signal (hydrodynamic trail). If the harbor seal swimming speed is sufficiently fast (around 2m/s), perhaps the water flow disturbance due to the head movement may be small. The advantage of the active sensing might not lie in accuracy but a fast response to hydrodynamic trail movements.

The artificial whiskers should be improved. The one made in this paper was just for a preliminary study. Since it is based on a microphone sensor, it can only sense the time varying components. Therefore this artificial whisker cannot sense the DC components of the deflection, but only changes of deflection. In biological terms, this sensor could be said to have only RA (rapidly adapting) cells but no SA (slowly adapting) cells. Sensors which mimic the follicle sinus-complex(FSC) of the pinnipeds should be made, but this will require more information on the FSC and knowledge of sensor manufacturing.

Also, making an array of such sensors may give more information about a given trail, sensing which direction it comes from, and (if it is a vortex) which axis is it is rotating to. Such whisker sensors could be used in applications such as swimming direction and speed estimation for a moving ship, or find trails made by fish or submarines under water.

While the artificial whisker sensor's shaft is a simply cylindrical in shape, the actual morphology of pinnipeds are different. Harbor seals' whiskers and California sea lions' whisker are both tapered and have a oval shaped cross section. Harbor seals' whiskers have a bumpy profile which are known to suppress VIV and its oval cross section is much more slender compared to the California sea lion's whisker cross section. Hence, the artificial whisker used in this paper is closer to the California sea lion's whisker. However, in order to look into the real mechanism of hydrodynamic sensing by pinnipeds, there are whisker characteristics which should be closely mimicked including the morphology.

If the Young's modulus, morphology (in scale) and the array structure of the whisker sensors could be mimicked, it is highly probably to obtain meaningful results, which might shed light on the sensitive pinniped whisker sensor systems.

It will also be very important to model the follicle of pinnipeds. To the author's knowledge, the parameters which the follicles are measured are yet unknown. Either by employing various types of sensors to mimic pinniped follicle (in this paper, microphone sensor was used to mimic the follicle), or first modeling the follicle and designing a sensor to closely mimic it, will both be plausible attempts to solve this mystery. The former approach might be more time consuming, but from such a process, it will show what kind is best for engineering applications. The latter approach will be a more subtle task, since it will require an intensive research in pinniped follicle structure from the 'sensing' point of view.

Appendix

A.1 Radial Distance Estimation Method using Tapered Whisker

In this section, the radial distance estimation method using a tapered whisker with the information of two different angles (protraction angle and tangential angle at an arbitrary point on the whisker) is derived.

First, the linear deflection equation was derived in Birdwell et al. (2007) . The following equations summarize the derivation.

First of all, the moment (or torque) on the whisker can be expressed as

$$M(x) = F(d - x), 0 \tag{3}$$

The area moment of inertia of an ideal tapered whisker could bze expressed as

$$I = \frac{\pi r^4}{4} \tag{4}$$

$$r = r_{base}(1 - \frac{x}{L}) \tag{5}$$

$$I = \frac{\pi}{4}(\frac{r_{base}}{L})^4(L - x)^4 = \alpha(L - x)^4 \tag{6}$$

where $\alpha = \frac{\pi}{4}(\frac{r_{base}}{L})^4$

From the Euler equation,

$$M(x) = EI\frac{(d^2y/dx^2)}{1 + (dy/dx)^2} \approx EI\frac{d^2y}{dx^2} \tag{7}$$

$$M(x) = F(d-x) = EI\frac{d^2y}{dx^2} = E\alpha(L-x)^4\frac{d^2y}{dx^2} \tag{8}$$

$$\frac{d^2y}{dx^2} = \frac{F}{E\alpha}\frac{d-x}{(L-x)^4} \tag{9}$$

$$\frac{dy}{dx} = \frac{F}{E\alpha}\frac{L+2d-3x}{6(L-x)^3} + C_1 \tag{10}$$

$$y = \frac{F}{E\alpha}[\frac{d-L}{6(L-x)^2} + \frac{1}{2(L-x)}] + C_1x + C_2 \tag{11}$$

Starting from equation 11, Birdwell et al. (2007) showed the analytical solution for a tapered cantilever beam deflection when force and force location is given (solution not shown). While the analytical solution is given in Birdwell et al. (2007) is for 'force on cantilever beam (fixed - free boundary condition), we derived an analytical solution for an 'active tapered beam'. The definition of 'active whisker' or 'active beam' is given in Kim and Möller (2006). For an active beam, two boundary conditions are given as

$$(1)y_{x=0} = 0 \tag{12}$$

$$(2)y_{x=d} = 0 \tag{13}$$

Using the the first boundary condition (equation 12) and equation 11,

$$y(x=0) = \frac{F}{E\alpha}[\frac{d-L}{6L^2} + \frac{1}{2L}] + C_2 = 0 \tag{14}$$

$$C_2 = -\frac{F}{E\alpha}[\frac{d-L}{6L^2} + \frac{1}{2L}] \tag{15}$$

can be derived.

Using the the second boundary condition (equation 13) and equation 11,

$$y(x=d) = \frac{F}{E\alpha}[\frac{d-L}{6(L-d)^2} + \frac{1}{2(L-d)}] + C_1d + C_2 = 0 \tag{16}$$

$$y(x=d) = \frac{F}{E\alpha}[\frac{d-L}{6(L-d)^2} + \frac{1}{2(L-d)}] + C_1d - \frac{F}{E\alpha}[\frac{d-L}{6L^2} + \frac{1}{2L}] = 0 \tag{17}$$

$$C_1 = \frac{F}{dE\alpha}\left(\frac{d-L}{6(L-d)^2} - \frac{1}{3(L-d)}\right) \tag{18}$$

can be derived.

Differentiating equation 11 with x,

$$\frac{dy}{dx} = \frac{F}{E\alpha}\frac{L+2d-3x}{6(L-x)^3} + C_1 = \frac{F}{E\alpha}\frac{L+2d-3x}{6(L-x)^3} + \frac{F}{dE\alpha}\left(\frac{d-L}{6(L-d)^2} - \frac{1}{3(L-d)}\right) \tag{19}$$

$$E\alpha\frac{dy}{dx} = \left(\frac{L+2d-3x}{6(L-x)^3} + \frac{1}{d}\left(\frac{d+2L}{6L^2} - \frac{1}{3(L-d)}\right)\right)\frac{M}{d} \tag{20}$$

For the case for $x=0$ and $x=h$ can be given as the following two equations.

$$E\alpha\frac{dy}{dx}|_{x=0} = \left(\frac{L+2d}{6L^3} + \frac{1}{d}\left(\frac{d+2L}{6L^2} - \frac{1}{3(L-d)}\right)\right)\frac{M}{d} \tag{21}$$

$$E\alpha\frac{dy}{dx}|_{x=h} = \left(\frac{L+2d-3h}{6(L-h)^3} + \frac{1}{d}\left(\frac{d+2L}{6L^2} - \frac{1}{3(L-d)}\right)\right)\frac{M}{d} \tag{22}$$

Dividing equation 22 with equation 21,

$$\frac{dy/dx|_{x=h}}{dy/dx|_{x=0}} = \frac{\left(\frac{L+2d-3h}{6(L-h)^3} + \frac{1}{d}\left(\frac{d+2L}{6L^2} - \frac{1}{3(L-d)}\right)\right)}{\left(\frac{L+2d}{6L^3} + \frac{1}{d}\left(\frac{d+2L}{6L^2} - \frac{1}{3(L-d)}\right)\right)} \tag{23}$$

Since dy/dx can be substituded with $tan\theta$ for small angle, equation 23 can be represented as

$$\frac{tan\theta_1}{tan\theta_0} = \frac{\left(\frac{L+2d-3h}{6(L-h)^3} + \frac{1}{d}\left(\frac{d+2L}{6L^2} - \frac{1}{3(L-d)}\right)\right)}{\left(\frac{L+2d}{6L^3} + \frac{1}{d}\left(\frac{d+2L}{6L^2} - \frac{1}{3(L-d)}\right)\right)} \tag{24}$$

where $tan\theta_1 = dy/dx|_1$ and $tan\theta_0 = dy/dx|_0$.

Using equation 24, the radial distance d can be calculated as

$$d = \frac{-B - \sqrt{B^2 - 4AC}}{2A} \tag{25}$$

where the A,B and C are the coefficients which are defined as the following.

$$A = \frac{tan\theta_1/tan\theta_0}{3L^3} - \frac{1}{3(L-h)^3} \tag{26}$$

$$B = \frac{L+3h}{6(L-h)^3} - \frac{1}{6L^2} \tag{27}$$

$$C = \frac{L^2-3hL}{6(L-h)^3} - \frac{1}{6L} \tag{28}$$

A.2 Passive Sensing Tapered Whisker Radial Distance Estimation

In this paper, passive sensing simulation for tapered whisker was used in order to compare it with active sensing simulation. The 'analytic passive sensing whisker model' is derived in this section. Starting from equation 11

$$y = \frac{F}{E\alpha}[\frac{d-L}{6(L-x)^2} + \frac{1}{2(L-x)}] + C_1x + C_2 \tag{29}$$

and using the boundary conditions $\frac{dy}{dx}|_{x=0}$ and $y|_{x=0} = 0$, the constant can be found. $C_1 = -\frac{F}{E\alpha}[\frac{L+2d}{6L^3}]$ and $C_2 = 0$. Finally, the equation could be expressed as

$$\frac{dy}{dx} = \frac{F}{E\alpha}[\frac{L-3x+2d}{6(L-x)^3} - \frac{L+2d}{6L^3}] \tag{30}$$

Since the protraction angle will always be zero, two tangential angles are measured from the whisker shaft. Naming the position for each sensor as $x = h_1$ and $x = h_2$ and inserting them into equation (30),

$$\frac{dy}{dx}|_{x=h_1} = \frac{F}{E\alpha}[\frac{L-3h_1+2d}{6(L-h_1)^3} - \frac{L+2d}{6L^3}] \tag{31}$$

$$\frac{dy}{dx}|_{x=h_2} = \frac{F}{E\alpha}[\frac{L-3h_2+2d}{6(L-h_2)^3} - \frac{L+2d}{6L^3}] \tag{32}$$

$$\frac{\frac{dy}{dx}|_{x=h_1}}{\frac{dy}{dx}|_{x=h_2}} = \frac{(L-h_2)^3[L^3(L-3h_1+2d)-(L-h_1)^3(L+2d)]}{(L-h_1)^3[L^3(L-3h_2+2d)-(L-h_2)^3(L+2d)]} \tag{33}$$

where $k = \frac{dy}{dx}|_{x=h_1} / \frac{dy}{dx}|_{x=h_2} = \frac{tan\theta_1}{tan\theta_2}$.

The final equation for radial distance estimation for passive sensing can be expressed as

$$d = \frac{(L-h_2)^3(L^4 - 3h_1L^3 - (L-h_1)^3L) - k(L-h_1)^3(L^4 - 3h_2L^3 - (L-h_2)^3L)}{2k(L-h_1)^3(L^3 - (L-h_2)^3) - 2(L-h_2)^3(L^3 - (L-h_1)^3)} \tag{34}$$

A.3 Radial Distance Estimation Equation Derivation Based on Deflection

The derivation of the equation of radial distance estimation base on deflection information starts from the

$$EIy = -\frac{1}{6}x^3Fu(x) + \frac{1}{6}(x-d)^3Fu(x-d) + \frac{1}{6}C_1x^3 + \frac{1}{2}C_2x^2 + C_3x + C_4 \tag{35}$$

where $F = M/a$. Inserting all the constants

$$EIy = -\frac{1}{6}x^3\frac{M}{d} + \frac{1}{2}Mx^2 - \frac{1}{3}Mdx = \frac{-Mx(x^2 - 3dx + 2d^2)}{6d} \tag{36}$$

hence, by putting in h_1 and h_2 where $h_1 \not\equiv h_2$

$$EIy(x = h_1) = \frac{-Mh_1(h_1^2 - 3dh_1 + 2d^2)}{6d} \tag{37}$$

$$EIy(x = h_2) = \frac{-Mh_2(h_2^2 - 3dh_2 + 2d^2)}{6d} \tag{38}$$

Using the two equations above, it could be summoned into

$$\frac{y(x = h_1)}{y(x = h_2)} = \frac{h_1(h_1^2 - 3dh_1 + 2d^2)}{h_2(h_2^2 - 3dh_2 + 2d^2)} \tag{39}$$

With the equation above, the radial distance could be estimated with the information of two different deflections.

Bibliography

A. Harvey, R. B. H. P. Z. M. (2001). Discriminative whisking in the head-fixed rat: optoelectronic monitoring during tactile detection and discrimination tasks. *Somatosensory & Motor Research*, 18(3):211–222.

Ahl, A. (1986). The role of vibrissae in behavior: a status review. *Veterinary Research Communications*, 10(1):245–268.

Ahn, S. and Kim, D. (2013a). Artificial whisker sensors' active and passive sensing characteristics in water (being prepared). *Adaptive Behavior*.

Ahn, S. and Kim, D. (2013b). Feasibility test for radial distance estimation methods with artificial whisker sensors (being prepared). *PloS one*.

Arabzadeh, E., Petersen, R., and Diamond, M. (2003). Encoding of whisker vibration by rat barrel cortex neurons: implications for texture discrimination. *The Journal of Neuroscience*, 23(27):9146–9154.

Arabzadeh, E., Zorzin, E., and Diamond, M. (2005). Neuronal encoding of texture in the whisker sensory pathway. *PLoS biology*, 3(1):155–165.

Assi, G., Bearman, P., and Kitney, N. (2009). Low drag solutions for suppressing vortex-induced vibration of circular cylinders. *Journal of Fluids and Structures*, 25(4):666–675.

Bearman, P. and Branković, M. (2004). Experimental studies of passive control of vortex-induced vibration. *European Journal of Mechanics-B/Fluids*, 23(1):9–15.

Beem, H., Hildner, M., and Triantafyllou, M. (2012). Characterization of a harbor seal whisker-inspired flow sensor. In *Oceans*, pages 1–4. IEEE.

Beem, H., Hildner, M., and Triantafyllou, M. (2013). Calibration and validation of a harbor seal whisker-inspired flow sensor. *Smart Materials and Structures*, 22(1):1–7.

Birdwell, J., Solomon, J., Thajchayapong, M., Taylor, M., Cheely, M., Towal, R., Conradt, J., and Hartmann, M. (2007). Biomechanical models for radial distance determination by the rat vibrissal system. *Journal of Neurophysiology*, 98(4):2439–2455.

Blackburn, H., Govardhan, R., and Williamson, C. (2001). A complementary numerical and physical investigation of vortex-induced vibration. *Journal of Fluids and Structures*, 15(3):481–488.

Blickhan, R., Krick, C., Zehren, D., Nachtigall, W., and Breithaupt, T. (1992). Generation of a vortex chain in the wake of a suhundulatory swimmer. *Naturwissenschaften*, 79(5):220–221.

Carvell, G. and Simons, D. (1990). Biometric analyses of vibrissal tactile discrimination in the rat. *The Journal of Neuroscience*, 10(8):2638–2648.

Chagnaud, B., Brücker, C., Hofmann, M., and Bleckmann, H. (2008). Measuring flow velocity and flow direction by spatial and temporal analysis of flow fluctuations. *The Journal of Neuroscience*, 28(17):4479–4487.

Clements, T. and Rahn, C. (2006). Three-dimensional contact imaging with an actuated whisker. *IEEE Transactions on Robotics*, 22(4):844–848.

Dehnhardt, G. and Kaminski, A. (1995). Sensitivity of the mystacial vibrissae of harbour seals (phoca vitulina) for size differences of actively touched objects. *Journal of Experimental Biology*, 198(11):2317–2323.

Dehnhardt, G., Mauck, B., Hanke, W., and Bleckmann, H. (2001). Hydrodynamic trail-following in harbor seals (phoca vitulina). *Science*, 293(5527):102–104.

Dehnhardt, G., Mauck, B., and Hyvärinen, H. (1998). Ambient temperature does not affect the tactile sensitivity of mystacial vibrissae in harbour seals. *Journal of Experimental Biology*, 201(22):3023–3029.

Drucker, E. and Lauder, G. (1999). Locomotor forces on a swimming fish: three-dimensional vortex wake dynamics quantified using digital particle image velocimetry. *Journal of Experimental Biology*, 202(18):2393–2412.

Eberhardt, W., Shakhsheer, Y., Calhoun, B., Paulus, J., and Appleby, M. (2011). A bio-inspired artificial whisker for fluid motion sensing with increased sensitivity and reliability. In *IEEE Sensors*, pages 982–985. IEEE.

Fend, M. (2005). Whisker-based texture discrimination on a mobile robot. *Advances in Artificial Life*, pages 302–311.

Fischer, F., Liapis, S., and Kallinderis, Y. (2004). Mitigation of current-driven, vortex-induced vibrations of a spar platform via smart thrusters. *Journal of Offshore Mechanics and Arctic Engineering*, 126:96.

Gabbai, R. and Benaroya, H. (2005). An overview of modeling and experiments of vortex-induced vibration of circular cylinders. *Journal of Sound and Vibration*, 282(3):575–616.

Ginter, C., DeWitt, T., Fish, F., and Marshall, C. (2012). Fused traditional and geometric morphometrics demonstrate pinniped whisker diversity. *PloS one*, 7(4):1–10.

Ginter, C., Fish, F., and Marshall, C. (2010). Morphological analysis of the bumpy profile of phocid vibrissae. *Marine Mammal Science*, 26(3):733–743.

Gläser, N., Wieskotten, S., Otter, C., Dehnhardt, G., and Hanke, W. (2011). Hydrodynamic trail following in a california sea lion (zalophus californianus). *Journal of Comparative Physiology A*, 197(2):141–151.

Govardhan, R. and Ramesh, O. (2005). A stroll down kármán street. *Resonance*, 10(8):25–37.

Hanke, F. and Dehnhardt, G. (2009). Aerial visual acuity in harbor seals (phoca vitulina) as a function of luminance. *Journal of Comparative Physiology A*, 195(7):643–650.

Hanke, F., Hanke, W., Scholtyssek, C., and Dehnhardt, G. (2009). Basic mechanisms in pinniped vision. *Experimental Brain Research*, 199(3):299–311.

Hanke, F., Scholtyssek, C., Hanke, W., and Dehnhardt, G. (2011). Contrast sensitivity in a harbor seal (phoca vitulina). *Journal of Comparative Physiology A*, 197(2):203–210.

Hanke, W. and Bleckmann, H. (2004). The hydrodynamic trails of lepomis gibbosus (centrarchidae), colomesus psittacus (tetraodontidae) and thysochromis ansorgii (cichlidae) investigated with scanning particle image velocimetry. *Journal of Experimental Biology*, 207(9):1585–1596.

Hanke, W., Brucker, C., and Bleckmann, H. (2000). The ageing of the low-frequency water disturbances caused by swimming goldfish and its possible relevance to prey detection. *Journal of Experimental Biology*, 203(7):1193–1200.

Hanke, W., Wieskotten, S., Miersch, L., Witte, M., Brede, M., Leder, A., and Dehnhardt, G. (2012a). On the wake flow dynamics behind harbor seal vibrissae–a fluid mechanical explanation for an extraordinary capability. *Nature-Inspired Fluid Mechanics*, pages 271–289.

Hanke, W., Wieskotten, S., Niesterok, B., Miersch, L., Witte, M., Brede, M., Leder, A., and Dehnhardt, G. (2012b). Hydrodynamic perception in pinnipeds. *Nature-Inspired Fluid Mechanics*, pages 255–270.

Hanke, W., Witte, M., Miersch, L., Brede, M., Oeffner, J., Michael, M., Hanke, F., Leder, A., and Dehnhardt, G. (2010). Harbor seal vibrissa morphology suppresses vortex-induced vibrations. *Journal of Experimental Biology*, 213(15):2665–2672.

Hans, H., Miao, J., and Triantafyllou, M. (2012). Characterization of von karman street with seal whisker-like sensor. In *IEEE Sensors*, pages 1–4. IEEE.

Hartlen, R. and Currie, I. (1970). Lift-oscillator model of vortex-induced vibration. *Journal of the Engineering Mechanics Division*, 96(5):577–591.

Hartmann, M. (2001). Active sensing capabilities of the rat whisker system. *Autonomous Robots*, 11(3):249–254.

Hartmann, M. (2009). Active touch, exploratory movements, and sensory prediction. *Integrative and Comparative Biology*, 49(6):681–690.

Jauvtis, N. and Williamson, C. (2004). The effect of two degrees of freedom on vortex-induced vibration at low mass and damping. *Journal of Fluid Mechanics*, 509(6):23–62.

Kaneko, M. (1994). Active antenna. In *IEEE Proceedings on Robotics and Automation*, pages 2665–2671.

Kaneko, M., Kanayama, N., and Tsuji, T. (1996). Vision based active antenna. In *IEEE International Conference on Robotics and Automation*, volume 3, pages 2555–2560.

Kaneko, M., Kanayama, N., and Tsuji, T. (1998). Active antenna for contact sensing. *RIEEE Transactions on Robotics and Automation*, 14(2):278–291.

Kim, D. and Moeller, R. (2004). A biomimetic whisker for texture discrimination and distance estimation. *From Animals to Animats*, 8:140–149.

Kim, D. and Möller, R. (2006). Passive sensing and active sensing of a biomimetic whisker. In *International Conference on the Simulation and Synthesis of Living Systems. Bloomington: Indiana University Press*, pages 127–131.

Kim, D. and Möller, R. (2007). Biomimetic whiskers for shape recognition. *Robotics and Autonomous Systems*, 55(3):229–243.

Krupa, D., Matell, M., Brisben, A., Oliveira, L., and Nicolelis, M. (2001). Behavioral properties of the trigeminal somatosensory system in rats performing whisker-dependent tactile discriminations. *The Journal of Neuroscience*, 21(15):5752–5763.

Lepora, N., Evans, M., Fox, C., Diamond, M., Gurney, K., and Prescott, T. (2010). Naive bayes texture classification applied to whisker data from a moving robot. In *The 2010 International Joint Conference on Neural Networks (IJCNN)*, pages 1–8.

Lepora, N., Fox, C., Evans, M., Mitchinson, B., Motiwala, A., Sullivan, J., Pearson, M., Welsby, J., Pipe, T., Gurney, K., et al. (2011). A general classifier of whisker data using stationary naive bayes: application to biotact robots. *Towards Autonomous Robotic Systems*, pages 13–23.

Matsumoto, M., Shiraishi, N., and Shirato, H. (1992). Rain-wind induced vibration of cables of cable-stayed bridges. *Journal of Wind Engineering and Industrial Aerodynamics*, 43(1):2011–2022.

Mauck, B., Eysel, U., and Dehnhardt, G. (2000). Selective heating of vibrissal follicles in seals (phoca vitulina) and dolphins (sotalia fluviatilis guianensis). *Journal of Experimental Biology*, 203(14):2125–2131.

Miersch, L., Hanke, W., Wieskotten, S., Hanke, F., Oeffner, J., Leder, A., Brede, M., Witte, M., and Dehnhardt, G. (2011). Flow sensing by pinniped whiskers. *Philosophical Transactions of the Royal Society B*, 366(1581):3077–3084.

Müller, U., Heuvel, B., Stamhuis, E., and Videler, J. (1997). Fish foot prints: morphology and energetics of the wake behind a continuously swimming mullet (chelon labrosus risso). *Journal of Experimental Biology*, 200(22):2893–2906.

Quist, B., Faruqi, R., and Hartmann, M. (2011). Variation in young's modulus along the length of a rat vibrissa. *Journal of Biomechanics*, page 27752781.

Rohr, J. and Fish, F. (2004). Strouhal numbers and optimization of swimming by odontocete cetaceans. *Journal of Experimental Biology*, 207(10):1633–1642.

Rooney, T., Pearson, M., Welsby, J., Horsfield, I., Sewell, R., and Dogramadzi, S. (2011). Artificial active whiskers for guiding underwater autonomous walking robots. pages 1–6.

Scholz, G. and Rahn, C. (2004). Profile sensing with an actuated whisker. *IEEE Transactions on Robotics and Automation*, 20(1):124–127.

Schulte-Pelkum, N., Wieskotten, S., Hanke, W., Dehnhardt, G., and Mauck, B. (2007). Tracking of biogenic hydrodynamic trails in harbour seals (phoca vitulina). *Journal of Experimental Biology*, 210(5):781–787.

Schultz, A., Solomon, J., Peshkin, M., and Hartmann, M. (2005). Multifunctional whisker arrays for distance detection, terrain mapping, and object feature extraction. In *IEEE International Conference on Robotics and Automation*, pages 2588–2593.

Schusterman, R. and Balliet, R. (2006). Aerial and underwater visual acuity in the california sea lion (zalophus californianus) as a function of luminance. *Annals of the New York Academy of Sciences*, 188(1):37–46.

Schusterman, R. et al. (1972). Visual acuity in pinnipeds. *The Behavior of Marine Mammals*, 2:469–492.

Solomon, J. and Hartmann, M. (2006). Biomechanics: robotic whiskers used to sense features. *Nature*, 443(7111):525–525.

Solomon, J. and Hartmann, M. (2008). Artificial whiskers suitable for array implementation: Accounting for lateral slip and surface friction. *IEEE Transactions on Robotics*, 24(5):1157–1167.

Solomon, J. and Hartmann, M. (2010). Extracting object contours with the sweep of a robotic whisker using torque information. *The International Journal of Robotics Research*, 29(9):1233–1245.

Solomon, J. and Hartmann, M. (2011). Radial distance determination in the rat vibrissal system and the effects of weber's law. *Philosophical Transactions of the Royal Society B*, 366(1581):3049–3057.

Stocking, J., Eberhardt, W., Shakhsheer, Y., Calhoun, B., Paulus, J., and Appleby, M.

(2010). A capacitance-based whisker-like artificial sensor for fluid motion sensing. In *IEEE Sensors*, pages 2224–2229. IEEE.

Szwed, M., Bagdasarian, K., and Ahissar, E. (2003). Encoding of vibrissal active touch. *Neuron*, 40(3):621–630.

Towal, R. and Hartmann, M. (2006). Right–left asymmetries in the whisking behavior of rats anticipate head movements. *The Journal of Neuroscience*, 26(34):8838–8846.

Towal, R. and Hartmann, M. (2008). Variability in velocity profiles during free-air whisking behavior of unrestrained rats. *Journal of Neurophysiology*, 100(2):740–752.

Towal, R. and Hartmann, M. (2010). Principles and applications of active tactile sensing strategies in the rat vibrissal system. In *IEEE Sensors*, pages 2230–2234.

Towal, R., Quist, B., Gopal, V., Solomon, J., and Hartmann, M. (2011). The morphology of the rat vibrissal array: a model for quantifying spatiotemporal patterns of whisker-object contact. *PLoS computational biology*, 7(4):1–17.

Triantafyllou, M. and Triantafyllou, G. (1995). An efficient swimming machine. *Scientific American*, 272(3):64–71.

Tytell, E. and Lauder, G. (2008). Hydrodynamics of the escape response in bluegill sunfish, lepomis macrochirus. *Journal of Experimental Biology*, 211(21):3359–3369.

Ueno, N. and Kaneko, M. (1994). Dynamic active antenna-a principle of dynamic sensing. In *IEEE International Conference on Robotics and Automation*, pages 1784–1790.

Valdivia y Alvarado, P., Subramaniam, V., and Triantafyllou, M. (2012). Design of a bio-inspired whisker sensor for underwater applications. In *IEEE Sensors*, pages 1–4. IEEE.

Vandiver, J. (1993). Dimensionless parameters important to the prediction of vortex-induced vibration of long, flexible cylinders in ocean currents. *Journal of Fluids and Structures*, 7(5):423–455.

Von Heimendahl, M., Itskov, P., Arabzadeh, E., and Diamond, M. (2007). Neuronal activity in rat barrel cortex underlying texture discrimination. *PLoS biology*, 5(11):2696–2708.

von Kármán, T. and Edson, L. (1967). *The wind and beyond*. Little, Brown & Company.

Wieskotten, S., Dehnhardt, G., Mauck, B., Miersch, L., and Hanke, W. (2010a). Hydrodynamic determination of the moving direction of an artificial fin by a harbour seal (phoca vitulina). *Journal of Experimental Biology*, 213(13):2194–2200.

Wieskotten, S., Dehnhardt, G., Mauck, B., Miersch, L., and Hanke, W. (2010b). The impact of glide phases on the trackability of hydrodynamic trails in harbour seals (phoca vitulina). *Journal of Experimental Biology*, 213(21):3734–3740.

Wieskotten, S., Mauck, B., Miersch, L., Dehnhardt, G., and Hanke, W. (2011). Hydrodynamic discrimination of wakes caused by objects of different size or shape in a harbour seal (phoca vitulina). *The Journal of Experimental Biology*, 214(11):1922–1930.

Williams, C. and Kramer, E. (2010). The advantages of a tapered whisker. *PloS one*, 5(1):1–8.

Wu, H., Sun, D., Lu, L., Teng, B., Tang, G., and Song, J. (2012). Experimental investigation on the suppression of vortex-induced vibration of long flexible riser by multiple control rods. *Journal of Fluids and Structures*, pages 115–132.

Yamamoto, C., Meneghini, J., Saltara, F., Fregonesi, R., and Ferrari, J. (2004). Numerical simulations of vortex-induced vibration on flexible cylinders. *Journal of Fluids and Structures*, 19(4):467–489.

Yu, X., Tao, J., and Berilla, J. (2010). A bio-inspired flow sensor. In *SPIE Smart Structures and Materials+ Nondestructive Evaluation and Health Monitoring*, pages 1–7. International Society for Optics and Photonics.